UNIVERSIDADE D
COIMBRA

Jacinta Maria Henriques Silva

FUNCTIONAL CONNECTIVITY AS A POTENTIAL BIOMARKER IN MULTIPLE SCLEROSIS USING FMRI

Dissertação no âmbito do Mestrado em Engenharia Biomédica orientada pelo Doutor João Valente Duarte e pelo Professor Doutor Miguel de Sá e Sousa de Castelo Branco e apresentada ao Departamento de Física da Faculdade de Ciências e Tecnologias da Universidade de Coimbra

setembro de 2022

Agradecimentos

Muitos foram os que me acompanharam de uma forma direta ou indireta durante a realização desta dissertação de Mestrado. A todos vocês, muito obrigado.

Começo por agradecer aos meus orientadores, ao Doutor Professor Miguel Castelo Branco, por quem expresso a minha admiração e ao Doutor João Duarte, a quem agradeço não só por toda a orientação, mas também pelas oportunidades, pelos conselhos e por toda a confiança. À Júlia um profundo agradecimento por ter sido não só uma amiga, mas também um grande apoio e ajuda durante este ano.

Ao Departamento de Física, para sempre DF, que ao longo destes 5 anos me fez sempre sentir em casa, e que me proporcionou tão boas memórias e pessoas que vou levar para a vida.

Agradeço à minha maltinha do DF, à Mariana, à Eva, aos meus afilhados, família de praxe, e ao grupo dos BCL em especial à Filipa e Filipe por todas as conversas, troca de experiências, e companheirismo. São sem sombra de dúvidas as melhores pessoas que podiam ter entrado na minha vida.

Às minhas amigas de Porto de Mós, obrigado por partilharem comigo o vosso dia-a-dia, e por toda a amizade ao longo de todos estes anos.

Por último, mas talvez o agradecimento mais importante, à minha família, em especial à minha mãe pelo apoio incondicional e pelas palavras certas nos momentos certos, que me deram sempre a força que eu precisava para continuar e alcançar os meus objetivos.

,

Resumo

A Esclerose Múltipla (EM) é uma doença complexa, ainda com causa desconhecida, que afeta principalmente a substância branca do sistema nervoso central dos humanos.

Apesar da imagem por ressonância magnética (IRM) ser a técnica de eleição para diagnosticar esta doença, esta apresenta algumas limitações que tornam o processo de diagnóstico e avaliação da progressão da doença uma tarefa complicada. Surge, assim, a motivação do estudo de biomarcadores funcionais. A Ressonância Magnética Funcional (em inglês, fMRI ou functional MRI) é uma técnica cada vez mais utilizada em investigação clínica, especialmente em condições de repouso (em inglês, resting-state fMRI ou rs-fMRI), e que permite obter padrões de activação e conectividade funcional (em inglês FC ou functional connectivity) na EM. Nesta dissertação, foram adquiridos dados de fMRI em condições de repouso e durante dois tipos de tarefa visual - uma de movimento visual passivo e outra de reconhecimento de movimento biológico.

O nosso principal objetivo foi comparar diferenças a nível da FC obtida através da técnica de Causalidade de Granger, entre doentes recentemente diagnosticados com EM e controlos saudáveis. Para além disso, a partir dos padrões de conectividade funcional medidos com fMRI calculámos medidas de conectividade (globais e locais), com base na teoria de grafos, e fizemos a análise da correlação entre a FC obtida dos doentes com os resultados da sua avaliação clínica e neuropsicológica.

Durante a análise das alterações da FC entre grupos, não foi possível observar qualquer aumento dos valores de conectividade nos doentes, ao contrário do reportado na literatura. Esta informação, em conjunto com os resultados das medidas globais baseadas na teoria de grafos, sugere que os doentes recrutados em fases muito iniciais da doença ainda não desenvolveram alterações significativas da organização global das redes neuronais. No entanto, as medidas locais baseadas na teoria dos grafos verificaram-se alteradas em várias regiões, com valores maioritariamente mais elevados nos doentes, sugerindo a presença de mecanismos compensatórios. Para além disso, também foram observadas diferenças entre os resultados obtidos em tarefa em relação com os obtidos em repouso, o que faz realçar a importância de estudar a FC utilizando diferentes paradigmas. Relativamente à correlação dos valores de conectividade com os resultados dos testes neuropsicológicos dos doentes, foram encontrados padrões interessantes que podem justificar tanto os défices físicos, como psicológicos na EM.

Finalmente, através de todas estas análises foi possível não só destacar o potencial benefício da utilização de fMRI em condições de tarefa, sugerindo que a utilização de tarefas tem vantagens na investigação de alterações da conetividade funcional, como também dar algumas visões sobre como alterações da conetividade funcional (fMRI-FC) podem estar relacionadas com a progressão e incapacidade da EM.

Palavras-Chave: Esclerose Múltipla, Ressonância Magnética Funcional (fMRI), Conetividade Funcional (direta), Causalidade de Granger e Teoria de Grafos.

Abstract

Multiple sclerosis (MS) is a complex disease, that mainly affects the white matter (WM) of the central nervous system, with several factors still unknown such as the cause of the disease.

Although structural Magnetic Resonance Imaging (MRI) is the gold standard technique to diagnose this disease, it has some limitations that make the process of diagnosing and assessing disease progression a challenging task. Thus, the motivation to study functional biomarkers arises.

Functional Magnetic Resonance Imaging (fMRI) is an increasingly used technique especially in resting-state conditions (rs-fMRI) to measure, describe and compare functional connectivity (FC) patterns in MS. However, the use of task-based fMRI can provide extra valuable information regarding how brain networks communicate. So, in this thesis, fMRI data were acquired in resting-state, as well as during two types of visual tasks - one passive visual motion task and one biological motion perception task.

The aim was to compare differences in FC obtained by Granger Causality, between early MS patients and healthy controls. In addition, we intend to extract connectivity measures (global and local) from graph theory and to correlate FC with the results of clinical and neuropsychological tests in patients.

During the FC analysis, no increase in connectivity values were observed in the patients and the same was observed for the global graph theory measures. These results go against to what was previously reported in literature. However, the local graph theory measures were found to be altered in several regions, with mostly higher values in patients, suggesting that compensatory mechanisms to limit disease damages are behind this increasing. Moreover, we also observed differences between task and resting-state results, which highlights the importance of studying FC using different paradigms. Lastly, when correlating connectivity values with neuropsychological test results, interesting patterns were found that may account for both physical and psychological deficits in MS.

Through all these studies, it was possible to highlight the potential benefit of using fMRI in task conditions over at rest which suggested that the use of tasks has advantages in investigating changes in functional connectivity. Finally, the outcomes of this work gave a few insights into better understanding how fMRI-FC is related to MS evolution and disability.

Keywords: Multiple Sclerosis, Functional Magnetic Resonance Imaging (fMRI), (direct) Functional Connectivity, Granger Causality and Graph Theory.

Contents

List of figures

List of Tables

List of Equations

Abbreviations

AAL3 Automated Anatomical Labeling atlas 3

AC Anatomical Connectivity

APCs Antigen-presenting Cells

BBB Blood Brain Barrier

BCT Brain Connectivity Toolbox

BICAMS Brief Cognitive Assessment for MS

BVMT Brief Visuospatial Memory Test

MS Multiple Sclerosis

CBF Cerebral Blood Flow

CBV Cerebral Blood Volume

CIS Clinical Isolated Syndrome

$CMRO_2$ Cerebral Metabolic Rate of Oxygen

CNS Central Nervous System

CSF Cerebrospinal Fluid

CNT Healthy controls

CVLT California Verbal Learning Test

dHb Deoxyhemoglobin

DAN Dorsal Attention Network

DIS Dissemination in Space (diagnostic criterion)

DIT Dissemination in Time Criterion (diagnostic criterion)

DMN Default Mode Network

EF Effective Connectivity

EDSS Expanded Disability Status Scale

FC Functional Connectivity

FLAIR Fluid-attenuated Inversion Recovery

fMRI Functional Magnetic Resonance Imaging

WM White Matter

GCA Granger Causality analysis

GLM General Linear Model

GM Grey Matter

H Hydrogen

Hb Hemoglobin

HRF Hemodynamic Response Function

HbO_2 Oxyhemoglobin

ICA Independent component Analysis

LIN Language Network

LWR Levinson-Wiggins-Robinson

MFIS Modified Fatigue Impact Scale

MP2RAGE Magnetization-prepared 2 rapid acquisition gradient echoes

MRI Magnetic Resonance Imaging

MS Multiple Sclerosis

MSC Multiple Sclerosis patients' group

MVGC Multivariate Granger Causality

O_2 Oxygen

PASAT Paces Auditory Serial Addition Test

PPMS Primary Progressive Multiple Sclerosis

PRMS Progressive Relapsing Multiple Sclerosis

PS Processing Speed

RF Radiofrequency Pulse

RME Reading the Mind in the Eyes

ROI Region of interest

RRMS Relapsing Remitting Multiple Sclerosis

RS-fMRI Resting-state functional magnetic resonance imaging

RUN V1MT Localizer run

RUNS BM Biological motion run

SDMT Symbol Digit Modalities Test

Sec Seconds

SMN Sensorimotor Network

SPMS Secondary Progressive Multiple Sclerosis

STC Slice Time Correction

TE Time of Echo

TE Transfer Entropy

TR Time of Repetition

VAR Vector Autoregression

1. Introduction

1.1. Motivation

Multiple Sclerosis (MS) is a chronic, autoimmune, and inflammatory disease that affects the myelin sheathing of axons, and one of the world's most frequent neurological disorders affecting the Central Nervous System (CNS) [1]. The loss of brain matter (atrophy) and the development of brain lesions have been extensively studied using brain imaging techniques such as Magnetic Resonance Imaging (MRI), and there is evidence that these alterations are potentially associated with not only physical, but also cognitive deficits.

According to 2020 data, there are over 2.8 million people diagnosed with MS, essentially young and middle-aged adults, with an average age of 32 years old, making the worldwide pooled incidence rate: 35.9 per 100.000 people [2].

MS is a condition with many factors still unknown, from its origin to its cause, with no cure and only debatably effective therapies focusing on controlling the progression of the disease [3]. Therefore, it is crucial to provide information about the pathophysiology of the disease, as well as to develop biomarkers related to the mechanisms that are responsible for disease progression, such as brain structural and functional alterations.

There is a growing interest in studies of human brain organization using resting-state Functional Magnetic Resonance Imaging (rs-fMRI). However, it is recognized that brain networks measured during resting-state do not exhibit comparable properties during task performance [4]. Therefore, we will investigate functional neuroimaging biomarkers of connectivity between brain regions, both during resting-state, i.e., when there is no explicit task, and most importantly, during task performance. We will take advantage of a visual motion paradigm of perceptual decision making, which depends strongly on the communication between distant and myelinated brain regions. Our hypothesis is that our paradigm might reveal changed functional connectivity patterns in patients with MS, due to alterations in neuronal communication. Another objective will be to correlate MS functional connectivity metrics with neuropsychological assessment of MS patients to explain potential cognitive and physical alterations.

These functional biomarkers might be a powerful tool to accurately follow disease progression and find more effective therapies.

1.2. Objectives and Original Contributions

Based on the current literature, the study of functional connectivity using task-based fMRI has not been much explored yet in the context of MS. Given that most of the analyses on brain networks using graph theory rely on functional connectivity of the brain during resting-state, the purpose of this thesis is to explore additional differences in directed FC in MS at the whole-brain level during the performance of two visual tasks, thus providing knowledge about specific brain function and organization. This is particularly interesting because the performance of a specific task could underline brain's characteristics, such as how easy information travels between distant brain regions, which could be damaged by MS and other neurodegenerative pathologies, therefore providing new biomarkers of the disease.

This work was focused on achieving the following:

- Implement FC models, such as Granger Causality (CC), to the acquired fMRI data for the construction of directed functional connectivity matrices and compare them between MS patients (MSC) and healthy controls (CNT). The fMRI data are acquired while participants are performing a passive visual motion task (V1MT), a visual biological motion perception task (BM), and also in resting state (RS), i.e., when there is no explicit task.

- Compute global and local graph theory measures of connectivity and compare them between groups.

- Investigate the relationship between brain connectivity and clinical features such as fatigue, disability scores, and neuropsychological evaluation in MS patients.

It should be noted that many patients' characteristics strongly differ between imaging studies in MS, namely regarding disease course and disease duration. In fact, there are few studies investigating changes in early MS. Additionally, most of the research on this topic considers patients with disease duration longer than the disease of the patients who participated in this thesis. Therefore, one motivation and objective of this work was to investigate altered patterns of connectivity in recently diagnosed patients with MS, thus in early disease stages. Nonetheless, some assumptions were made based on previous studies: increased functional connectivity was expected in MS patients, particularly during the most demanding task, due to compensatory mechanisms (neuroplasticity), and changes were also expected between MSC and CNT in the global and local graph theory measures with a

decreasing trend of values of network efficiency, resultant from loss of long-range connections.

This thesis was integrated in the project “Biomuscle”, supported by Fundação para a Ciência e Tecnologia, with reference PTDC/MEC-NEU/31973/2017.

1.3. Thesis Outline

The following is a brief summary of each of the seven main chapters that constitute this thesis. The present chapter is an introduction chapter where motivation, main purpose of the study, as well as its alignment is presented. Chapter 2 provides all the basic principles of fMRI and functional connectivity after the theoretical explanation of the principles and concepts about MS. Chapter 3 summarizes the current MS studies in the context of task-related fMRI and rs-fMRI as well as the studies that explore functional connectivity using graph theory. Chapter 4 overviews the methodology used to acquire and analyze the data, offering a detailed description of the experimental design and an explanation of how the graph theory connectivity measures were computed. In Chapter 5 the obtained results are shown and discussed. In chapter 6 besides presenting the limitations of the study, possible future work to be developed is also mentioned. Chapter 7 concludes this thesis work and highlights the principal points found in chapter 5.

Finally, a detailed listing of all the bibliographic references used is presented, as well as a section of appendices, with supplementary tables.

2. Concepts

2.1. Multiple Sclerosis

2.1.1. Pathogenesis

MS is an inflammatory disease of the CNS that mainly affects the white matter (WM) of the brain. The causes of the development of MS are not yet well understood, although the main factors responsible for the immune system dysregulation are thought to be genetic, as well as environmental, such as exposure to viral and bacterial agents, leading to activation of autoreactive T-cells [1], [4], [5].

When autoimmune T cells, whose function is to attack antigens coming from the CNS, are activated in the periphery, they transpose the blood-brain barrier and cross the perivascular space (**Figure 1-1**). In fact, Microglial and B cells are the antigen-presenting cells (APCs) (**Figure 1-2)** that contribute to a cell-mediated inflammatory reaction triggering the release of antibodies and suppressive cytokines (**Figure 1-3**), causing demyelination accompanied by axonal loss and/or injury (**Figure 1-4**)[5].

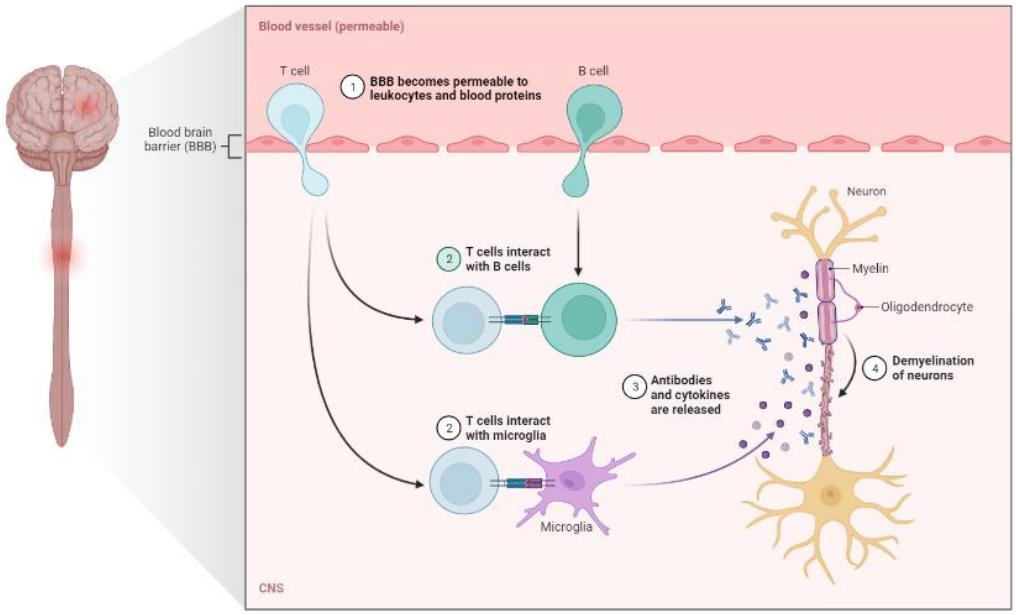

Figure 1- Representative diagram of the main stages of the Pathogenesis of MS (template available at BioRender.com).

The main pathological characteristic of MS is the appearance of lesions called plaques, which are focal areas of demyelination with variable levels of inflammation predominantly in periventricular WM, optic nerves, brainstem, cerebellum, and spinal cord.

When this happens, myelin sheaths are damaged, nerve impulses slowed or even stopped, and, consequently, symptoms arise [6]. The symptoms include several manifestations such as sensorimotor disturbances (most frequently unilateral numbness and tingling), vertigo, fatigue, constipation, vision changes, or bladder and sexual dysfunction [1].

There is no cure for MS. In this context, multiple treatment options are available and must be chosen according to the patient's needs. The treatments currently proposed for MS management are used to decrease the inflammatory activity and flare-ups caused by the disease short-term, allowing an improvement in the patient's quality of life and reducing the disability acquired over time [7].

2.1.2. Diagnosis

The diagnosis of MS is essentially supported by a pattern of symptoms consistent with the disease and confirmed by MRI analysis of the brain and cerebrospinal fluid (CSF) markers [8]. Given the concern with the diagnosis as early as possible, to initiate the best and most reliable treatment, there were many attempts to develop criteria which could facilitate this task.

The McDonald Criteria is the international standard for diagnosing MS, having as requirements to form a diagnosis: the occurrence of two or more lesions in the WM of CNS (Dissemination in Space criterion – DIS), occurrence of two or more relapses during MS (Dissemination in Time criterion - DIT) which must be confirmed after three months of the previous relapse by clinical signs on MRI images or analysis of CSF to prove chronic CNS inflammation [1], [9].

To be updated with the research on how MS arises and progresses in patients, the McDonald Criteria have been reviewed several times. The newest revision was made in 2017 (Thompson et al.,[9]). The most considerable adjustment was that oligoclonal bands can now be taken as a substitute for atypical CSF findings, establishing the diagnosis of MS after the first clinical attack or after a single brain MRI [8]. These criteria are summarized in table 1.

Table 1- 2017 McDonald Criteria for MS diagnosis [9].

Number of attacks	Number of lesions with objective clinical evidence	Additional data needed for a diagnosis
≥ 2	≥ 2	None (but MRI is recommended)
≥ 2	1	Dissemination in space (DIS) via: • An additional clinical attack implicating a different CNS site OR • MRI
1	≥ 2	Dissemination in time (DIT) via: • An additional clinical attack OR • MRI OR • Demonstration of CSF-specific oligoclonal bands
1	1	Dissemination in space (DIS) via: • An additional clinical attack implicating a different CNS site OR • MRI AND Dissemination in time (DIT) via: • An additional clinical attack implicating a different CNS site OR • MRI OR • CSF-specific oligoclonal bands

2.1.3. Subtypes of MS and Clinical Features

A red flag of the disease is marked by a "clinically isolated syndrome" (CIS), a monophasic clinical episode that lasts longer than twenty-four hours comparable to a typically multiple sclerosis relapse. Individuals who have experienced CIS commonly present optic neuritis, spinal cord, brainstem and/or hemispheric lesions [9].

CIS is not considered a phenotype of MS since it does not accomplish dissemination in time base on the criteria in section 2.1.2 but can eventually develop into relapsing-remitting MS, evidencing that the pathological changes form a continuous spectrum since one subtype of MS can evolve into another [7]. Thus, MS is split into four clinical subtypes: Relapsing-Remitting Multiple Sclerosis (RRMS), Secondary Progressive Multiple Sclerosis (SPMS), Primary Progressive Multiple Sclerosis (PPMS) and Progressive Relapsing Multiple Sclerosis (PRMS) [1], [9].

- *Relapsing-Remitting MS*:

  It is characterized by relapses (flare-ups or attacks) followed by periods with no symptoms and/or clinical improvement, also called remission periods. The time between attacks is unpredictable and can go from months to years.

  Due to excessive persistent inflammation at each relapse, the degree of disability increases, which can only be partially recovered. This form of MS is present in about 80% of patients, being the most common disease course.
- *Secondary Progressive MS:*

  Developed in patients with relapsing-remitting form, within 10 to 15 years of diagnosis. With secondary progressive MS, symptoms continuously get worse with or without remission periods.
- *Primary Progressive MS*:

  Affects 15% of MS patients, with no relapses and remissions, it is characterized by a gradual disability accumulation that starts on its onset. Its higher resistance against treatment also characterizes it.
- *Progressive Relapsing MS:*

  Is a rare form of MS, affecting nearly 5% of MS patients with a noticeable progressive line of sporadic relapses and worsening symptoms, but without remission periods.

In summary, the clinical course of the disease usually follows a pattern over time characterized by acute relapses with worsening of the symptoms, progressive decline of neurological function, or a mixture of both [7].

2.1.4. Expanded Disability Status Scale

Describing disease progression in the context of MS through specific instruments is fundamental, and it allows for a more viable understanding of how much patients are clinically impaired [10]. One of the most common symptoms of MS is physical disability. To assess it, the EDSS or Kurtzke Scale gives international guidance on how MS patients' walking function changes through time. A grade ranging from 0 (normal) to 10 (death) is given by the results determined with the neurological examination, that take into consideration: body coordination and balance, bowel and bladder, visual, physical, and cognitive issues. The greater the EDSS score, the worse is the ambulatory disability [11].

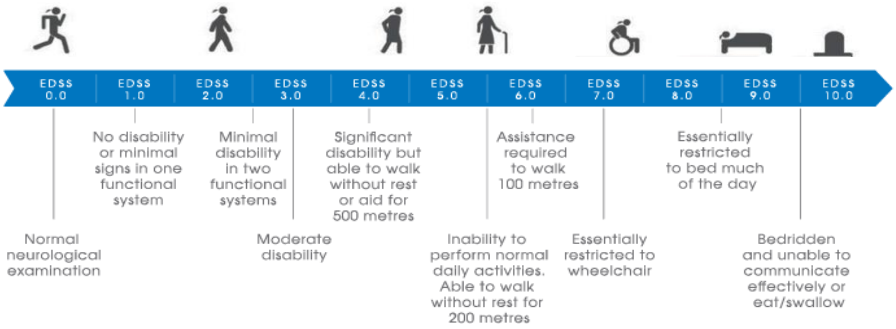

Figure 2- Representative scheme of the Expanded Disability Scale (EDSS). This is a numerical scale with 0.5 unit increments levels between 0 and 10. Adapted from https://hsctindia.com/edss.

Values between 1.0 - 4.5 correspond to easiness in moving around, whilst values between 5.0 - 9.5 correspond to patients with very low degree of ambulatory ability [10].

That said, EDSS is the most recognized MS scale since it has been in use for a long time. One of its main advantages, is that it allows modern clinical trials to be compared against older ones. However, it has some limitations since it does not consider emotional problems [10].

2.2. Magnetic Resonance Imaging (MRI)

2.2.1. Physics principles behind MRI

MRI is based on nuclear magnetic resonance, i.e., the interaction of certain atomic nuclei with external magnetic fields. In fact, the hydrogen (H) nuclei are the most used for MRI, because of their high abundance in the human body and due the fact that they carry nuclear spin. Each spin precesses at an exact frequency (f_0), proportional to the strength of the external magnetic field applied (B_0) and the gyromagnetic ratio (γ), a specific constant for each particle [12], [13]. This relationship can be explained by the Larmor's equation (equation 1):

$$f_0 = \gamma B_0 \text{ (Equation 1)}$$

When the subject is brought into a strong magnetic field, most of the spinning protons become aligned with the direction of B_0. Then, an electromagnetic wave, more commonly known as radiofrequency pulse (RF), is sent to an area of the body. If this RF pulse has a frequency equal to the precessing frequency of the proton, the protons will be

perturbed, and transit to a higher energy level away from its original state and start to align with a certain angle in relation to the B_0. Furthermore, the spins that were precessing with random phase, now also precess in aligned phase after the RF pulse. Thus, their net magnetization vector is no longer parallel to the magnetic field, being now divided into two components: a net longitudinal magnetization in the direction of the magnetic field and a transverse magnetization component, typically perpendicular to the field.

After the RF pulse stops, the protons attempt to restore the original orientations and de-phase as well, thus emitting RF energy. As a result, the transverse magnetization disappears in a process called transverse relaxation, due to the spin-spin interactions (characterized by the transverse relaxation constant T2) and inhomogeneities in B_0 (actually causing T2 to be the so-called T2*), while the longitudinal magnetization grows to its original length (characterized by longitudinal relaxation constant T1). Anytime during this relaxation process, as the magnetic field varies, an electric current will be detected in the receiver coil and then translated into the MRI signal [14].

The physical principles of fMRI are identical to MRI, the main difference is in the acquisition parameters and pulse sequences selected for the appropriate T2* contrast. The most significant parameters are the Repetition Time (TR), i.e., the interval between the application of one RF pulse (or excitation) and the next pulse, and the Time of Echo (TE), i.e., the peak of the echo (signal) that will be read from the coil [12], [13], [15]. With an appropriate choice of parameters, it is possible to create images sensitive to T1, T2, or T2* effects. Notably, the T2* signal is the basis of functional MRI, because it is susceptible to neurovascular changes.

2.2.2. Functional Magnetic Resonance imaging (fMRI)

Functional MRI has been a profoundly successful technique, developing and adding to our insight about the human brain function.

While MRI was developed in the late 1970s and early 80s, it would be another decade before it was realized that MRI could be used to detect and map, non-invasively, human brain activation. In 1992, a technique sensitive to the changes of blood oxygenation emerged, which was the starting point of fMRI [14], [16].

While structural MRI measures the anatomical properties of the brain, fMRI is a neuroimaging technique that is used to measure the blood-oxygen-level-dependent (BOLD) signal, which is related to brain activity.

BOLD contrast mechanism

The beauty of functional MRI is that we can have both exogenous and endogenous contrast agents influencing the local magnetic homogeneity. In most studies, the BOLD contrast mechanism is the preference, where the hemoglobin (Hb) itself is a contrast agent that depends on its oxygenation levels.

Since hemoglobin is the protein which transports oxygen (O_2) through the circulatory system, it has on its structure subunits (iron ions) with an affinity for O_2. When Hb binds to oxygen, it is designated oxyhemoglobin (HbO_2) and when oxygen is released, it is designated deoxyhemoglobin (dHb). dHb due to four unpaired electrons becomes strongly paramagnetic. Thus, distortions on the local signal arise, because of an additional and precise field gradient within and around the blood vessels. Unlike dHb, HbO_2 has no unpaired electrons, so it is weakly diamagnetic (low distortion on the local signal) [13], [14].

BOLD imaging takes advantage of these imbalances in the magnetic properties between the two forms of Hb to indirectly measure brain activity [13], [14].

BOLD Phenomenon

It is precisely in this versatility of the MRI technique that lies the possibility of producing fMRI images, which reflect the level of activity of nerve cells in each region of the brain.

The fundamental underlying physiological principle is the relationship between the neural activity of these cells and the dynamics of the blood in their neighborhood – *neurovascular coupling*. Therefore, when neuronal activity increases after neuronal stimulation, there is a need for glucose and oxygen in the brain regions responsible for that activation. To deliver those substrates an increase in cerebral blood volume (CBV) and cerebral blood flow (CBF) occurs. Consequently, the amount of oxygen removed from the blood increases, meaning that there will be also an increase in the cerebral metabolic rate of oxygen ($CMRO_2$) [17], [18].

In agreement with the description above, the MRI signal should drop since the paramagnetic dHb disturbs the homogeneity of the magnetic field. However, because the increase in CBF has a bigger contribution, it overcompensates the decrease in O_2. Thus, even if there is an increase of $CMRO_2$, the amount of oxygen provided exceeds the oxygen consumption [13], [14], [17].

Thus, the outcome of neural excitation shows local increases in the signal strength, because of the decrease of deoxyhemoglobin concentration, originating the BOLD contrast mechanism [19].

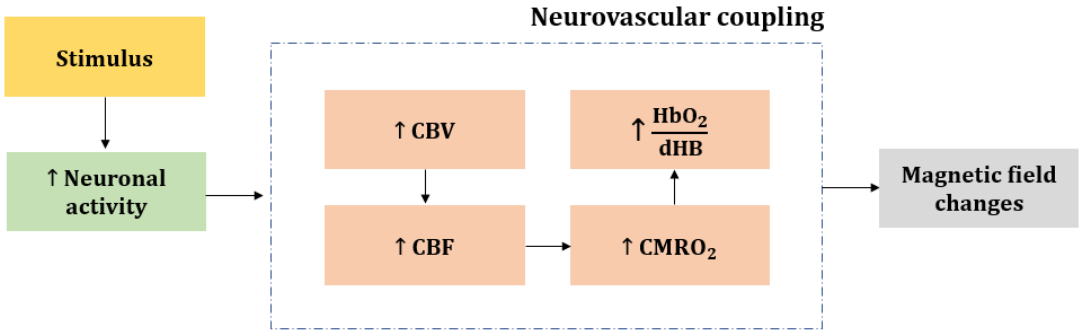

Figure 3- Flowchart of the processes triggered after the onset of a stimulus (adapted from [19]).

BOLD hemodynamic response

The vascular response to a stimulus is called the hemodynamic response function, or HRF. The HRF has a known shape, with an initial deviation from the baseline described as the initial dip, as a result of the quick response to increased neuronal activity. After 2 seconds, an increase in the signal can be seen due to a decrease in the concentration of dHb, as the flow of oxygenated blood increases as a consequence of the quantity of O_2 received being much higher than needed. This results on a brusque positive response, reaching a maximum peak 6 seconds after stimulus onset. Finally, after the stimulation/activation ends, subsequently causing a large accumulation of dHB, since CBF and $CMRO_2$ returned to their standard values, there is a decrease in BOLD signal intensity and an undershoot, after which the signal returns to baseline. However, the distensibility of the vessels (CBV) requires more time to reach the baseline [18], [19].

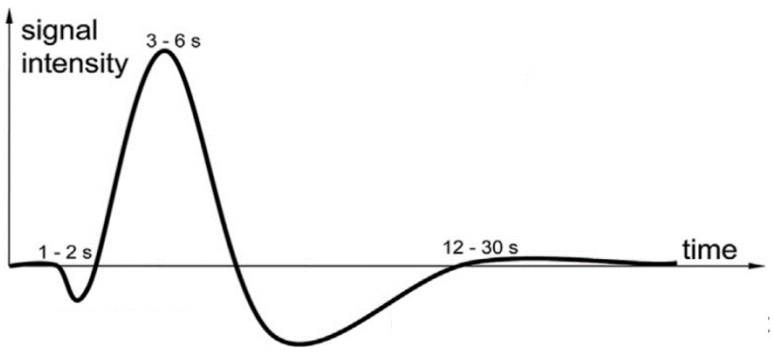

Figure 4- Standard BOLD hemodynamic response function (adapted from [18]).

The shape of the HRF can be helpful to understand the behavior of the BOLD signal in response to any random neural activity condition. For example, an "active" condition, when there is specific task performance, or a "passive" condition, during which there is no explicit task/stimulus (rest), have distinct BOLD signatures [15].

Resting-state functional magnetic resonance imaging (rs-fMRI) is mostly used to interpret the low frequency fluctuations of the BOLD signal. This allows us to explore the intrinsic brain organization and spontaneous connections between brain regions. However, this approach is limited to track the flow of information, since phasic alterations in brain activity are always occurring, and thus hard to analyze [18], [20].

We believe that task-based experiments are the best way for assessing brain function and connectivity, and its relationship with cognitive functions, which can highlight the differences between the group of patients with MS (MSC) and the group of healthy control participants (CNT). This could be to the fact that, since a specific task is being performed, there will be more demand on the connection between regions, and therefore, only then differences will be revealed established [4].

2.2.3. fMRI analysis

Functional runs (task or resting-state), consists of a timeseries of 3D functional volume data i.e., a four-dimensional volume (4D, space and time dimensions). Each functional volume is made up of 2D slices acquired at various points throughout the TR and when stacking all slices together they form a 3D image of the brain, that is, a volume made up of voxels.

Data pre-processing

After data acquisition and before studying connectivity matrices, it is important to identify and correct fluctuations of no interest in the data. Image artifacts may result from physiological noise (heartbeats, respiration, drowsiness, patient motion) or thermal noise (MRI system electronics, field inhomogeneities) [21], [22]. Thus, to remove noise inducing BOLD signal changes, functional data must be pre-processed. A summary of the common pre-processing steps is presented in Table 2. The specific steps applied to our data will be presented discussed in the next chapter.

Table 2- Definition of the most common pre-processing steps.

Slice Timing Correction (STC)	Each fMRI volume of the brain is acquired as a set of 2D slices at different times, which means that one brain volume has an accumulation of offset delays between the first slice and all remaining slices. To achieve an accurate statistical analysis, these slice-dependent delays must be corrected. In STC, this is done by shifting the time series of all slices to a reference time-point [22].
Realignment and motion correction	It is quite common during image acquisition that the patient moves unintentionally. Even the smallest movements will create motion artifacts and variations in the signal, decreasing the quality of the data. By characterizing motion in relation to a reference volume, which is more suitable for the other volumes to line up, with 6 parameters (3 translations and 3 rotations) we can correct motion induced signal changes [13].
Geometric distortions correction	fMRI data is usually collected using echo planar imaging (EPI) sequences, and thus geometric distortions are inevitably present. This step intends to correct this problem that cause the EPI functional data to not being spatially aligned with the structural MRI scans [23].
Bias Field Correction	Each tissue has a characteristic intensity, which will change with variations in the magnetic field. With the Bias Field Correction method, the images are standardized and corrected, making the intensity of each tissue more homogeneous and uniform.
Coregistration	Align the functional data to the high spatial resolution of structural data, so that functional activations can be spatially localized [13], [22].
Segmentation	Its main aim is to divide the structural image into different segments (GM, WM, CSF, bone,soft tissue, and air). With this, it gets easier to visualize each region, which is very important for extracting information or estimate noise contributions to the signal only within tissues of interest (masks) [13].
Physiological noise correction	The use of this correction is made because sometimes respiration and cardiac pulsations generate time-varying signals that can be confounded with neural activity. Therefore, the effect of the physiological noise will be minimized [21].
Smoothing	Smoothing can improve signal-to-noise ratio (SNR) because its objective is to blur the measured signal in near voxels, so noise will get averaged out, and the signal of interest not significantly affected. It will also optimize inter-subject spatial correspondence [13].
Temporal filtering	Low frequency fluctuations do not matter in the signal, particularly in task paradigms, and therefore, high-pass filtering is applied to detect and remove this noise [27].

The last step in the fMRI analysis is the statistical analysis of the pre-processed signal with the aim of testing/verifying a hypothesis, e.g., whether two conditions cause a different brain response or not. To perform this analysis, the General Linear Model can be used [13].

2.3. Brain Connectivity

Brain connectivity refers to how the brain networks are organized and how is the process of information exchange. It can be used to investigate how the brain adapts in different conditions and how its changes relate with cognitive states [29]. It has evolved as an approach to infer about functional integration between functionally segregated regions. Functional segregation refers to the anatomical division of functionally specialized areas, while functional integration refers to how quickly these modules link together and information flows between them [25].

There are many different ways to study and measure brain connectivity, each depending on the method used for the analysis. Therefore, analysis of brain connectivity can be divided into three types: Anatomical (or structural) connectivity, Functional Connectivity (FC), without causal assumptions, and Effective Connectivity, which model's causal influences between regions [25], [26].

As mentioned before, in section 1.2, the study of this dissertation is based on FC during two visual tasks and also in resting state. Thus, any reference to brain connectivity in the future will be correlated to this type of connectivity network.

The foundation of FC lies on the statistical dependencies or temporal correlations between different brain regions without any undertaking as to how these connections are caused. Approaches to investigate functional connectivity in fMRI are divided according to whether they are used to estimate undirected or directed FC. For example, measures like independent component analysis (ICA) or Pearson Correlation assume that all brain regions are spatially and/or temporally independent. Contrarily, Granger Causality (GC) relies on temporal precedence, i.e., how past values of one brain region predict the current value of a distinct brain region [27], [28].

In the next section, the focus will be the analysis through GC, since it was the connectivity model implemented in this thesis.

2.3.1 Granger Causality (GC)

Wiener–Granger Causality, or G-causality, was proposed in 1969. Firstly, this method was widely used in the field of econometrics, but now, due to its simplicity, it can be applied in neuroscience, specifically as a measure of directed functional connectivity [29].

While employing GC analysis (GCA) to fMRI, data must respect a set of assumptions to overcome some problems reported. The TR, which is often in the range of seconds, is one of the most challenging fMRI properties when using GCA. This is problematic since neural responses take milliseconds or less, and so this difference in timescales can lead to inaccurate data and analysis. Other restrictions related to conditions that GCA must meet are: the data should be stationary, and the variables stochastic and linear. Linearity governs the way in which the variables interact, which is not what happens in the human brain. However, linear VAR modeling and GC are sensitive to the linear components of the data because of the similarity with transfer entropy (TE) [29].

Despite some limitations, with this statistical method it is possible to establish a hypothesis about which regions of the brain are functionally connected and the direction of their information exchange based on the notion that the "cause" precedes the effect.

In its simplest (unconditional, time-domain) form, G-causality assumes that if the prediction of a time-series $X(t)$ is improved by the knowledge of the past of a second time-series Y(t), better than using only the information already in the past of $X(t)$, then Y "G-causes" X. This idea can be traced in terms of linear vector autoregressive (VAR) models, a mathematical approach model in which the value of a variable at a particular time is firstly fit as a (linear) weighted sum of its own past (equation 2) and then the past of another variable (equation 3) [4], [29].

$$X_t = \sum_{i=1}^{p} A_i \,.\, X(t-i) + \varepsilon_1(t) \qquad \text{(Equation 2)}$$

$$X_t = \sum_{i=1}^{p} A_i \,.\, X(t-i) \; + \; \sum_{j=1}^{p} B_j \,.\, Y(t-j) + \varepsilon_2(t) \qquad \text{(Equation 3)}$$

Here, p is the model order, i.e., the number of past observations (time-steps), A_i and B_j are regressors of the model, X and Y are the average of BOLD time series of each region, and ε_1 and ε_2 the residual errors. When ε_2 is smaller than ε_1 then the prediction of time

series X values are improved by using the values of time series Y. The directed Granger Causality between Y and X can be defined as:

$$F_{y\to x} = log\frac{var(\varepsilon_1(t))}{var(\varepsilon_2(t))} \quad \text{(Equation 4)}$$

Whereby, $F_{y\to x}$ represents the temporal dependence between the two timeseries. If there are three or more time series, a multivariate analysis can be performed (Conditional, time domain) using the above approach.

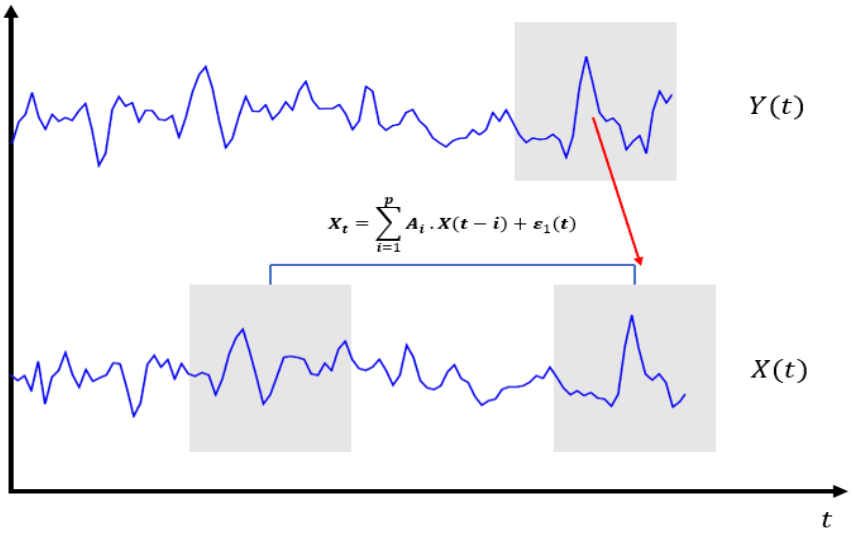

Figure 5- Diagram of the framework sustaining Granger causality analysis [4]. The basic principle of GC is based on temporal precedence. The past of Y(t) is checked, as is the past of X(t), and if the past of Y(t) can help predict the future of X(t) better than only X's own past then Y "G-causes" X (adapted from [4], [25]).

Supposing the existence of three time series X_t, Y_t and Z_t, the Granger Causality between X and Y conditioned by Z can be understood as "the degree to which the past of Y helps anticipate X, over and beyond the degree to which X is already predicted by its own past and the past of Z" as stated by Barnet et al., [29]. As a result, spurious Y→X causality may be reported if Y → X has no direct causal relationship, but X and Y are dependent on Z. Therefore, if common dependencies are present in the data, it is possible to "condition out" these false/spurious causalities.

2.3.2. Graph Theory – The Fundamentals

Complex systems are better understood when represented mathematically as graphs. Therefore, as the human brain establishes various interactions between regions producing complex behaviors [26], [30], [31], graph theory approaches can be adopted for this analysis. Hence, it provides a powerful way to quantitatively describe the topological organization of the brain networks.

In this regard, a graph can be interpreted as a set of nodes (vertices) denoting brain regions linked by (edges) representing their interactions [26], [31]. Based on the nature of the edges, their weight and directionality, four types of graphs can be classified (figure 6).

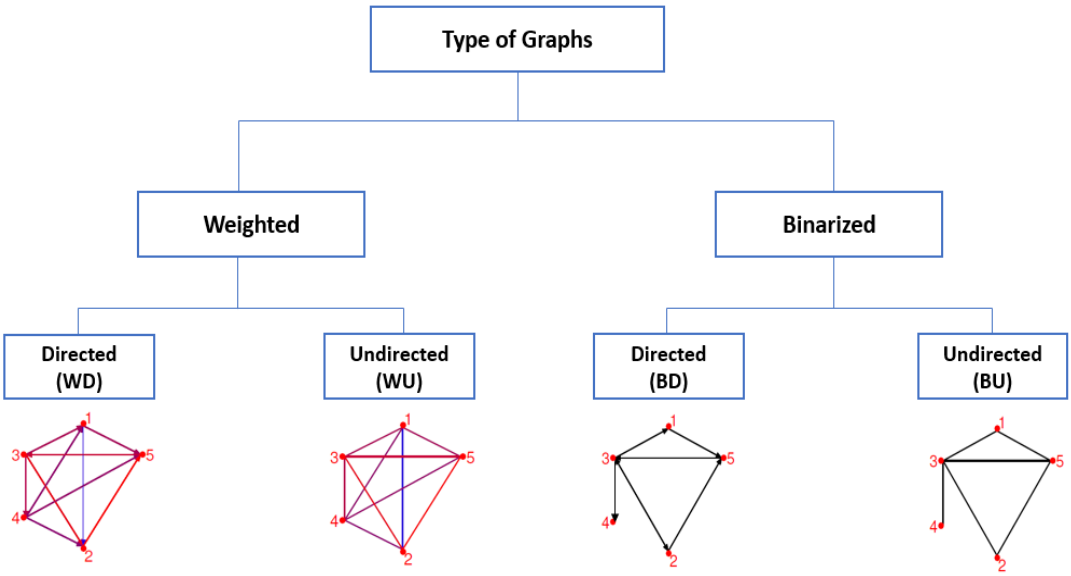

Figure 6- Different types of Graphs and respective representation. (WD) The edges are associated with a real number indicating the strength of the connection and are directed (node i can be connected to node j without node j being connected with node i; (WU) The edges are associated with a number that defines the strength of the connection and are undirected (therefore, if node i is connected to node j, node j is also connected to node i); (BD) The edges can be either 0 (absence of connection) or 1 (existence of connection) and are directed; (BU) The edges can be either 0 (absence of connection) or 1 (existence of connection) and are undirected (adapted from [34]]).

In binary graphs, the edges only denote whether a connection exists. In weighted graphs, a truer representation of a connection is made, representing the strength of correlation or "causality" of the connections. Thus, weighted graphs help to find quantitative insights into functional connectivity like the amount of information flowing through regions, while directed graphs provide insights about the direction of the interactions and can help e.g., to evidence changes in brain lateralization. Combining the two is the perfect match.

An alternative way to represent a graph is using a connectivity matrix, where each row and column represents the nodes and the elements of the matrix represent the edges between nodes; for example, the element (i,j) represents the edge that goes from node i to node j . In undirected graphs the connectivity matrix is symmetric [31].

The general steps to perform a graph theory analysis involve [4], [28]:

1. The selection of the nodes (in this case, brain regions) through anatomical parcellation schemes or atlases;
2. Averaging fMRI time series of all voxels within each node;
3. The choice of the connectivity method to produce an NxN connectivity matrix or a graph that is based on the connections between the N nodes;
4. The calculation of the connectivity metrics of interest and comparison of these metrics to the equivalent parameters of a different group [26].

Figure 7 illustrates a brain network construction and graph theory analysis using fMRI. It is organized according to the steps described previously.

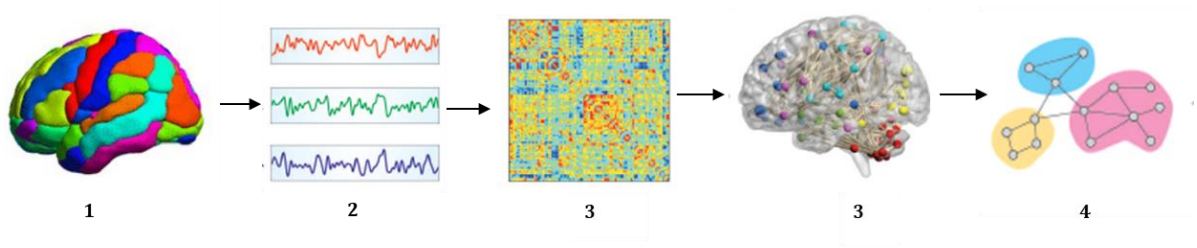

Figure 7- Flowchart exemplifying the steps to perform a graph theory analysis using fMRI. (adapted from [26]).

2.3.3 Graph Theory – Measures

Due to the complexity of the neuronal networks and its uniqueness between individuals or groups, it is essential to calculate connectivity metrics, as they will quantify and reflect behaviors of the network (e.g., integration, segregation, centrality, and resilience) [25], [28], [31].

Naturally, questions emerge during the network analysis, and some can be explained by the concept of integration and segregation, explained in the previous section. However, others remain unanswered such as: Is one node more important than other in the

network and what is the level of impairment that might be expected following an insult to a specific network?

The first question is directly intertwined with the concept of centrality: centrality analysis aims to identify important network elements (hubs), nodes with strong roles in brain function. The other question can only be answered through resilience, the capability of a system to maintain its fundamental functionality when suffering an insult [31].

Graph measures can be divided into two types: global metrics, which refer to global properties of a graph (they provide a single value per graph), and local/nodal metrics, which refer to properties of the nodes of a graph (they provide a vector of numbers, one for each node of the graph).

Table 3- Overview of major graph theory connectivity measures.

	Connectivity measures	**Properties**	**Definition**
Segregation	Clustering Coefficient	nodal	Connection probability that the nearest neighbors of a node are also neighbours of each other. If the mean clustering coefficient for the network is high, this indicates prevalence of clustered networks [31].
	Modularity	global	The degree to which the network can be subdivided into clearly separated and nonoverlapping groups (modules) [26].
Integration	Characteristic Path Length	global	It is one of the most robust measures of the network, defined as the average of all shortest paths between all pairs of nodes in the network [31], [32].
	Global Efficiency	global	It is inversely related to the characteristic path length. Measures the ability of parallel information to travel across the network [30].
	Local Efficiency	nodal	Efficiency of a node calculated on the subnetwork created by the node's neighbourhood. Measures the ability of information to be exchanged if the node is removed from the network [30].
	Small-wordmess index	global	Measure of the balance between the degree of network segregation versus network integration [26], [31].
Centrality	Degree	nodal	The degree of a node is the number of links connected to that node. The higher the degree of a node, the more that node influences the others, which could mean that they have a bigger importance in the network [31]. • In degree: number of links that converge for the node. • Out degree: number of links that diverge from the node.
	Strength	nodal	Very similar to the "degree" measure. It is the sum of the link weights connected to a node. For directed networks [31]: •In-strength: sum of converge link weights • Out-strength: sum of divergent link weights.
	Eccentricity	nodal	Maximal shortest path between a certain node and any other node of the network. Reflects the easiness of a node to be functionally reached by all other nodes. The minimum eccentricity is called the graph radius. The maximum eccentricity is the graph diameter, i.e., the largest distance between any two nodes of the network [33].
	Betweennes Centrality	nodal	Number of times a node is in the shortest path of other two nodes. Quantifies which node has more control in the information flow of the network [25], [34].
	Subgraph Centrality	nodal	Sum of the closed walks in the network starting and ending at a particular node. A smaller value means that the length of the closed walk is shorter giving higher importance to the influence of the node on centrality [31].
	K-coreness Centrality	nodal	K-core analysis helps us to find the sub-graphs that are densely connected and then identify the best paths for fast and good transfer of information [35].

	Participation Coefficient	nodal	Quantifies the relation between a node's connections within its own community and to other nodes from other communities. If a node has low participation coefficient it means that most of its connections are restricted to its community. Moreover, if it has high participation coefficient, the majority of the connections are with nodes from different communities [36].
	Eigenvector centrality	nodal	Eigenvector centrality determines the level of influence of a node over the network based on a given score: the higher the score, the higher the number of connections that the node makes, and the greater the level of influence of the node within the network [37].
	Pagerank Centrality	nodal	The PageRank centrality is a variant of the Eigenvector centrality score, but because it uses incoming links ("in degree") it is used in directed networks [37].
	Within module degree	nodal	Quantifies the relation between a node and the nodes from the same community. It is the opposite of the participation coefficient [38]. Therefore, if a node has a high within module degree, it means that most of its connections are within their community [36].
	Local Flow Coefficient	nodal	Capacity of a specific node to conduct information. Defined as the number of paths of length two divided by the number of possible paths of length two that pass through that node [4].
	Global Flow Coefficient	global	Average local flow coefficients over the network [4].
	Total Flow Coefficient	nodal	Measures the number of paths that flows across each node [4].
Resilience	Assortativity	global	Calculates whether most of the nodes of the network are connected to nodes with a similar degree [34]. A positive assortativity indicates a strong and resilient core where high degree nodes are connected. On the other hand, negative assortativity indicates a vulnerable core and the existence of widely distributed hubs [32].

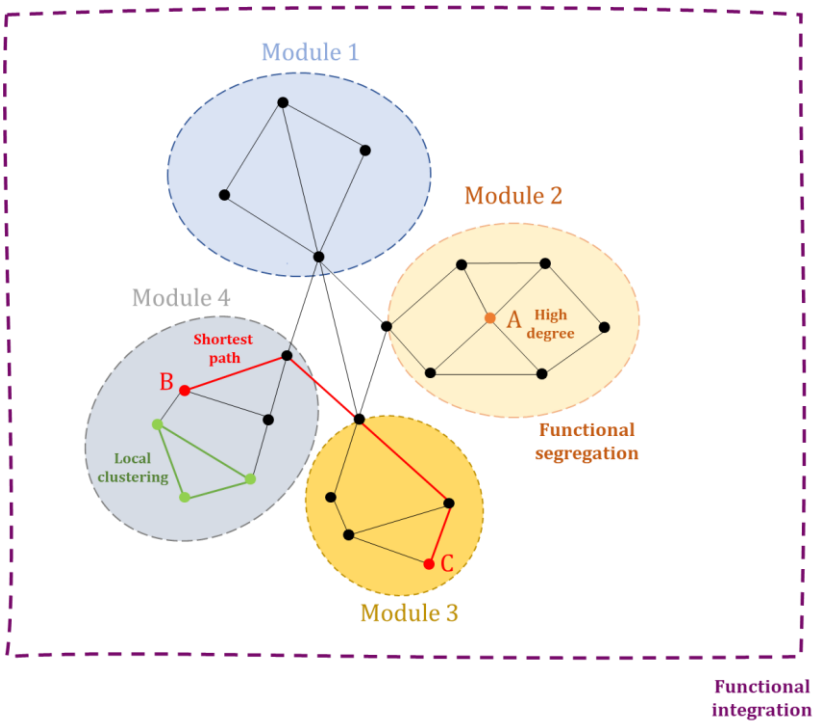

Figure 8- Illustration of what functional integration and segregation represent, as well as some measures from graph theory. There are four modules in the graph, in module 2, node A has the highest number of edges connected to it, so it has a higher degree. In red is represented the minimum number of edges to go from node B to node C (characteristic path length) and in green is represented local clustering, which is the propensity of nodes to form neighbourhood triangles, revealing information about the network's organization (adapted from [38]).

3. State of the art

3.1. The role of structural MRI in MS

Different conventional MRI sequences, such as T2-weighted imaging, and T1-weighted imaging, will provide different kinds of information about MS structural lesions [39].

The most characteristic MS lesions occur in the WM, mainly in the periventricular and juxtacortical regions, corpus callosum, and temporal stems. Abnormalities in the grey matter can also be displayed in MS patients, consistent with axonal damage frequently in progressive disease stages. As a matter of fact, GM lesions damage (cortical lesions, cortical atrophy, iron accumulation, and cortical thickness changes) became more associated with the symptoms often present in MS patients than WM lesions. However, they remain undetected by conventional MRI [40], [41].

The sensitivity of T2-weighted images allows the detection of WM lesions which appear as focal areas of hyperintensity. Nonetheless, the scans do not depict whether a WM lesion is due to inflammation, demyelination, or axonal loss, i.e., there is a lack of specificity. Besides T2-visible lesions, T1-weighted images (without contrast) reveal highly hypointense lesions, often known as “black holes”, which are linked with more severe tissue injury and are frequently chronic lesions. Remarkably, when a contrast agent like gadolinium is used on a T1-weighted image, active and inactive lesions can be distinguished because this agent only enters the cells when the brain-blood barrier is compromised, i.e., when permeability increases. This means that enhanced lesions will represent areas of ongoing inflammation [39]–[41].

Patients with MS may also have spinal cord lesions, primarily atrophy, which can be found in all MS phenotypes. Although this atrophy can serve as a biomarker, its relevance is restricted, due to the presence of edema that would hide any destructive changes that have occurred [39].

In general, despite its diagnostic sensitivity, conventional MRI lacks specificity. Therefore, non-conventional MRI approaches have emerged, such as fMRI, a very powerful imaging technique that allows to investigate changes in functional connectivity and potentially find biomarkers for forecasting the disease progression [42].

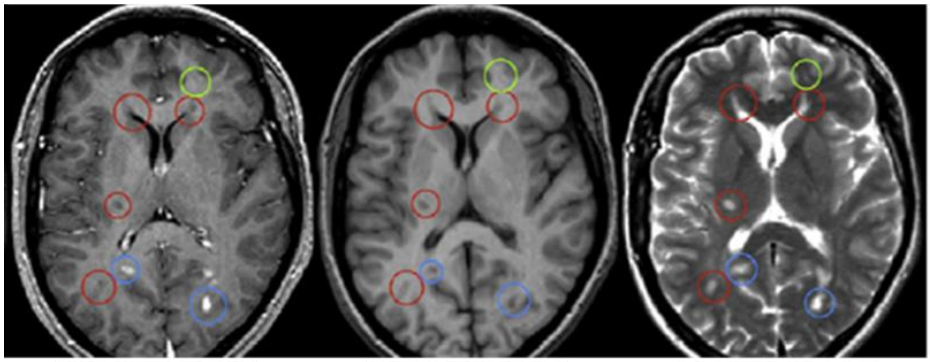

A B C

Figure 9- A) T1 Gd-enhanced, B) T1-weighted, C) T2- weighted images of MS lesions. Yellow: T2 lesions, Blue: Ring-enhancing lesion, Red: black holes. (adapted from [40]).

3.2. Functional connectivity in MS

Functional connectivity has been a topic of interest for almost three decades now. Therefore, it is important to take into consideration some of the work that has already been made in this field before diving into the work developed in this thesis. [43]

Focusing on studies summarized by Fleischer [27] and Rocca et al.,[44] it becomes clear that most of them used resting state fMRI analyses. Their main results focus on the fact that RRMS patients, compared with CNT, presented FC increases suggesting that a potential brain compensatory mechanism was occurring. This phenomenon maybe called neuroplasticity and it is related to the recruitment of more connections, or more recruitment of the same connections, to maintain the brain's function despite the presence of ongoing structural damage. In fact, an increased functional activation both in the basal ganglia and thalamus, parts of the default mode network (DMN) and the sensorimotor network (SMN), was reported in RRMS patients [44].

Furthermore, Droby et al., [45] observed that in patients with RRMS, the rs-FC values did not greatly differ. Meijer et al., [46] also noticed that at early RRMS there were no rs-FC changes. This combination of findings led to the hypothesis that there is preservation of brain function in the early stages of MS.

The majority of task-based studies revealed that people with RRMS tend to activate not only regions involved in the task, but also additional regions. This formation of new connections and information pathways could be explained by neuroplasticity. For example, Audoin et al., [47] and Mainero et al., [48] found in patients with RRMS altered patterns of activation in the areas involved in the PASAT (Paces Auditory Serial Addition Test) task, but also activation in other areas mainly in cortical regions associated to executive processing. Staffen et al., [49] observed the same hyperactivation of brain areas that participated in the PVSAT (Paced Visual Serial Addition Test).

Interestingly, there is evidence that RRMS patients tend to compensate for the occurrence of tissue damage by increasing FC in the non-dominant hemisphere [50].

Preziosa et al., [51] infers that the two brain hemispheres have a different susceptibility to damage accumulation. Agcaoglu et al., [52], Tahedl et al., [53] and Veréb et al., [54] observed FC decreases within the left cerebral, which corroborates the idea of Charil et al., [55] which argues that lesions preferentially appear in the left hemisphere.

In Filippi et al., [56] and Pool et al., [57] hand dominance was also linked to interhemispheric lesion dispersion, evidenced by greater evidence of lesions in the dominant hemisphere. As the dominant hemisphere is the left for right-handed people, this hemisphere will be more vulnerable to injury and accumulation of lesions for this population.

This field of functional connectivity in MS has become more and more complex, being very difficult to interpret. That said, brain reorganization and function should be analyzed using approaches that provide a more thorough understanding of the brain, such as graph theory measures.

3.3. Graph theory measures in MS

Graph theoretical network measurements are the perfect way to contextualize and understand what truly happens to the overall status of the whole brain network in MS, beyond poorly understood local increases or decreases in connectivity. Currently there is vast research on brain functional connectivity, but only a few studies have used graph theory to analyse fMRI data in patients with MS, again mostly focused on resting state connectivity.

Five studies (Shu et al., [58], Rocca et al., [32], Welton et al., [59], Tommasin et al., [60], Abidin et al., [61]) investigated functional connectivity using graph theory in Multiple Sclerosis during resting state.

Shu et al., [58] designed an experiment to explore alterations of both the structural and functional connectivity in CIS and MS patients. Focusing on the functional connectivity, first Pearson correlation and subsequently an absolute threshold were applied to construct the brain network of 3 groups of participants: 35 CNT, 41 CIS and 32 RRMS. After that, several global measures (clustering coefficient, characteristic path length, global efficiency, mean local efficiency, small-worldness index, strength) and one local measure (nodal efficiency) were calculated. They found no significant changes in global measures between CIS and the other two groups, lower local efficiency and clustering coefficient in MS patients compared to healthy controls, and increased efficiency in the left cuneus of the CIS patients while MS showed decreases in efficiency in the same ROI. Another aspect is that functional network changes seemed to be correlated with physical and cognitive impairment in MS patients but not CIS patients.

In summary, the presence of changes in MS and not in CIS may indicate that the brain in the early stages of the disease deals with the loss of connections through functional plasticity.

Rocca and colleagues (Rocca et al., [32]) evaluated, using graph theory, distinct modifications of brain network organization among MS phenotypes, and if its disruption promotes clinical manifestations. The authors found a decrease in global integration supported by higher values of characteristic path length and assortativity, and lower values of global efficiency in MS patients. On the other hand, they found preservation of segregation supported by the fact that there were no significant changes in clustering coefficient. Therefore, changes in the global network were identified between MSC patients and healthy controls but not between the different MS phenotypes. At a nodal level, they also found changes in hubs distribution marked by loss, a different lateralization or formation of hubs in MS patients, that were not seen in the healthy control group.

Notably, global and nodal changes of the network organization are associated with disability (physical and cognitive impairment).

Welton et al., [59] aimed to understand the significance of brain network measures in MS patients with cognitive impairment. For this, they used Pearson correlation analysis as a basis for constructing the connectivity matrices. This is the study with the largest network (164 ROIs) in which global measures such as clustering coefficient, modularity,

characteristic path length, global efficiency and small-worldness index were analysed. The results point to a more segregated network, since higher values of clustering coefficient and modularity were observed in MS patients, but a less efficient network, with higher values of characteristic path length and lower values of global efficiency in MS patients.

In Tommasin et al.,[60] the focus of the study was knowing how FC reorganization is linked to tissue damage and disability. FC matrices were calculated by using independent component analysis (ICA) and only global efficiency and degree centrality were extracted to study the brain integration process. The results suggest that the increased segregation may be related to cognitive functions and decrease integration with reduced global efficiency and degree centrality of the basal ganglia, attentive and control networks in the MS patients, which may result from structural disconnections and saturation of compensatory mechanisms.

Unlike most of the studies that have been using conventional linear correlation methods, Abidin et al., [61] proposed that large-scale Granger Causality with graph theory may be a better approach to capture changes in brain network organization. They focused on differences at a global and regional level in CIS patients. In fact, some subtle differences were detected at a global level like increase of clustering coefficient and modularity, which can be indicators of a compensatory response in early stages of MS. At the nodal level, multiple metrics' changes in precentral, frontal gyrus and some portions of the parietal lobe were detected as well. The graph theory measures used in this study were: clustering coefficient, modularity, global efficiency, assortativity, mean degree (in- and out-degree) at a global level and strength, degree, local efficiency, and nodal clustering coefficient at nodal level.

Even though several approaches to assess graph theoretical analysis can be used (Pearson correlation, ICA or Granger Causality), changes in MS always seem to follow the scheme shown in figure 11. At the early stages of disease, when structural damages are minor, there is often a loss of distant connections and increases in modularity, as well as decreases in global efficiency along with longer characteristic path lengths. All these observations suggest a compensatory mechanism that maintains cognitive functions, however as time passes by, functional compensation reaches a saturable level, resulting in significant loss of connections and network efficiency, leading to irreversible disease progression and cognitive impairment [44], [62].

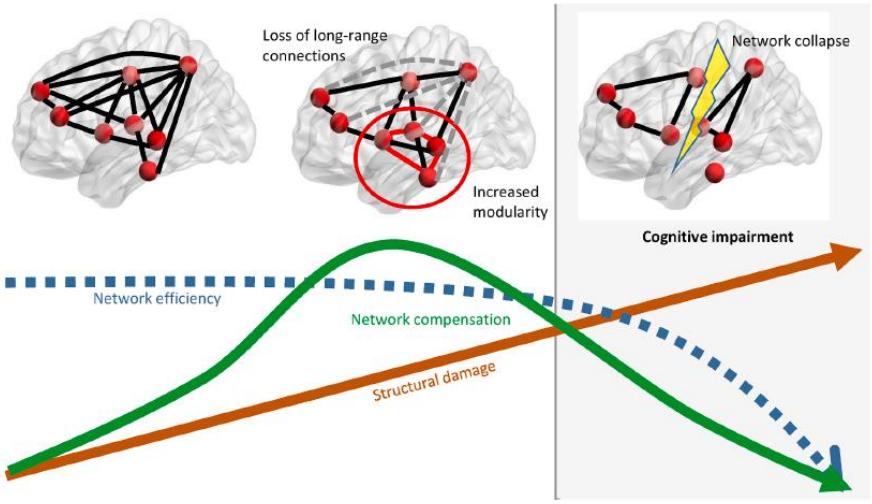

Figure 11- Schematic representation of how the neuronal network is reorganized through graph theory analysis in the course of cognitive impairment [44].

Three task-related fMRI studies (Ashtiani et al., [35], Ashtiani et al., [33], Azarmi et al., [4]) have analyzed graph theory measures in patients with Multiple Sclerosis. To follow the related work a summary of the main topics of the studies is presented in table 4.

Ashtiani et al., [35] studied the changes in brain functional connectivity topologies of RRMS patients during the performance of a cognitive task (PASAT) comparing them with matched healthy controls. They employed Pearson correlation analysis to determine the following measures: mean clustering coefficient, modularity, transitivity, characteristic path length, global efficiency, assortativity and small-worldness index at a global level, and degree, participation coefficient, diversity centrality, betweenness centrality, subgraph centrality, k-coreness centrality, pagerank centrality and eigenvector centrality at a nodal level. Their main conclusions were that in the global measures only the clustering coefficient, modularity and small-worldness index showed significant differences between the two groups (decreased values in the MSC group), which could be caused by increasing WM damage.

Also, almost all the nodal measures were different between groups in regions that seem to be involved in cognitive deficits, but interestingly in participation coefficient only the right putamen was significant between groups.

One year later Ashtiani et al., [33] with the same group of participants, and using the PASAT task, implemented Modular Structures Sparse Weights instead of Pearson correlation to construct the weighted functional connectivity networks and determine global and nodal measures. The results showed that only modularity out of six global measures is different between groups. The decrease of modularity in MS patients is in line with the above study, which led the authors to propose that changes in modularity can serve

as an early detector of cognitive impairment. Again, almost all the nodal measures, mainly the eccentricity, strength, within-module degree, eigenvector centrality, identified significantly different regions between groups. These nodal graph measures can be helpful to detect brain regions that are affected by cognitive deficits.

Azarmi et al., [4] presented a research study with the same goal as Ashtiani et al., [40]. GCA was the approach chosen to assess functional connectivity and they calculated the most frequent global and local graph measures, also adding the global flow coefficient, a measure that was never extracted and studied before. The results showed that only the global flow coefficient is statistically different between RRMS patients and healthy controls. In the case of nodal measures only subgraph centrality didn't have significantly different regions between groups. This study is the most similar to this thesis, and established GC as a method to assess changes in brain networks of MS patients.

Table 4- Summary of the studies using graph measures in task-based fMRI.

	Ashtiani et al., [35]	**Ashtiani et al., [33]**	**Azarmi et al., [4]**
Participants	8 RRMS 12 CNT	8 RRMS 12 CNT	8 RRMS 12 CNT
Parcellation	whole brain 116 ROIs (AAL)	whole brain 116 ROIs (AAL)	whole brain 116 ROIs (AAL)
Brain network	Pearson Correlation Analysis	Modular Structures Sparse Weights	Granger Causality
Threshold	Proportional Thresholding: 0.06-0.3 (steps of 0.01)	Proportional Thresholding: 0.1-0.5 (steps of 0.01)	Proportional Thresholding: 0.06-0.3 (steps of 0.01)
Global measures	Clustering coefficient, modularity, transitivity, characteristic path length, global efficiency, assortativity, global flow coefficient.	Clustering coefficient, modularity, transitivity, characteristic path length, global efficiency, mean local efficiency.	Clustering coefficient, modularity, transitivity, characteristic path length, global efficiency, assortativity, global flow coefficient.
Nodal measures	Degree, participation coefficient, centrality; diversity, betweenness, subgraph, k-coreness, pagerank, eigenvector centrality.	Nodal clustering coefficient, local efficiency, eccentricity, node strength, within-module degree, participation coefficient; betweenness, diversity, eigenvector centrality.	Total, in- and out-degree, participation coefficient, local flow coefficient; betweenness, subgraph, k-coreness and pagerank centrality.

Even though performing a task is more challenging and leads to higher signal noise than resting state [32], we believe that it can activate connections of the brain that are not specific to the task, and that would otherwise be undetectable. This will allow us to find and

eventually understand compensatory mechanisms that might be happening in MS, namely those leading to cognitive impairment.

4. Methods

The data analyzed in this thesis were collected in the context of the funded scientific project BIOMUSCLE (PTDC/MEC-NEU/31973/2017). Patients were recruited and clinically evaluated by the members of the project at the Neurology Department of the Hospital of University of Coimbra and met the criteria for MS diagnosis according to McDonald Criteria [9]. All the participants filled out written informed consent forms before the experiment.

4.1. Experimental Setup

4.1.1. Participants

A total of eighteen RRMS patients in the early stages of the disease (mean age 31.92 ± 8.09 years), and seventeen age-, sex-, and education-matched healthy controls with ages ranging from 20 to 50 years (mean age 30.70 ± 8.07 years), were recruited for this study.

The demographic information of the participants is reported in Table 5.

Table 5- Details of study participants.

	CNT	MSC
N	17	18
Age (mean ± std, in years)	30.70 ± 8.07	31.89 ± 8.15
Disease duration (mean ± std, in years)		0.91 ± 1.81
Education (mean ± std, in years)	16.10 ± 2.81	13.83 ± 2.22
Gender (Female/Male)	10 / 7	10 / 8
Handedness (Right/Left)	17 / 0	18 / 0

All the MS patients performed six clinical and neuropsychological tests, including the Expanded Disability Status Scale (EDSS) and the Modified Fatigue Impact Scale (MFIS), which measure physical impairment and the impact of fatigue, respectively. Three tests are embedded in the Brief International Cognitive Assessment for MS (BICAMS) and assess cognitive functions, namely processing speed declines (Symbol Digit Modalities Test-SDMT), performance during auditory and verbal memory tasks (California Verbal Learning Test-CVLT), and visuospatial learning and memory abilities (Brief Visuospatial Memory Test-BVMT). The last one in an emotion recognition test (Reading the Mind in the Eyes-RME).

- EDSS is a scale ranging from 0 (normal neurological status) to 10 (death from MS) that may change as the patient's physical impairment evolves during the course of the disease (median score of the MS patients of this study: **1.75,** range: **1.5-5**). Higher scores represent worse disability [10,11].
- MFIS is a self-reported questionnaire that assesses the impact and severity of fatigue in MS patient's daily lives [63,64]. The scores can go from 0 to 84 [65]. Higher scores represent more fatigue. The scores of the MS patients ranged from 3 to 62 (mean score ± std: **31.78 ± 16.15**).
- SDMT is a written/oral task lasting for 90 seconds designed to assess cognitive processing speed. Higher scores are associated with faster processing speeds, i.e., highest number of correct responses [66]. The scores go from 0 to 110 [67]. The MS patients had scores between 35 and 71 (mean score ± std: **52.28 ± 9.43**).
- CVLT is an oral assessment of auditory and verbal memory. It is based on the ability to memorize a list of 16 words and in 5 attempts state as many words as possible [66]. The scores go from 0 to 80 [68]. Higher scores indicate better auditory and verbal memory. The scores of the MS patients from the study range from 39 to 73 (mean score ± std: **50.56 ± 8.66**).
- BVMT is a paper-pencil test that measures visuospatial learning as well as memory abilities. It is assumed that the higher the score in BVMT, higher cognitive ability. The scores can go from 0 to 36 [67]. The MS patients presented score ranging from 9 to 36 (mean score ± std: **24.44 ± 7.68**).
- RME assesses dysfunction in social cognition by identifying other people's mental states through photographs of their eyes [67]. The scores of MS patients range from 18 to 30 (mean score ± std: **24.22 ± 3.39**), but they can go from 0 to 36. Higher scores indicate better cognitive function.

4.1.2. MRI acquisition

Imaging was performed at the Portuguese Brain Imaging Network facilities (Coimbra, Portugal) on a 3T Siemens MAGNETOM Prisma Fit MRI scanner (Siemens, Erlangen, Germany) using a 64-channel RF receive coil. In order to minimize head motion and scanner noise related discomfort, foam cushions and earplugs were used, respectively. fMRI data was acquired using a 2D simultaneous multi-slice (SMS) gradient-echo echoplanar imaging (GE-EPI) sequence (6× SMS and 2×in-plane GRAPPA accelerations), with whole brain coverage and the following parameters: TR/TE = 1000/37 ms, voxel size = 2.0×2.0×2.0 mm3, 72 axial slices (whole-brain coverage), FOV = 200×200 mm2, FA = 68°, and phase encoding in the anterior-posterior direction. The start of each trial was synchronised with

the acquisition of the functional images. A short EPI acquisition (10 volumes) with reversed phase encoding direction (posterior-anterior) was also performed prior to each fMRI run, for image geometric distortion correction. A 3D anatomical T1-weighted MP2RAGE (TR = 5000 ms, TE = 3.11 ms; 192 interleaved slices with isotropic voxel size of 1 mm3) was also collected for subsequent image registration.

4.1.3. Experimental design

All the participants were submitted to two visual stimulation tasks, one passive task of visual motion of dot patterns and one perceptual visual task of biological motion perception, followed by a resting-state run.

Passive visual task

The task with passive visual stimuli will also be referred to as V1MT run, as it was also used to localize regions in the visual cortex, such as the human middle temporal area (hMT+/V5), which is known to respond well to simple motion paradigms.

The V1MT run consisted of 10 blocks of 18 seconds, with each block consisting of a fixation period of 6 seconds, a period showing stationary white dots for another 6 seconds and one final period in which the dots are travelling towards and away from a central fixation cross at a constant speed (5 deg/sec) for another 6 seconds [63][64].

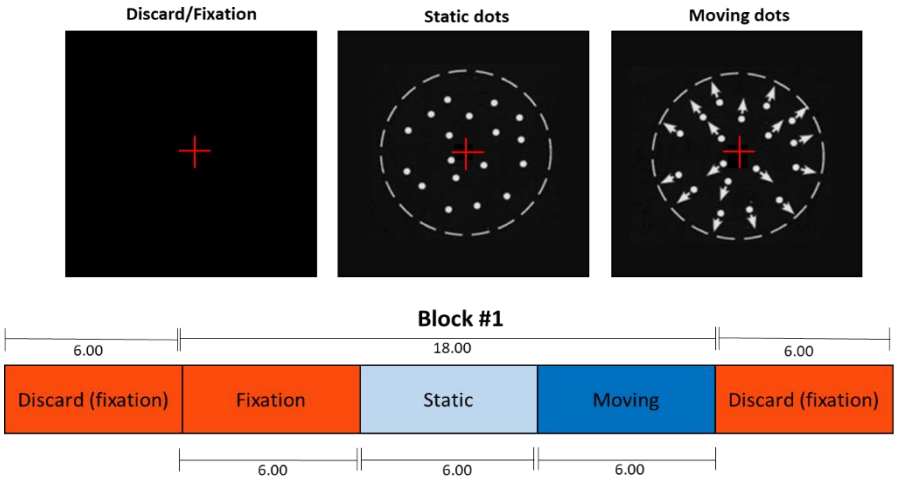

Figure 12- Schematic representation of the passive visual task. The duration of each period is indicated in seconds. Participants do not have to discriminate any movement, just fixate the red cross during the whole task. (adapted from Huk et al. [64])

Biological motion task

Biological motion (BM) stimuli were created based on the familiar shape of a male walker and were composed of 12 white point-lights displayed on a black background, in the positions of the main joints of the body. The walker is facing left or right on a sagittal (profile) view and walks always in the same spot (no translation).

Each BM run consisted of 12 stimulation blocks of 18 seconds, each one followed by a 22 seconds' fixation block. In each run, 4 or 5 stimulation blocks (depending on the starting block) presented the whole body of the point-light walker was shown facing rightwards or leftwards (B: body blocks), 4 or 5 stimulation blocks showed only one point-light at the right ankle and moving rightwards of leftwards (F: foot blocks), and 3 stimulation blocks showed the 12 point-lights of the whole body but randomly positioned across the y axis, with their original trajectory across the x axis (S: scrambled blocks). Participants performed two runs of BM, thus a total of 9 body, 9 foot and 6 scrambled stimulation blocks were collected.

In each stimulation block, eight motion trials were shown consecutively. In each trial, a motion pattern (either body, foot or scrambled, depending on the type of block) was shown for 0.75 seconds, pseudo-randomly towards left or right.

After each motion pattern, participants were asked to discriminate whether motion patterns were towards the left or right. The answers were given via button press during a 1.5 second period, in which a central white cross was shown.

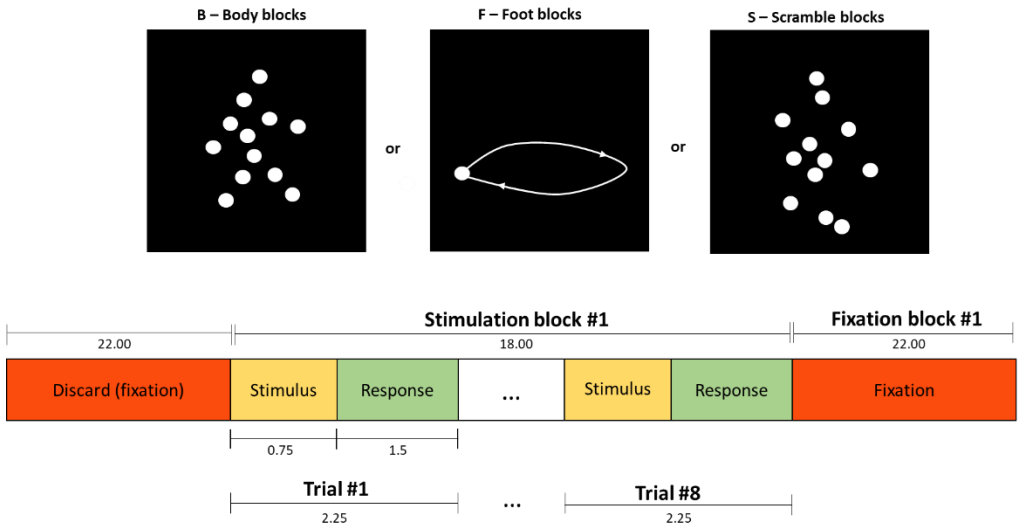

Figure 13- Schematic representation of the biological motion task. The duration of each period is indicated in seconds. In each stimulation block there were eight trials; In each trial the stimulus interval represents a motion pattern of B, F or S., depending on the type of block. (adapted from Duarte et al.[47])

Resting State

The resting state run consist of one fixation block (equal to the ones in the other two paradigms), of 480 seconds. The participants only have to fixate a central red cross.

4.1.4. Pre-processing

The pre-processing fMRI data was implemented in MATLAB, through the SPM12 and the PhysIO toolbox, however for image distortion correction, FMRIB software Library (FSL) was the better choice.

Therefore, in this thesis the pre-processing was performed with the pipeline described by Soares et al., [65]. In more detail this pipeline can be divided into 2 phases, the first one starts with the data to be submitted to: 1) Slice timing; 2) realignment and motion correction, being the reference volume the first one; 3) correction of geometric distortions with the acquisition of two undistorted GE images at two different echo-times (TE); 4) bias field correction.

The second phase of the preprocessing corresponds to rectifying non-neuronal fluctuations generated by e.g., head motion, cardiac and respiratory signals. For this, (1) the functional images were aligned with the reference anatomical images (coregistration) and (2) WM and ventricular CSF masked extracted, (segmentation). Noise fluctuations were insert in PhysIO toolbox, which were calculated the noise regressors of the BOLD signal. With this toolbox, it's also possible to detect sudden movement peaks, called “motion outliers”, originated, for example, when a person moves very quickly or sneezes inside the scan.

Then the “clean images” from the regression were brain masked and the pre-processing was completed with spatial smoothing with a 3 mm full-width-at-half-maximum (FWHM) isotropic Gaussian kernel and high-pass temporal filtering with a cut-off period of 12s, 80s and 100 for the run V1MT, run BM and run RS respectively.

4.2. Brain Network construction

4.2.1. Brain anatomical parcellation

In the present study, each participant's brain was divided into 170 regions of interest (ROIs), 92 cortical and 78 subcortical, defined by the Automated Anatomical Labeling 3 (AAL3) atlas [66]. Because patients even in the earliest stages of the disease might show a shift in functional hemispheric lateralization, the atlas was organized to better visualize whether there is greater connectivity in the right (non-dominant) hemisphere or not. Thus, the index numbers from 1 to 80 are regions from the left hemisphere, the 81-90 are midline structures and 91-170 are regions from the right hemisphere. Table 6 gives the names and abbreviations of the 170 ROIs.

Table 6- AAL3 regions. The first number shown in column 1, is for the left hemisphere, and the second number is for the right hemisphere. This does not apply to the lobules of vermis and raphe nuclei, because these are midline structures.

Index	Anatomical description	Abbreviation	Index	Anatomical description	Abbreviation
1, 91	Precentral gyrus	PreCG	46, 136	Temporal pole: middle temporal gyrus	TPOmid
2, 92	Superior frontal gyrus-dorsolateral	SFG	47, 137	Inferior temporal gyrus	ITG
3, 93	Middle frontal gyrus	MFG	48, 138	Crus I of cerebellar hemisphere	CERCRU1
4, 94	Inferior frontal gyrus-opercular part	IFGoperc	49, 139	Crus II of cerebellar hemisphere	CERCRU2
5, 95	Inferior frontal gyrus-triangular part	IFGtriang	50, 140	Lobule III of cerebellar hemisphere	CER3
6, 96	IFG pars orbitalis	IFGorb	51, 141	Lobule IV-V of cerebellar hemisphere	CER4_5
7, 97	Rolandic operculum	ROL	52, 142	Lobule VI of cerebellar hemisphere	CER6
8, 98	Supplementary motor area	SMA	53, 143	Lobule VIIB of cerebellar hemisphere	CER7b
9, 99	Olfactory cortex	OLF	54, 144	Lobule VIII of cerebellar hemisphere	CER8
10, 100	Superior frontal gyrus-medial	SFGmedial	55, 145	Lobule IX of cerebellar hemisphere	CER9
11, 101	Superior frontal gyrus-medial orbital	PFCventmed	56, 146	Lobule X of cerebellar hemisphere	CER10
12, 102	Gyrus rectus	REC	57, 147	Thalamus-Anteroventral Nucleus	tAV
13, 103	Medial orbital gyrus	OFCmed	58, 148	Lateral posterior	tLP
14, 104	Anterior orbital gyrus	OFCant	59, 149	Ventral anterior	tVA
15, 105	Posterior orbital gyrus	OFCpost	60, 150	Ventral lateral	tVL
16, 106	Lateral orbital gyrus	OFClat	61, 151	Ventral posterolateral	tVPL
17, 107	Insula	INS	62, 152	Intralaminar	tIL
18, 108	Anterior cingulate & paracingulate gyri	ACC	63, 153	Reuniens	tRe
19, 109	Middle cingulate & paracingulate gyri	MCC	64, 154	Mediodorsal medial magnocellular	tMDm
20, 110	Posterior cingulate gyrus	PCC	65, 155	Mediodorsal lateral parvocellular	tMDl
21, 111	Hippocampus	HIP	66, 156	Lateral geniculate	TLgn
22, 112	Parahippocampal gyrus	PHG	67, 157	Medial Geniculate	tMGN
23, 113	Amygdala	AMYG	68, 158	Pulvinar anterior	tPuA
24, 114	Calcarine fissure and surrounding cortex	CAL	69, 159	Pulvinar medial	tPuM
25, 115	Cuneus	CUN	70, 160	Pulvinar lateral	tPuL
26, 116	Lingual gyrus	LING	71, 161	Pulvinar inferior	tPuI
27, 117	Superior occipital gyrus	SOG	72, 162	Anterior cingulate cortex-subgenual	ACCsub
28, 118	Middle occipital gyrus	MOG	73, 163	Anterior cingulate cortex-pregenual	ACCpre
29, 119	Inferior occipital gyrus	IOG	74, 164	Anterior cingulate cortex-supracallosal	ACCsup
30, 120	Fusiform gyrus	FFG	75, 165	Nucleus accumbens	Nacc
31, 121	Postcentral gyrus	PoCG	76, 166	Ventral tegmental area	VTA
32, 122	Superior parietal gyrus	SPG	77, 167	Substantia nigra-pars compacta	SNpc
33, 123	Inferior parietal gyrus - excluding supramarginal and angular gyri	IPG	78, 168	Substantia nigra-pars reticulata	SNpr
34, 124	SupraMarginal gyrus	SMG	79, 169	Red nucleus	tRe
35, 125	Angular gyrus	ANG	80, 170	Locus coeruleus	LC
36, 126	Precuneus	PCUN	81	Lobule I-II of vermis	VER1_2
37, 127	Paracentral lobule	PCL	82	Lobule III of vermis	VER3
38, 128	Caudate nucleus	CAU	83	Lobule IV-V of vermis	VER4_5
39, 129	Lenticular nucleus-Putamen	PUT	84	Lobule VI of vermis	VER6
40, 130	Lenticular nucleus-Pallidum	PAL	85	Lobule VII of vermis	VER7
41, 131	Thalamus	THA	86	Lobule VIII of vermis	VER8
42, 132	Heschls gyrus	HES	87	Lobule IX of vermis	VER9
43, 133	Superior temporal gyrus	STG	88	Lobule X of vermis	VER10
44, 134	Temporal pole: superior temporal gyrus	TPOsup	89	Raphe nucleus-dorsal	RapheD
45, 135	Middle temporal gyrus	MTG	90	Raphe nucleus-median	RapheM

4.2.2. Average time course extraction

To construct functional brain networks, time course extraction was achieved through a function specifically created to extract the time courses from all the 170 ROIs by averaging the BOLD signal from all voxels within each ROI. The function is going to convert the 4D fMRI file into a 2D matrix and create a mask variable with the same size as the atlas. The mask will go through each which voxel in the brain and return 0s or 1s. If returns the number 1 it means that the voxel belongs to that ROI, and it will store that time course. At the end, it uses the mean function to calculate the average time course for the whole ROI. This process is repeated on a loop for each AAL3 ROI.

4.2.3. Granger Causality – Connectivity Matrix

Granger Causality was applied using the Multivariate Granger Causality (MVGC) toolbox Version 1.3 for MATLAB (https://github.com/lcbarnett/MVGC1). The toolbox uses a package of functions to perform conditional and unconditional GCA in the time or frequency domains. These functions are correctly compiled into a script provided by the toolbox, in order to simplify the determination of some important parameters, such as the model order, residual errors, and regressors coefficients and statistical analysis [29]. Due to computational demands, the choice was to perform a more traditional approach, i.e., a bivariate (unconditional) GCA analysis (see equation 2 for reference) in the time domain, for each participant and for each task individually (BM runs were concatenated).

Apart from the experimental design, the following inputs are required and the choices we made to proceed with the analysis are the following [29]:

- **Number of trials:** equivalent to the number of blocks. This parameter is equal to 1 because each run is only evaluated after all the blocks, not after each block.
- **Number of observations per trial:** equivalent to the number of volumes per run. For the V1MT run it is 192 volumes, for the BM runs it is 1004 volumes (the BM runs were concatenated, and each BM run had 502 volumes), and for the RS run it is 480 volumes.
- **VAR model estimation regression mode**: Levinson-Wiggins-Robinson (LWR) algorithm.
- **Information criteria regression mode**: LWR algorithm.
- **Model order estimation method:** Bayesian Information Criteria (BIC).
- **Statistical test for MVGC**: Granger's F-test.

At the end of this analysis, a squared ROI x ROI matrix is generated (figure 14 - a), where each element represents the Granger F-value between the corresponding pair of ROIs, reflecting directed functional connectivity (FC), from ROI A (in x axis) to ROI B (in y axis). The higher the F-value, the higher the FC. The other matrix (figure 14 - b) shows the p-values as the result of the F-test used for statistical analysis of Granger F-values, where the theoretical null distribution is Y doesn't "G-cause" X. So, if the null hypothesis is rejected Y "G-causes" X. To better highlight which connections are statistically significant, the matrix of the p-value <0.05 is corrected for false discovery rate (FDR) and thresholded at 0.05, yielding a binary matrix of significant (1) and non-significant (0) connections (figure 14 - c).

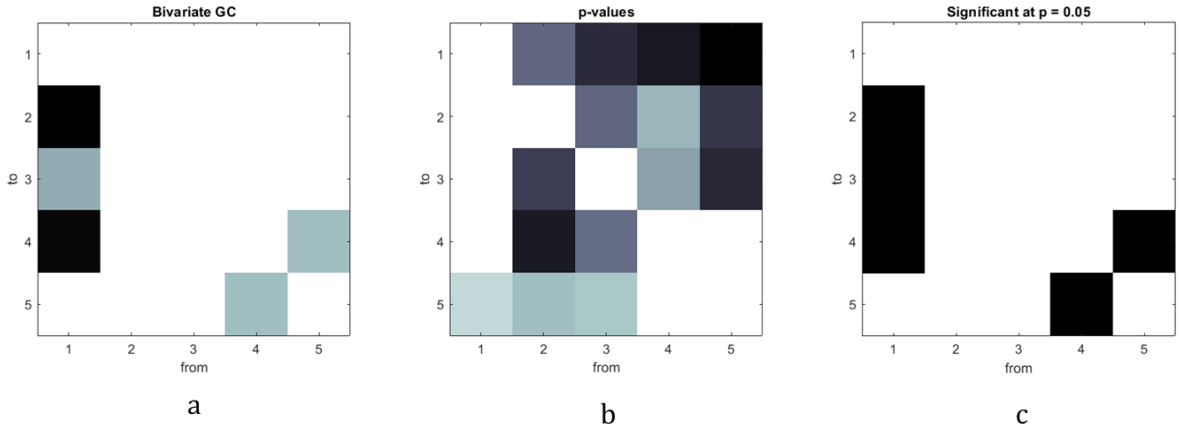

Figure 14- a) Bivariate GC matrix. b) Matrix with the p-values as the results of the statistical analysis with the F-test of Granger F-values. c) Binary matrix with white squares representing the non-significant connections and the black squares representing the significant connections.

4.2.4. Connectivity Matrix Thresholding

Before obtaining theory graph metrics, a threshold is usually applied to connectivity matrices. By applying a threshold to the connectivity matrices, spurious connections (connections that do not contain meaningful information) will be removed, and the remaining strong correlations in the connectivity matrix will be obtained [31][67]. Furthermore, thresholding might be useful to analyze equally dense connectivity matrices.

Whether or not a difference in connection density is considered a confound determines which method to use [64]. The two most used methods to perform network thresholding are the "absolute" and "proportional" thresholding.

Applying a single, absolute threshold to the connectivity matrix of all participants is the simplest thresholding approach. Below the threshold, all elements are set to zero, while

the elements above that threshold are preserved [4]. This approach has as its main flaw, fluctuations in the number of edges between participants, which can change various measurements of functional brain connectivity, such as degree centrality [31].

Aiming to address this limitation, proportional thresholding ensures the same number of connections across all participants [31][32], which is very meaningful when analyzing brain networks between groups. Hence, we constructed the brain network of each participant considering the proportional approach. Since there's no ideal threshold value, we followed the approach of published studies, cited below, of extracting metrics for a range of threshold values.

Miri Ashtiani et al., [35] claim that choosing a threshold range among 0.10 and 0.50 for proportional thresholding meant that the matrices would be neither sparse nor dense. Azarmi et al., [4] employed a range of 0.06-0.30 with increments of 0.01. Since this study has many similarities with this thesis, we opted to enlarge this range, choosing proportional threshold (PTh) values ranging from 0.06 to 0.32 with steps of 0.01, in order to investigate possible changes in the network. Thus, the graph theory metrics were extracted for each participant twenty-seven times.

4.2.5. Graph theory connectivity measures

Global and nodal/local connectivity measures were calculated via the Brain Connectivity Matlab toolbox (BCT) (http://www.brain-connectivity-toolbox.net), by using functions applicable to weighted connectivity matrices.

Various connectivity measures described in section 2.2.3 can be employed in whole-brain analyses. Thus, the choice of which ones to extract for this study was made analyzing the frequency with which they appear in the literature. Segregation brain measures such as mean clustering coefficient and modularity were extracted. Moreover, integration measures such as characteristic path length, global efficiency and local efficiency were extracted as well. Assortativity was used as measure of resilience and all centrality measures that can be applied to directed and weighted matrices were also calculated (eccentricity, radius, diameter, total degree, in-degree, out-degree, total strength, in-strength, out-strength, betweenness centrality, within-module degree, participation coefficient, subgraph centrality, k-coreness centrality, local, global, and total flow coefficient).

Finally, PageRank centrality was used instead of eigenvector centrality because its computation applies to directed networks [4], [44], which is the case of these matrices.

The small-worldness index was not extracted as the calculation of this measure requires the number of edges as an input, the total value of which cannot exceed 16256. As we have 28900 edges in this study, this measure was impossible to obtain. Moreover, this measure also requires an undirected connectivity matrix as input, which again does not apply to the matrices obtained with GCA.

5. Results and Discussion

5.1. Mean of the connectivity matrices

After the calculation of the individual matrices for each participant, the overall mean connectivity was computed for each participant and each task. These results are presented in table 7. Hereafter, the group of healthy controls is referred to as CNT, and the group of MS patients as MSC.

Table 7- Mean connectivity matrix of each participant, in all runs.

		Mean of F - values		
	Participants	**Run V1MT**	**Run BM**	**Run RS**
CNT	1	0.0261	0.0706	0.0231
	2	0.0319	0.0504	0.0187
	3	0.0156	0.0510	0.0368
	4	0.0366	0.0658	0.0221
	5	0.0203	0.0540	0.0081
	6	0.0120	0.0306	0.0118
	7	0.0128	0.0415	0.0065
	8	0.0230	0.0320	0.0079
	9	0.0183	0.0440	0.0189
	10	0.0134	0.0445	0.0146
	11	0.0273	0.0372	0.0216
	12	0.0123	0.0425	0.0137
	13	0.0265	0.0427	0.0088
	14	0.0170	0.0521	0.0164
	15	0.0181	0.0461	0.0155
	16	0.0194	0.0490	0.0128
	17	0.0217	0.0438	0.0089
MSC	1	0.0211	0.0396	0.0225
	2	0.0175	0.0338	0.0101
	3	0.0136	0.0339	0.0219
	4	0.0123	0.0494	0.0168
	5	0.0125	0.0374	0.0158
	6	0.0153	0.0402	0.0187
	7	0.0241	0.0445	0.0446
	8	0.0213	0.0384	0.0362
	9	0.0177	0.0538	0.0267
	10	0.0128	0.0352	0.0284
	11	0.0241	0.0492	0.0219
	12	0.0158	0.0484	0.0216
	13	0.0141	0.0329	0.0176
	14	0.0210	0.0420	0.0297
	15	0.0136	0.0371	0.0272
	16	0.0156	0.0514	0.0137
	17	0.0140	0.0464	0.0152
	18	0.0174	0.0486	0.0213

Table 8- Total mean F-value ± standard deviation of each group, in each run.

	Mean F value		
	Run V1MT	Run BM	Run RS
CNT	0.0207 ± 0.0071	0.0469 ± 0.0103	0.0237 ± 0.0096
MSC	0.0174 ± 0.0039	0.0423 ± 0.0067	0.0228 ± 0.0084

Comparing the groups in the different runs relying only on the average F-values of each participant is challenging. Even so, the biggest distinction that can be observed at first glance is that the BM run of the CNT and MSC group, compared to the other runs, has higher F-values. This can be explained by the fact that this is a more demanding task which recruits more regions. Hereafter, to test differences between groups, means and standard deviations of the individual F-values matrices were calculated (presented in table 8). This was done by averaging the participants' matrices across groups (CNT and MSC), obtaining a single mean matrix (displayed in figure 16), with mean F-values and standard deviation, for each group in each run.

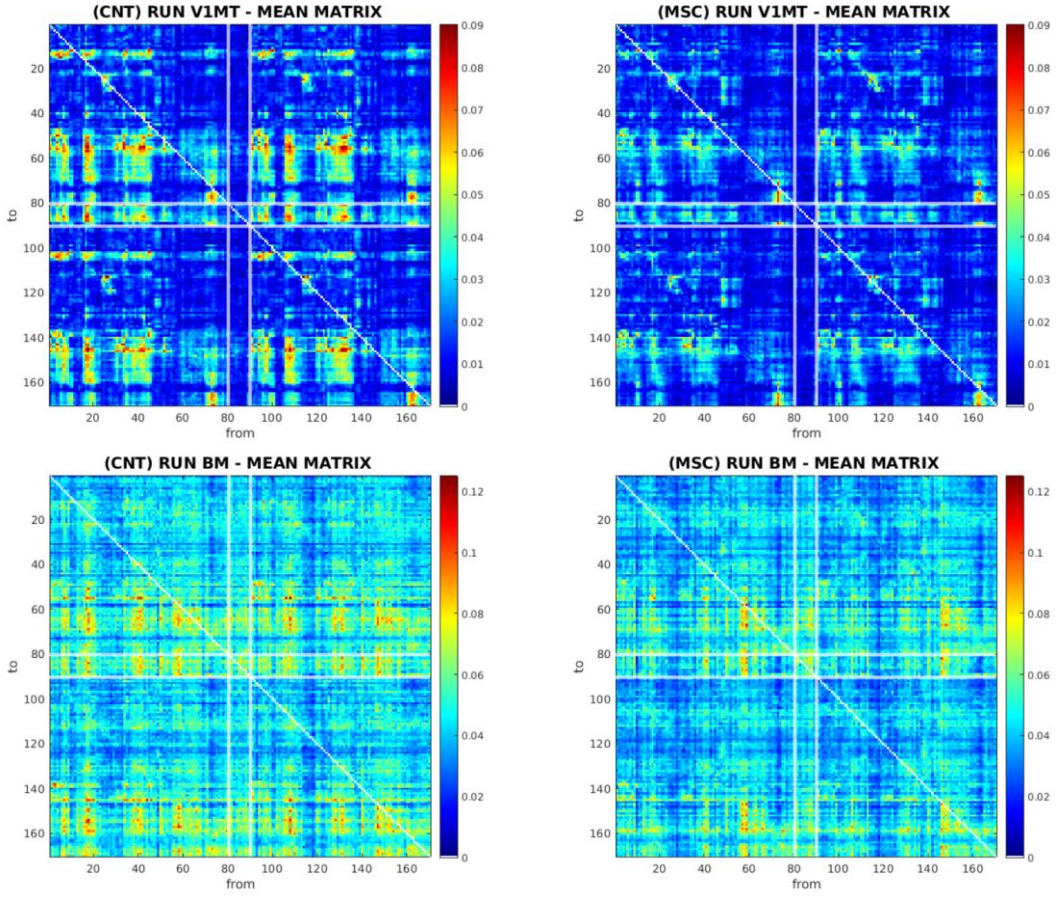

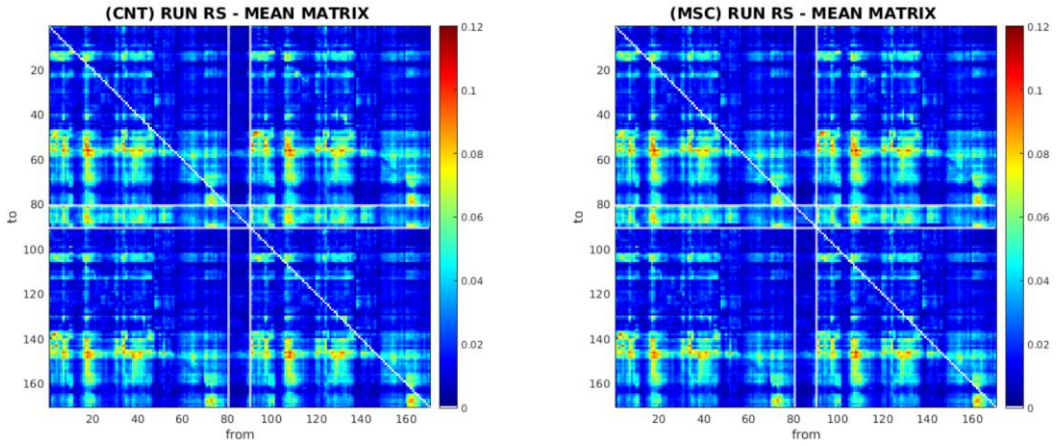

Figure 16- Average matrix of the CNT (left column) and MSC (right column) groups, in run V1MT (top row), run BM (middle row) and run RD (bottom row). The color bar represents the F-values.

When comparing the MS patients with healthy controls, it can be observed that, on average, the F-values have a tendency to be smaller. This happens in every run, but is more noticeable in the BM run, as there is a decrease of 0.0046 units, while in the V1MT run it is 0.0039 units and in the RS run 0.0009 units. Visually, this smaller difference in the RS run is very noticeable since the mean matrices of both groups are very similar.

To validate these observations, we compared the number of significant connections between the different experimental conditions, since F-values theoretically have no biological interpretation, but a mathematical interpretation. For this effect we extracted the F-values of only the statistically significant connections (with p-value<0.05, FDR corrected) for both groups (CNT and MSC) and all runs (V1MT, BM, and RS).

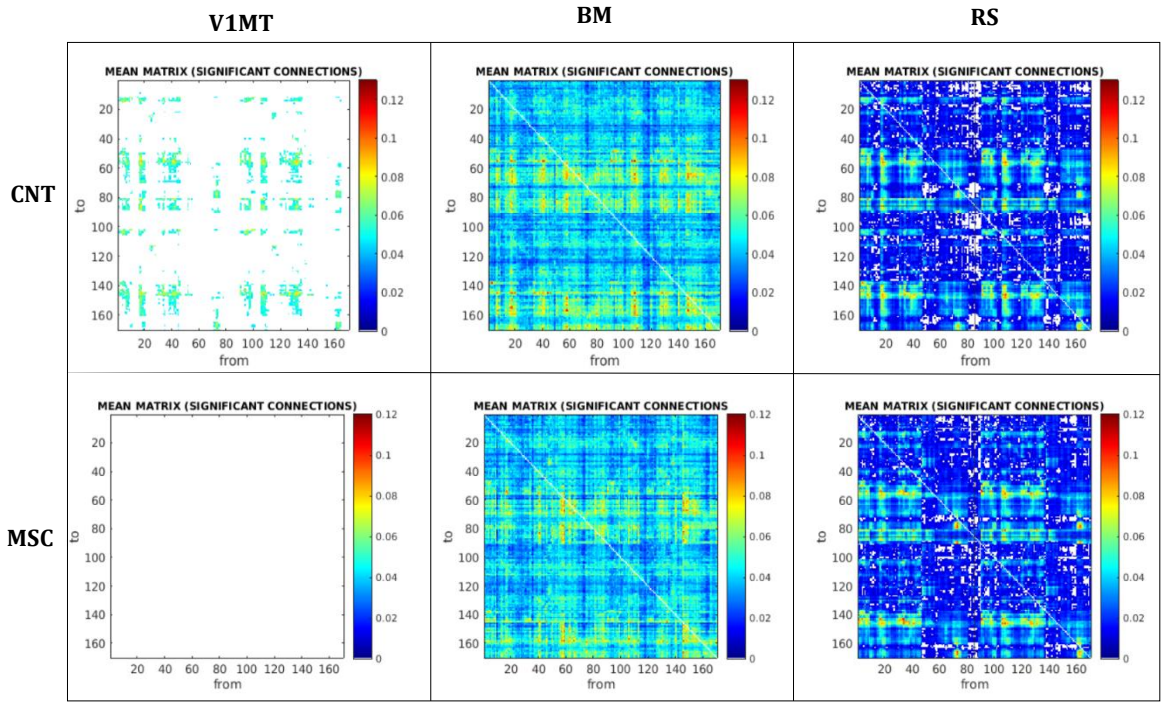

Figure 17- Results of the within-groups statistical analysis. (top row) F-values of the statistically significant connections in CNT, in each run. (bottom row) F-values of the statistically significant connections in MSC, in each run. The color bar represents the F-values.

In the CNT group, it can be observed that there is an increase of the number of connections in the BM run relative to the other runs (V1MT and RS).

Also, in the RS run, the number of connections is bigger than in the V1MT run, in both the CNT and MSC groups.

One unexpected observed aspect is that every connection established between two regions in the BM runs is statistically significant even after the correction for multiple comparisons. This might be because of the larger number of volumes per run, which makes mathematical computations more robust and statistical differences more evident. This happens again in RS run, but not in the V1MT run, since it is the run with the fewest volumes. Also, the higher F-values in this BM run can be explained by the increase in the complexity of the task, which involves decision-making and that inherently recruits more brain regions for the efficient information flow and processing.

These results are in line with those observed based on the mean F-values, which reinforces that aspects observed during task performance are not so obvious in resting-state. Although this is not a direct comparison between the mean F-values of the groups, our results appear to be contradictory to most of the studies done in this context, that report increases in functional connectivity in early stages of the disease both in task and rs-FC, as a compensatory mechanism in response to brain injuries (Rocca et al., [44]).

One hypothesis for this result is the fact that this work focuses on very recently diagnosed patients, so it is likely that they have not yet developed these compensatory mechanisms. Indeed, in Droby's [45] RRMS patients, who had a mean disease duration of 3.7 years it was shown that FC did not change dramatically, which is in line with our results that also show very minimal differences. Our results may also suggest that, once again, due to the recent diagnosis, it is not possible to observe the same results as in the literature in a whole-brain scenario, although it does not mean that in a more restricted network this sensitivity to detect other outcomes will not occur.

5.2. Between-Groups Statistical analysis

The aim of the between-group statistical analysis is to identify the connections that were different between groups as a consequence of the disease.

The Kolmogorov-Smirnov normality test was applied for every group and run, and all the distributions returned as not normal. Thus, the Wilcoxon rank sum test was used to find the different connections between CNT and MSC groups with a significance level of 0.05 and not corrected for multiple comparisons, as to apply a more exploratory approach. Considering the high number of connections and the relatively low number of subjects in each group, correcting for so many tests could be too conservative and lead us to miss some potentially interesting effects, especially subtle or small differences that might exist in early disease phases as in our case.

If the null hypothesis is rejected, it means that in that connection the two independent groups do not have the same median, therefore that connection is statistically significantly different between groups.

To find out in which direction the FC is altered, in MS patients relative to healthy controls, the difference between the medians of the F-values of the two groups (MSC-CNT) was calculated for each significantly different connection. These results are presented in matrix form below, in figure 18. The red cells in the rightmost matrices indicate positive differences, which means that the F-values are higher in the MSC group, and the blue cells indicate negative differences, so that the F-values are higher in the CNT.

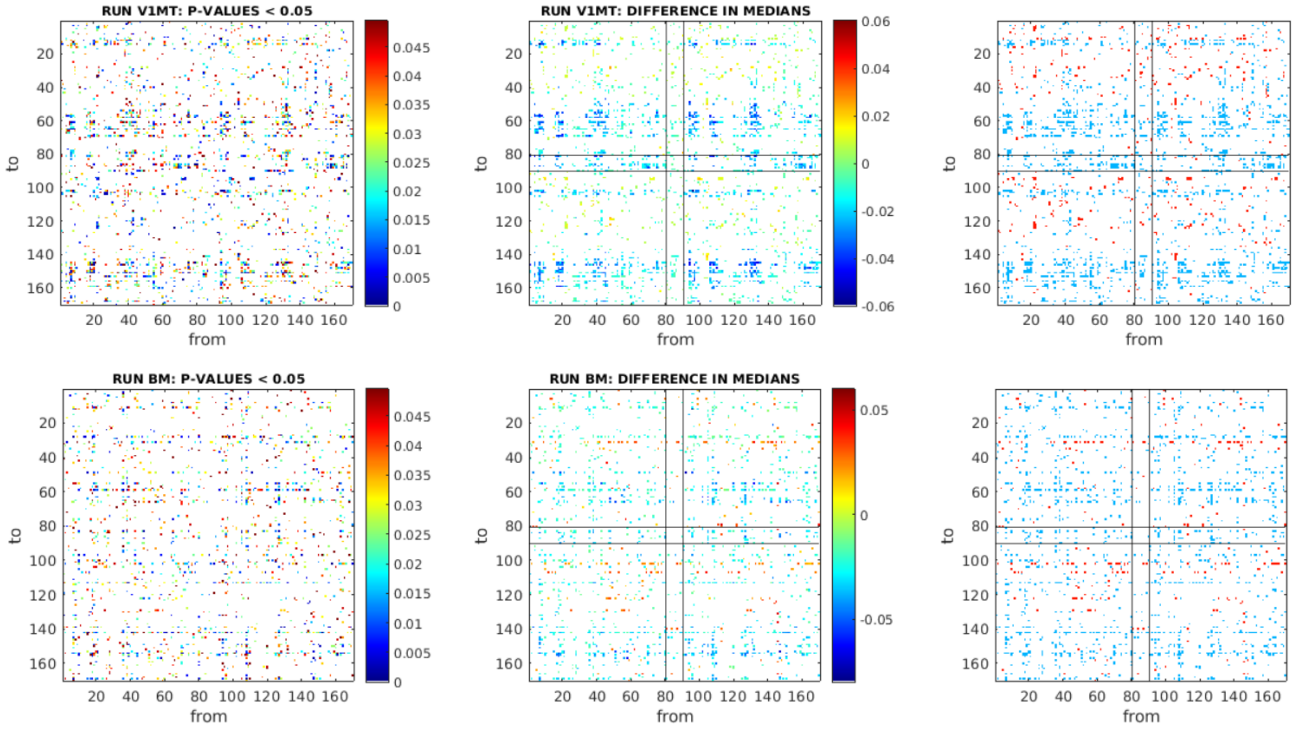

Figure 18- Results after performing the non-parametric Wilcoxon rank-sum test for all the runs (V1MT, BM, and RS). (left column) p-values of the connections that are statistically significantly different between groups (null hypothesis rejected, p< 0.05). (middle column) Matrix in which each element is the difference between the medians of two independent groups (MSC-CNT) in the same statistical significantly different connections. The colorbar expresses the difference in the median of F-values, from negative values to 0 means that the median in the healthy control group is higher, and from 0 up to the maximum value, represents a higher median in the MS patients'. (right column) Binary matrix to better identify in which connections the previous hypotheses take place. Red points are where median of MSC > median of CNT and the blue points shows where the opposite happens.

In the V1MT run, the number of connections with higher F-values in the MS patients' group (412 red cells) is lower than the number of connections with higher F-values in healthy controls (1869 blue cells).

In comparison to the V1MT run, in the BM run there are fewer connections that are significantly different between groups. Nevertheless, the number of connections with higher F-values in the MS patients' group (299 red cells) is again lower than the number of connections with increased F-values in the CNT group (1478 blue cells).

The RS run presents the lowest number of statistically significant different connections between groups, and there is higher balance between the number of connections with increased F-values in the MS patients (539 red cell) and the number of connections with increased F-values in the healthy controls (813 blue cells).

These results agree with what we already concluded in the previous section, that during task performance there are more differences than in resting state conditions.

Additionally, to the calculation of the differences between the medians of the F-values of the two groups, the mean of those differences was also calculated for the group of intra-hemispherical, inter-hemispherical, and non-hemispherical (including medial regions) connections, to have broader understanding of the degree of differences in each side of the brain.

Table 9- Mean values of the differences (MSC-CNT) previously calculated in specific areas of the brain. Shaded areas indicate where the greatest differences in connectivity between groups were found. The abbreviations are as follow: L- left; M- medial; R- right.

V1MT	**L -> L**	**M -> L**	**R -> L**
	-0.0136	-5.5365e-4	-0.0123
	L -> M	**M -> M**	**R -> M**
	-0.0204	-0.0062	-0.0204
	L -> R	**M -> R**	**R -> R**
	-0.0135	-0.0056	-0.0132
BM	**L -> L**	**M -> L**	**R -> L**
	-0.0177	-0.0046	-0.0176
	L -> M	**M -> M**	**R -> M**
	-0.1085	-2.2306e-4	-0.0267
	L -> R	**M -> R**	**R -> R**
	-0.0194	-0.0162	-0.0217
RS	**L -> L**	**M -> L**	**R -> L**
	-0.0029	-0.0053	-0.0043
	L -> M	**M -> M**	**R -> M**
	-0.0123	-0.0060	-0.0127
	L -> R	**M -> R**	**R -> R**
	-0.0034	-0.0053	-0.0048

Looking at the table, all the differences are negative, which means that generally the connections have a higher F-value in the healthy control group. The most striking feature is that in all runs, the greatest differences in connectivity between groups are seen in the connections projected from the left and right hemisphere to the medial zones (cerebellar vermis and raphe nuclei). Differences, yet minor, are most noticeable in task runs.

Connections to the vermis are associated with limb movements and body posture, which can become impaired with disease progression. The existing information about raphe nuclei is mostly on their role as a neurotransmitter of serotonin, but not much is known about their efferent pathways. Thus, changes in these connections in the future should be taken into consideration as they may serve as a biomarker of the disease.

5.3. Graph Theory Connectivity Measures

The main aim of this section is to find differences in network measures between the groups CNT and MSC. After running the KS test for normality, we employed the non-parametric Wilcoxon rank sum test, in order to assess differences in network connectivity metrics of graph theory. Statistical significance was considered (for $p<0.05$). A final note worth mentioning is that results are presented without correction for multiple comparisons, with the same rationale explained above. With FDR correction no differences remained statistically significant.

5.3.1. Global Connectivity Measures

For all the proportional thresholding values (PTh's) and participants, the following eight global connectivity measures were explored: mean clustering coefficient, assortativity, global efficiency, modularity, global flow coefficient, characteristic path length, radius and diameter. In turn, a single value and standard deviation for each PTh was obtained for the mentioned measures, as a result of the average calculated over each group (table 13, table 14 and table 15 of appendix I).

Then, to have a better perspective of how these measures vary across PTh values, boxplots were built with the distribution of their values for each group, with a line connecting their average values, so that it was easier to visualise patterns of behavior. As identifying this pattern was not always clear, new boxplots were built, but this time with the distribution of the mean values across thresholds for each measure (27 values, one for each threshold), which made it simpler to interpret the results.

RUN V1MT

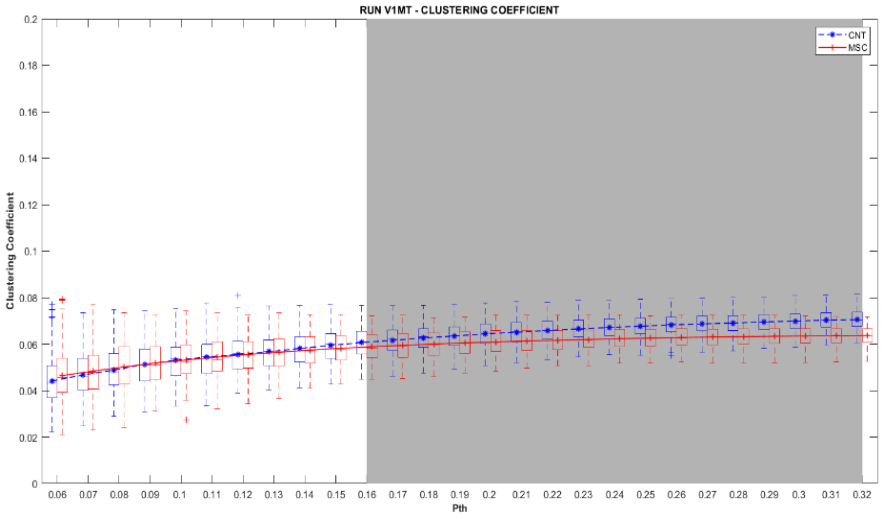

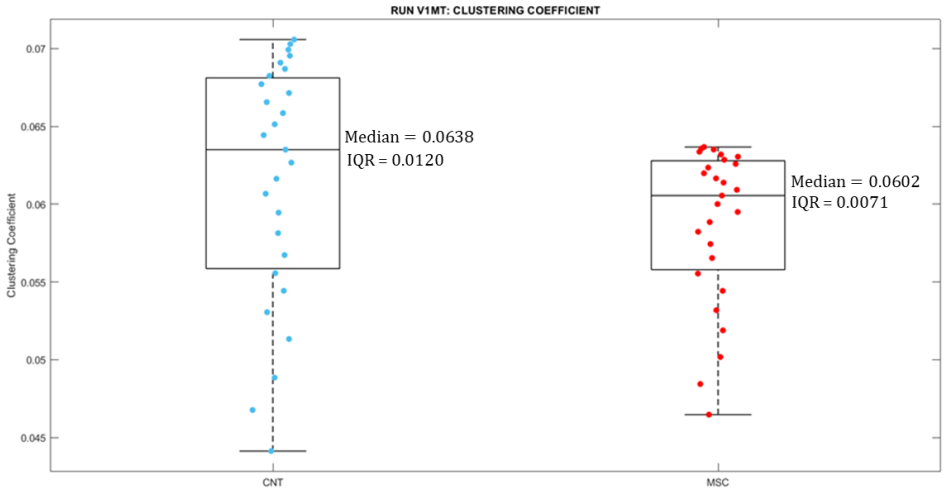

Figure 19- (top) Boxplot of the distribution of the **mean clustering coefficient** values in CNT (blue line) and MSC (red line) over the selected range of thresholds, shaded areas indicate the PTh's where between-group differences were statistically significant. (bottom) Boxplots with the distribution of the mean values of the mean clustering coefficient at each threshold in both groups. IQR: inter-quartile range.

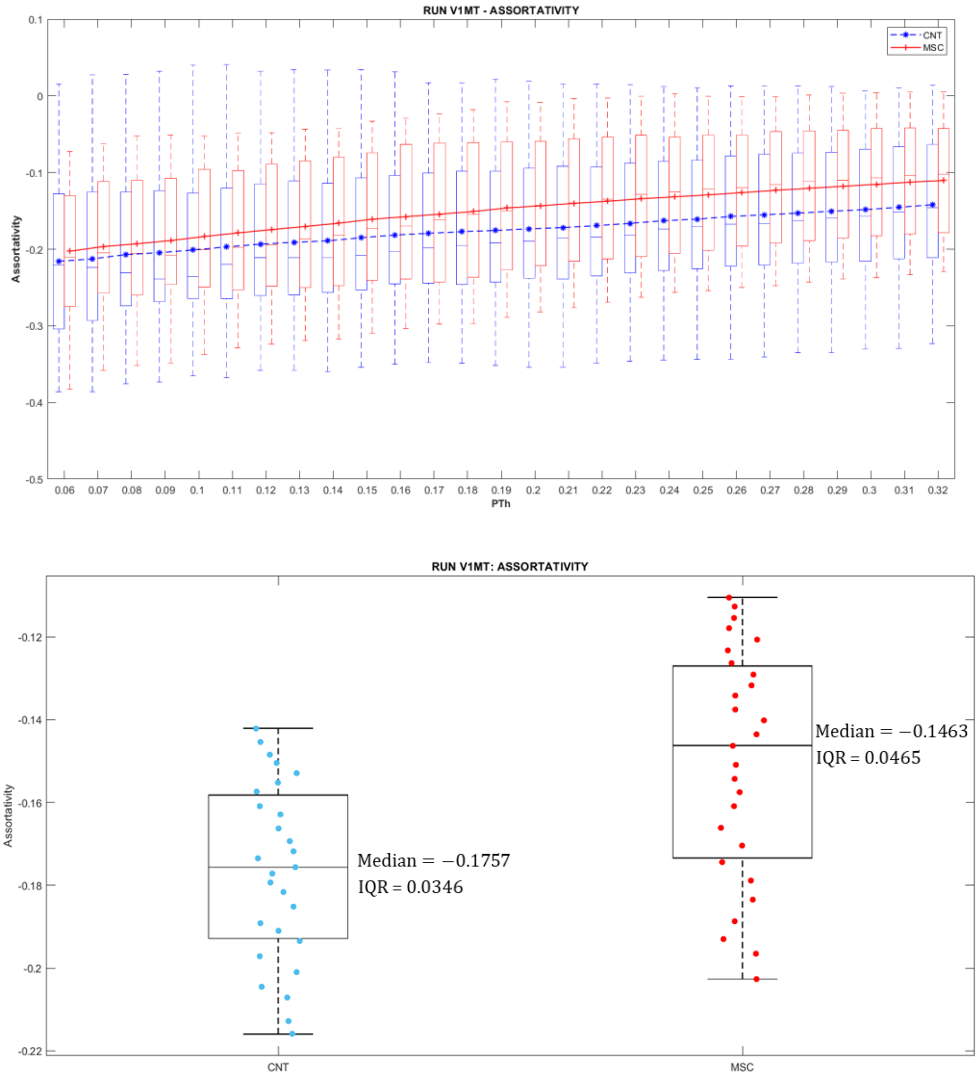

Figure 20- (top) Boxplot of the distribution of the **assortativity** values in healthy controls (blue line) and MS patients (red line) over the selected range of thresholds. (bottom) Boxplots with the distribution of the mean values of the assortativity at each threshold in both groups. IQR: inter-quartile range.

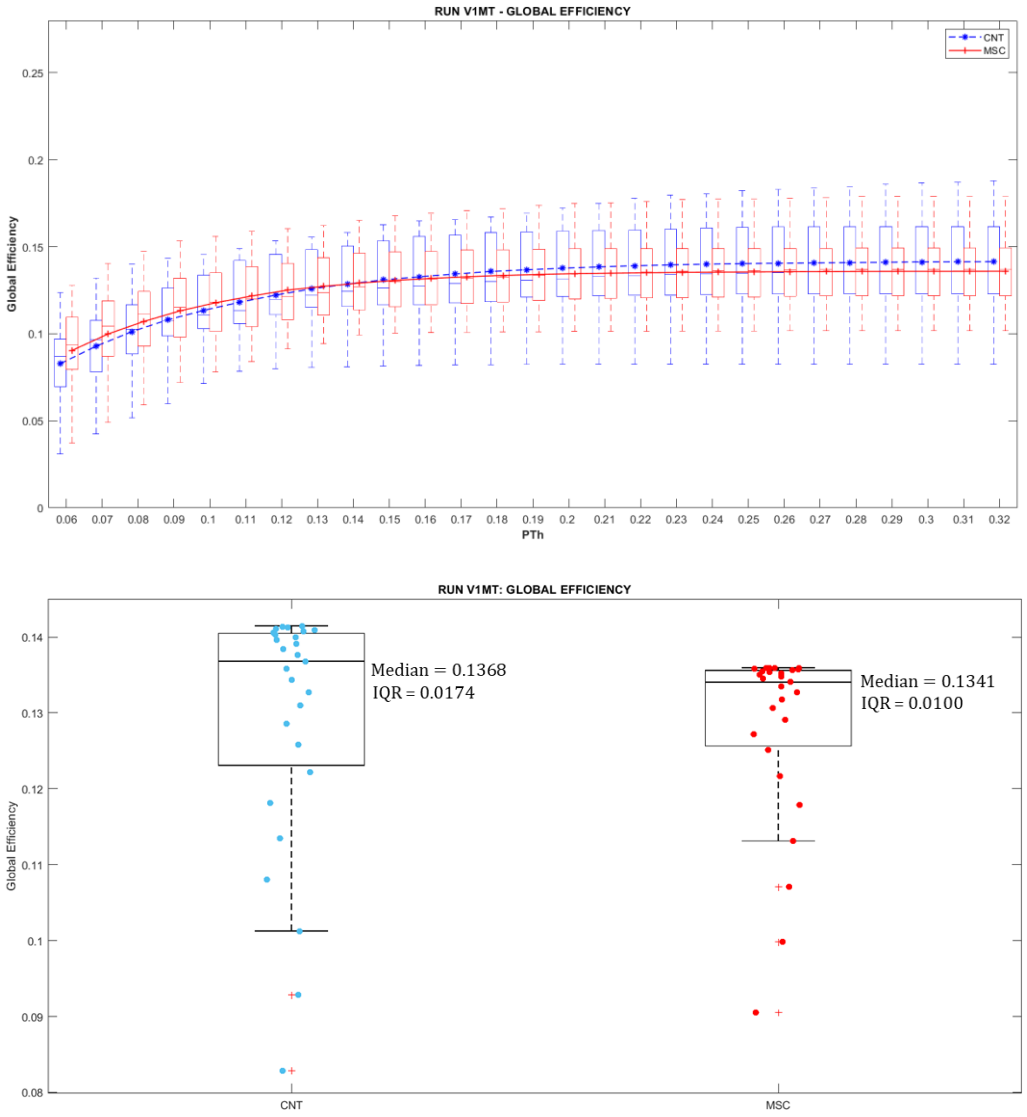

Figure 21- (top) Boxplot of the distribution of the **global efficiency** values in healthy controls (blue line) and MS patients (red line) over the selected range of thresholds. (bottom) Boxplots with the distribution of the mean values of the global efficiency at each threshold in both groups. IQR: inter-quartile range

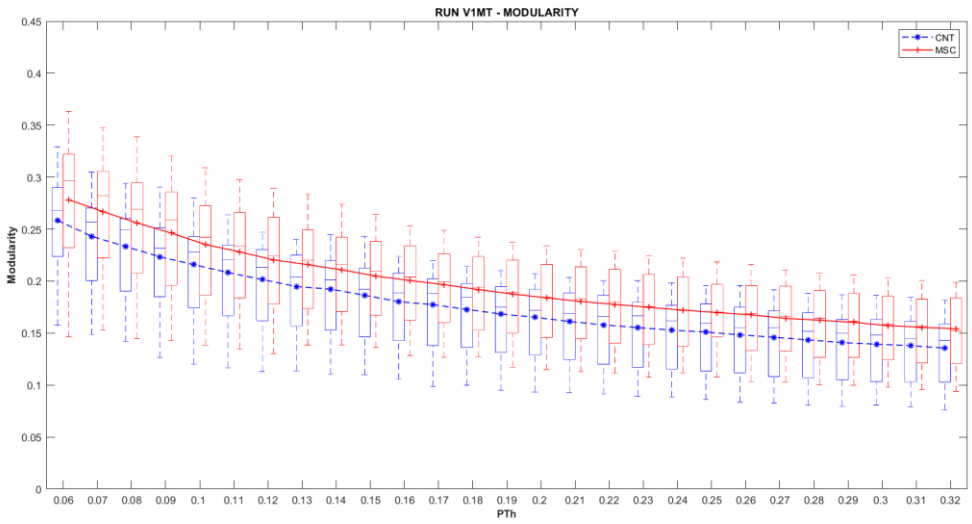

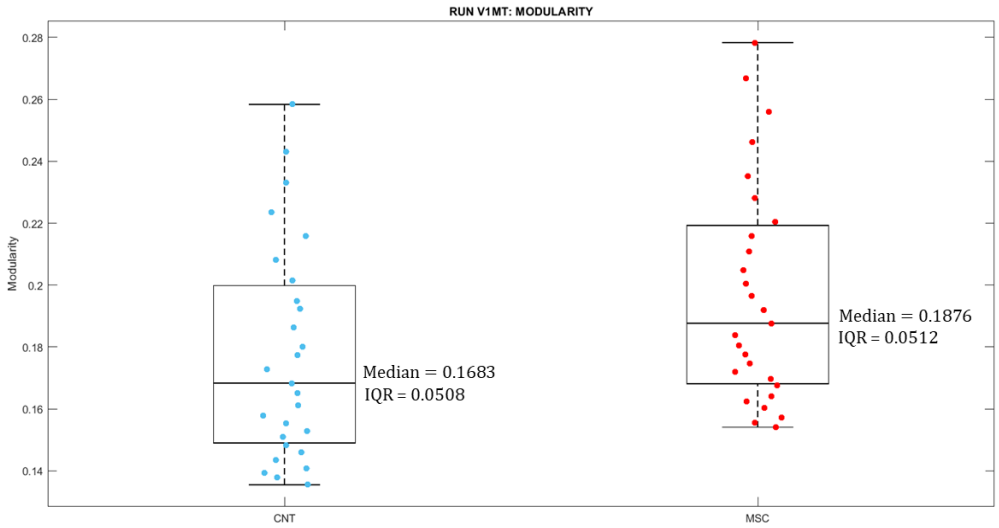

Figure 22- (top) Boxplot of the distribution of the **modularity** values in healthy controls (blue line) and MS patients (red line) over the selected range of thresholds. (bottom) Boxplots with distribution of the mean values of the global efficiency at each threshold in both groups. IQR: inter-quartile range.

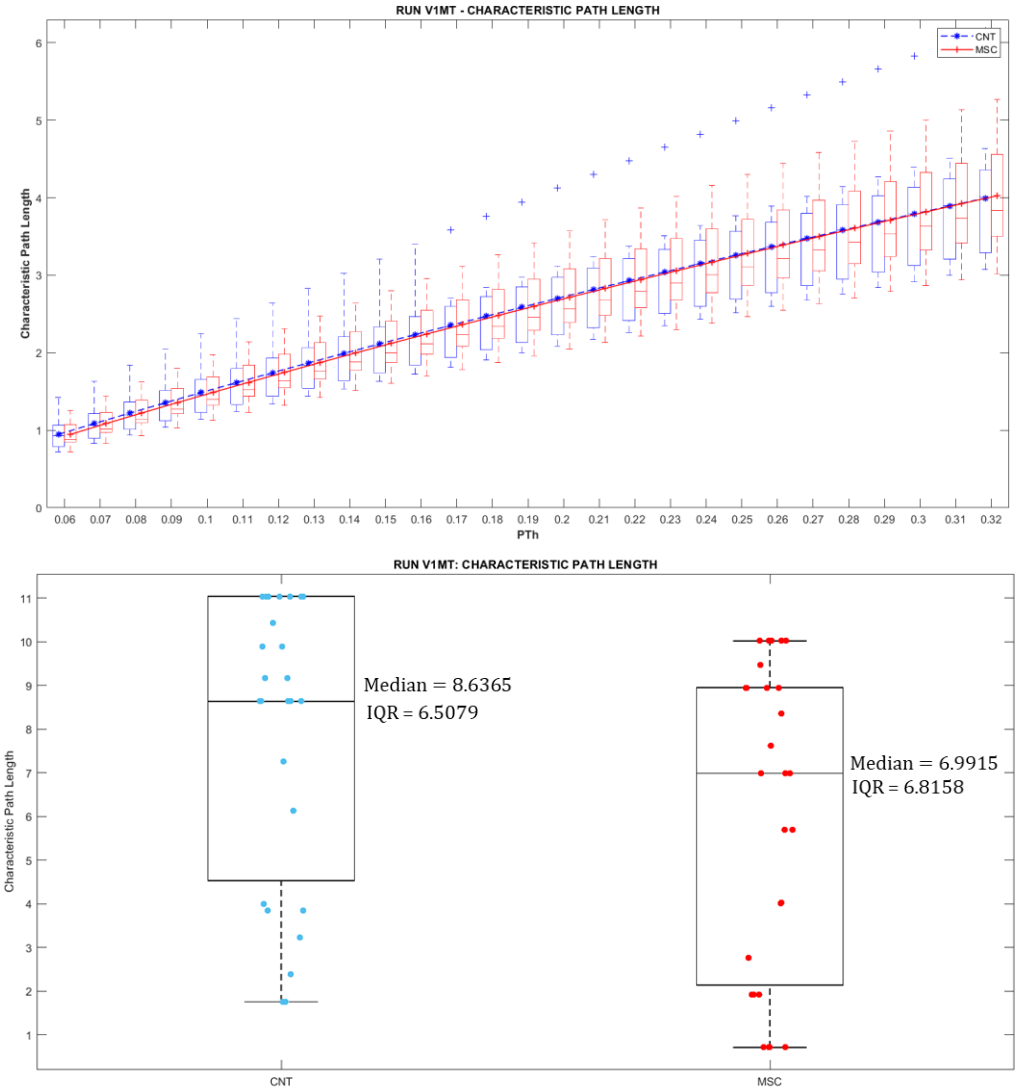

Figure 23- (top) Boxplot of the distribution of the **characteristic path length** values in healthy controls (blue line) and MS patients (red line) over the selected range of thresholds. (bottom) Boxplots with the distribution of the mean values of the characteristic path length at each threshold in both groups. IQR: inter-quartile range.

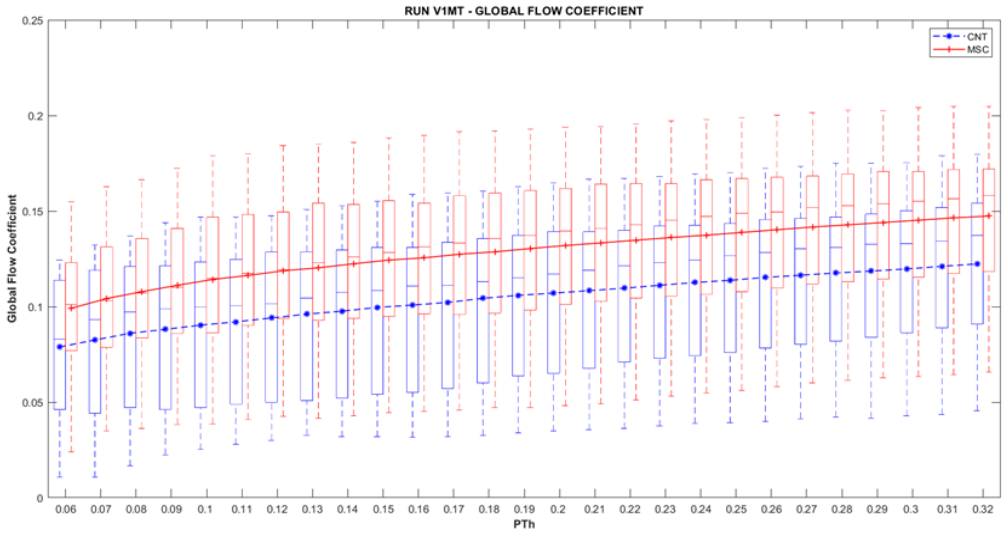

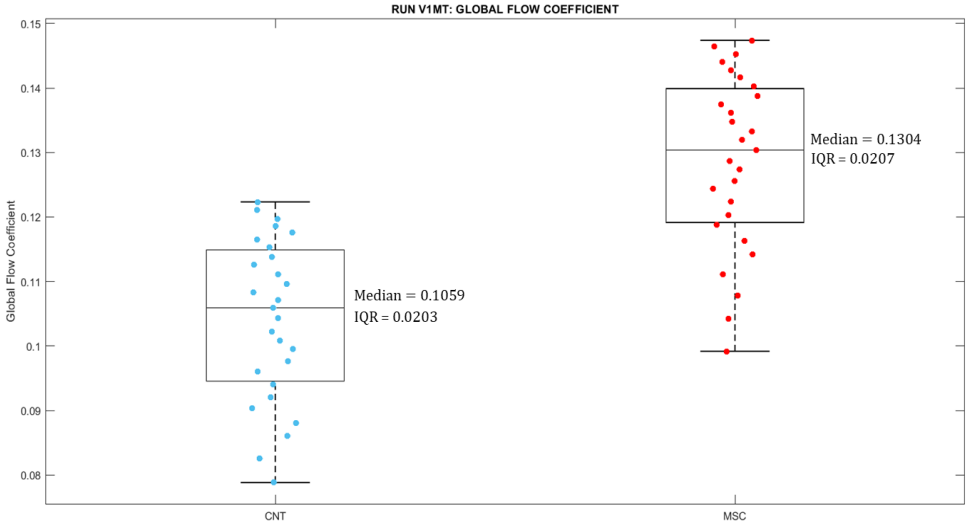

Figure 24- (top) Boxplot of the distribution of the **global flow coefficient** values in healthy controls (blue line) and MS patients (red line) over the selected range of thresholds. (bottom) Boxplots with the distribution of the mean values of the global flow coefficient at each threshold in both groups. IQR: inter-quartile range.

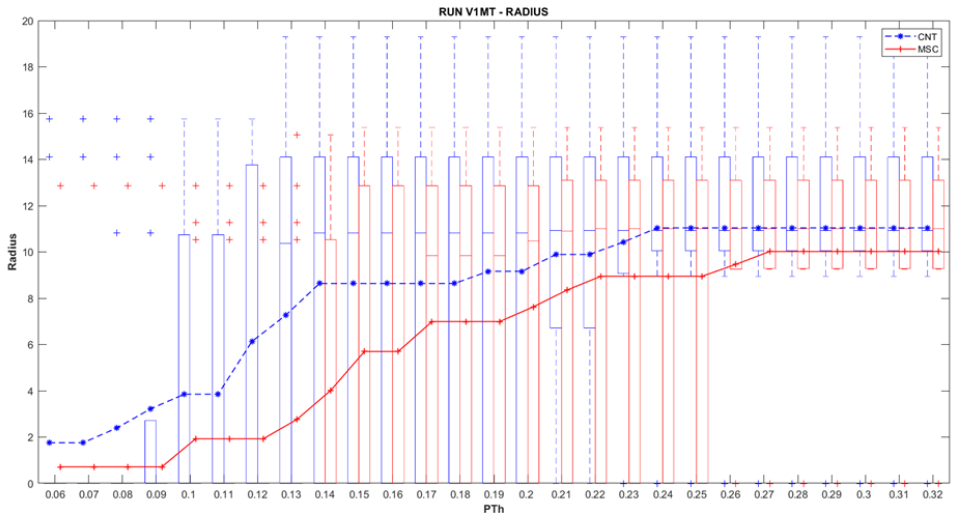

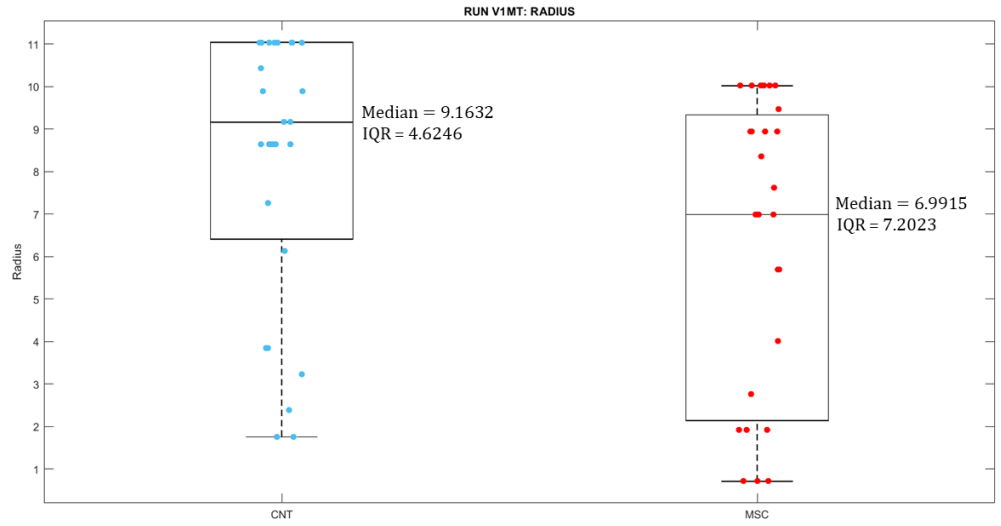

Figure 25- (top) Boxplot of the distribution of the **radius** values in healthy controls (blue line) and MS patients (red line) over the selected range of thresholds. (bottom) Box plots with the distribution of the mean values of the radius at each threshold in both groups. IQR: inter-quartile range.

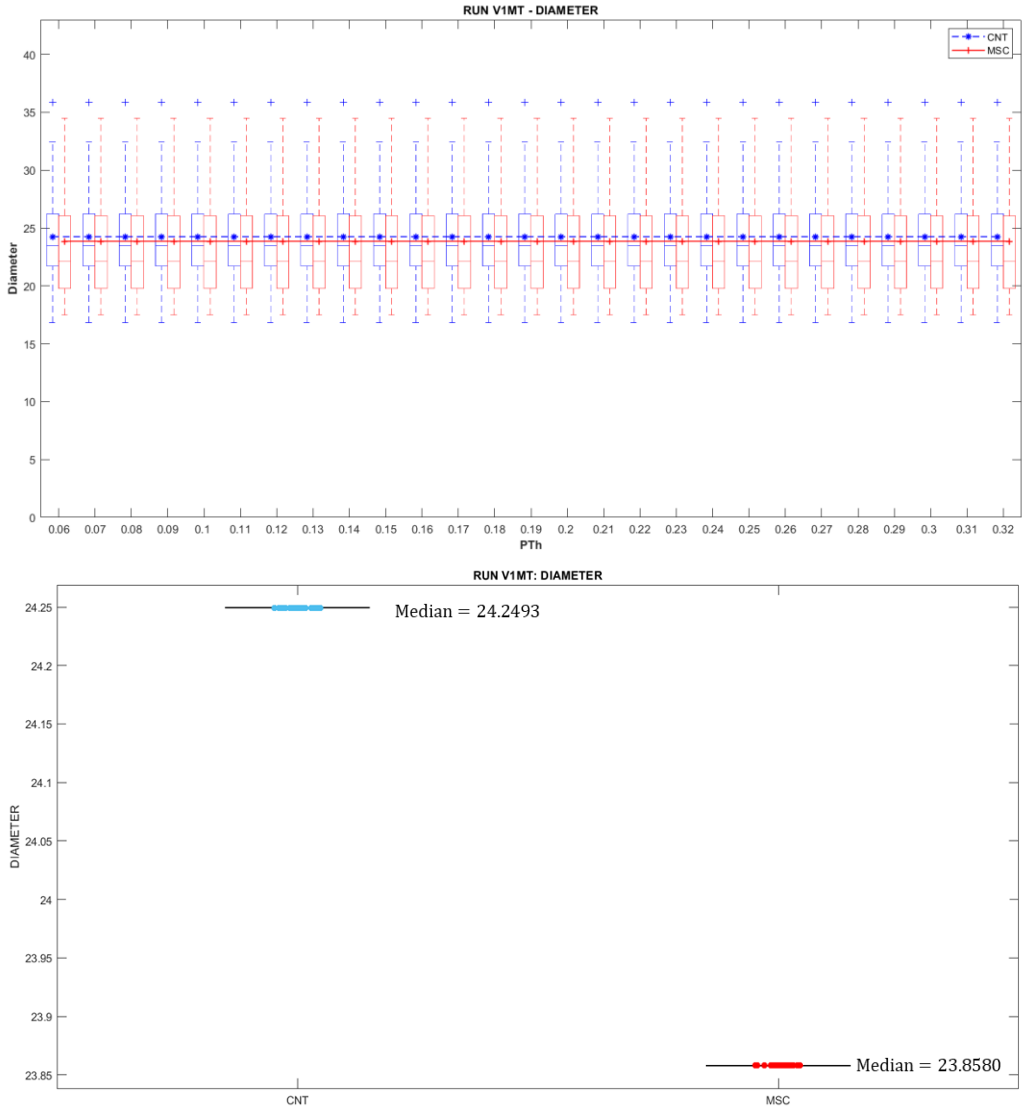

Figure 26- (top) Boxplot of the distribution of the **diameter** values in healthy controls (blue line) and MS patients (red line) over the selected range of thresholds. (bottom) Boxplots with the distribution of the mean values of the diameter at each threshold in both groups. IQR: inter-quartile range.

RUN BM

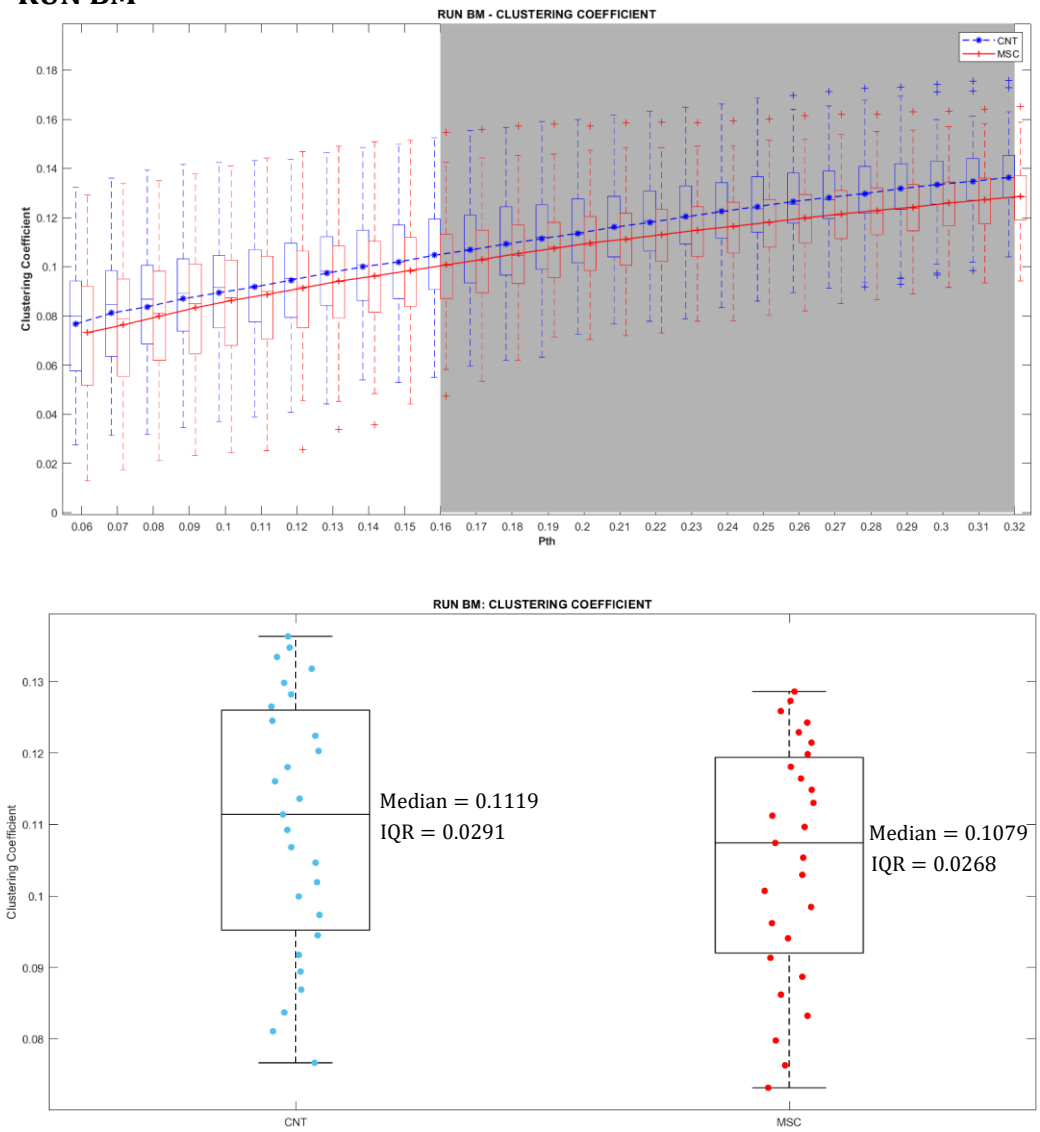

Figure 27- (top) Boxplot of the distribution of the **mean clustering coefficient** values in CNT (blue line) and MSC (red line) over the selected range of thresholds, shaded areas indicate the PTh's where between-group differences were statistically significant. (bottom) Boxplots with the distribution of the mean values of the mean clustering coefficient at each threshold in both groups. IQR: inter-quartile range.

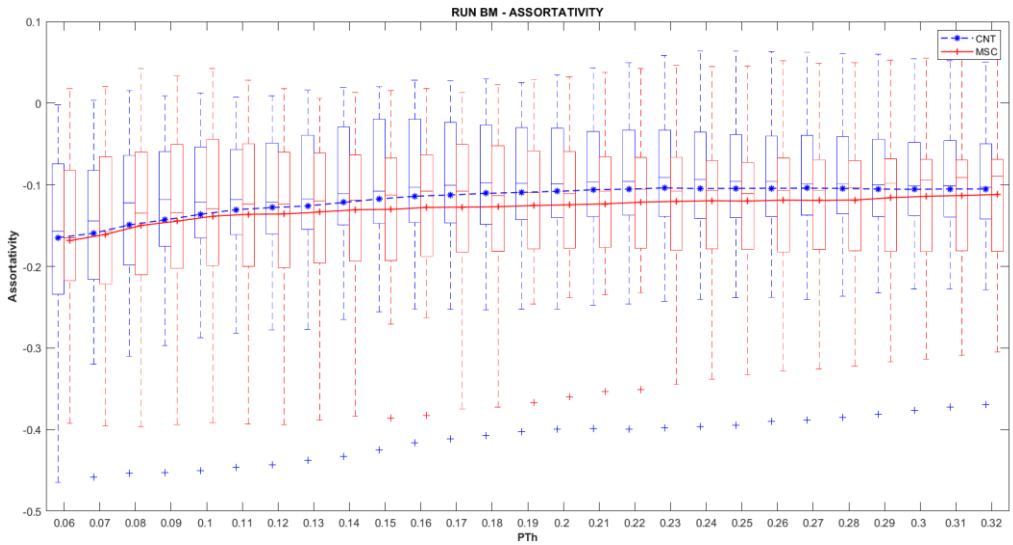

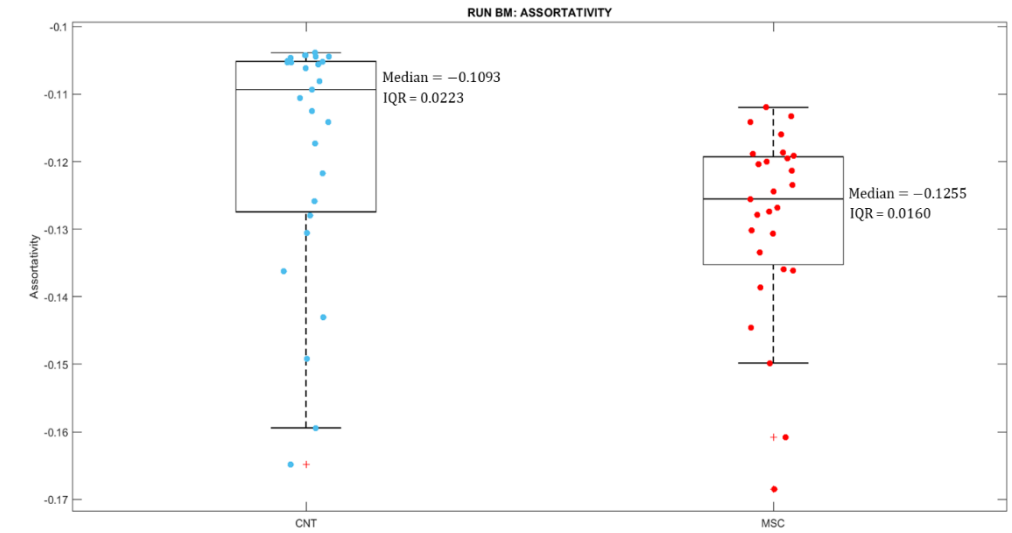

Figure 28- (top) Boxplot of the distribution of the **assortativity** values in healthy controls (blue line) and MS patients (red line) over the selected range of thresholds. (bottom) Boxplots with the distribution of the mean values of the assortativity at each threshold in both groups. IQR: inter-quartile range.

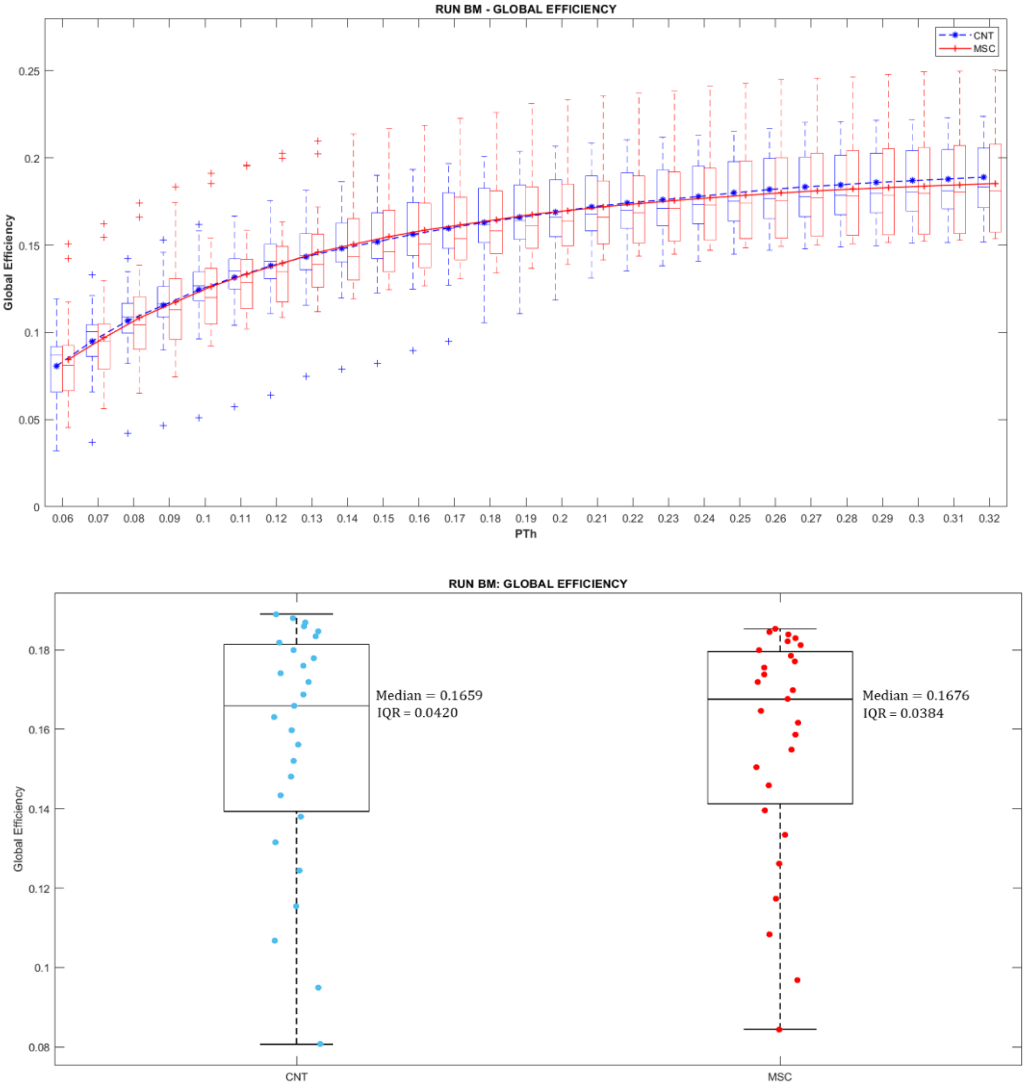

Figure 29- (top) Boxplot of the distribution of the **global efficiency** values in healthy controls (blue line) and MS patients (red line) over the selected range of thresholds. (bottom) Boxplots with the distribution of the mean values of the global efficiency at each threshold in both groups. IQR: inter-quartile range.

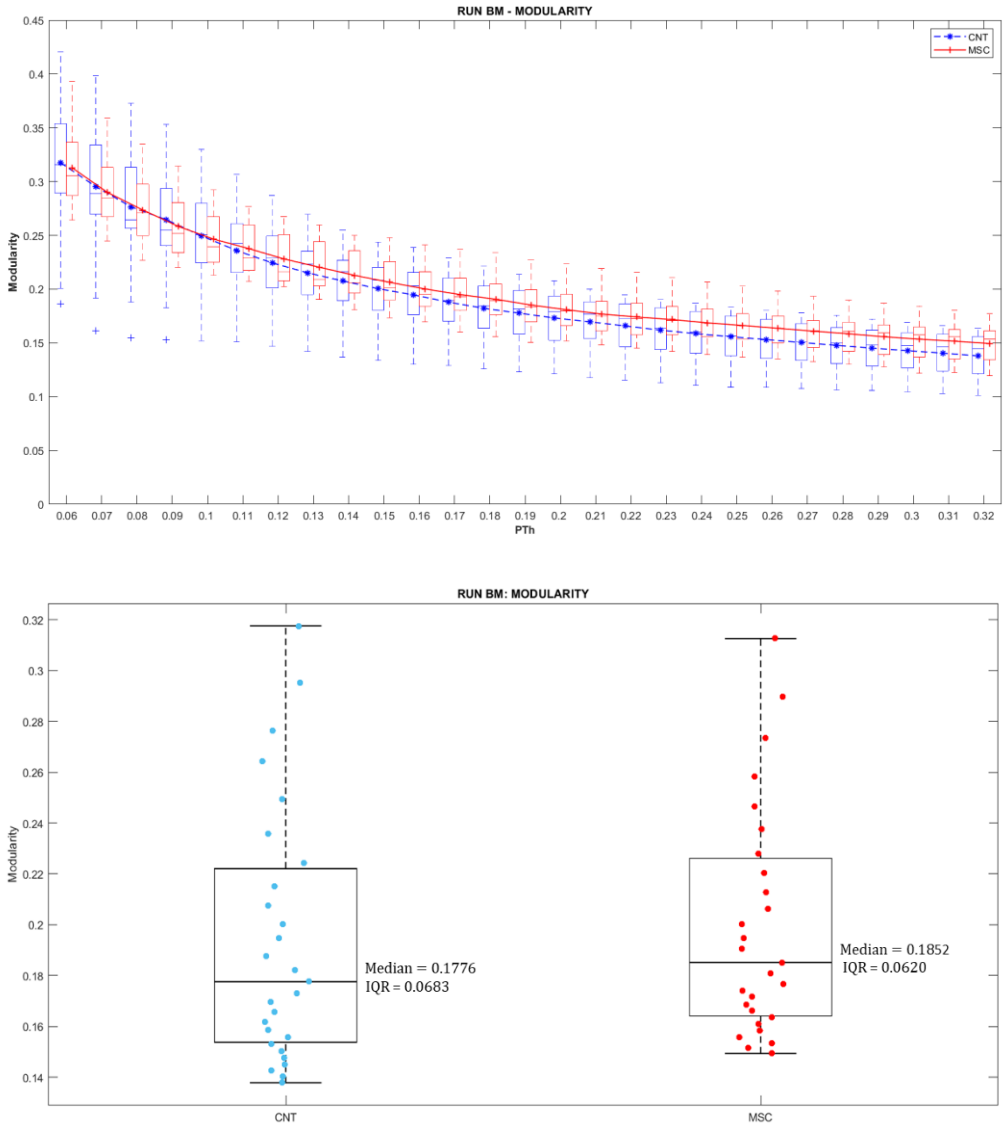

Figure 30- (top) Boxplot of the distribution of the **modularity** values in healthy controls (blue line) and MS patients (red line) over the selected range of thresholds. (bottom) Boxplots with distribution of the mean values of the global efficiency at each threshold in both groups. IQR: inter-quartile range.

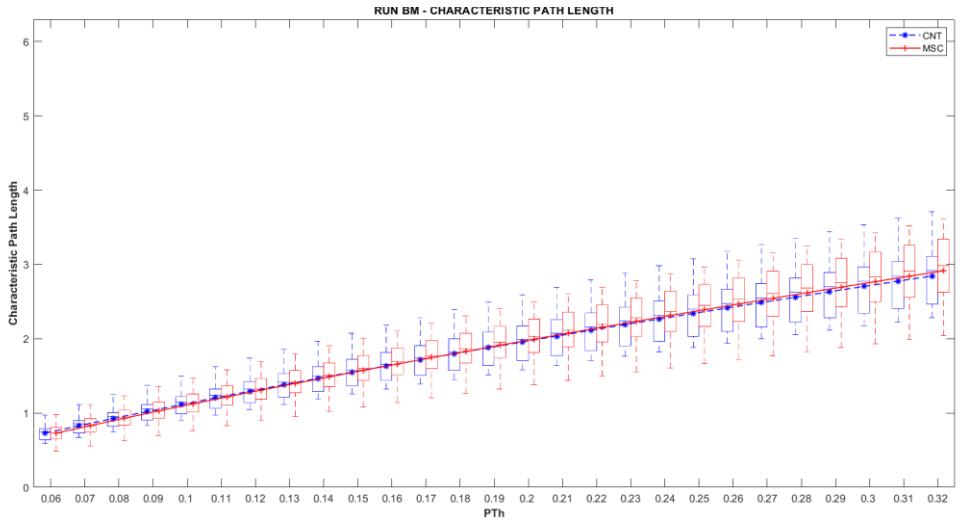

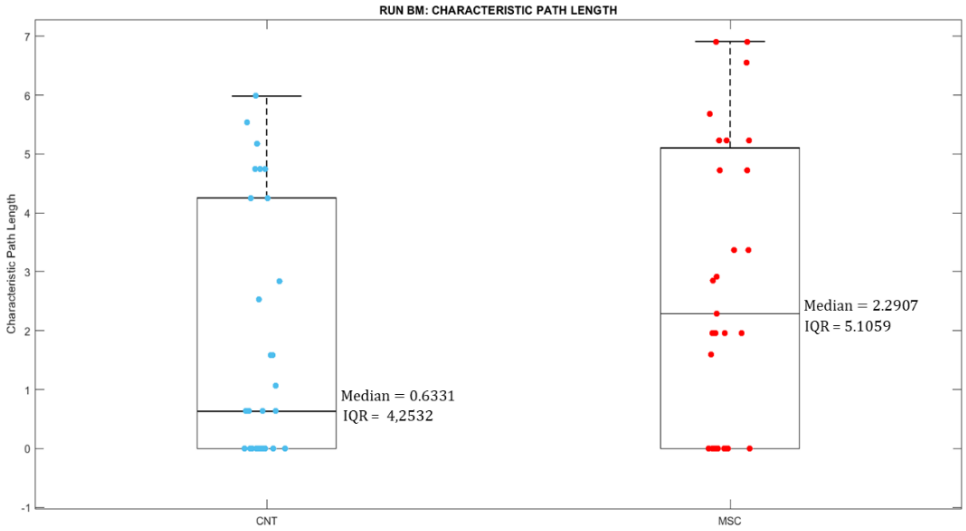

Figure 31- (top) Boxplot of the distribution of the **characteristic path length** values in healthy controls (blue line) and MS patients (red line) over the selected range of thresholds. (bottom) Boxplots with the distribution of the mean values of the characteristic path length at each threshold in both groups. IQR: inter-quartile range.

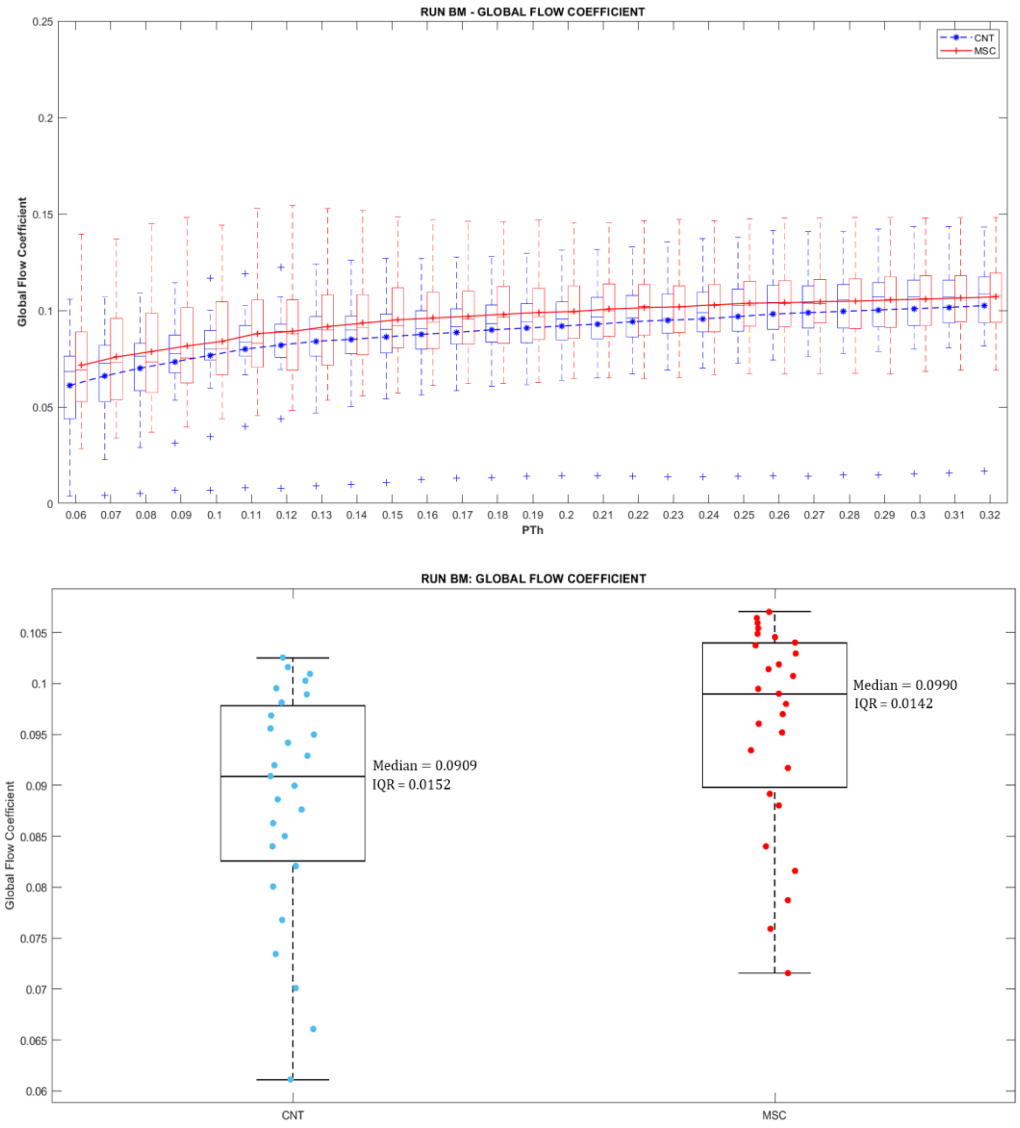

Figure 32- top) Boxplot of the distribution of the **global flow coefficient** values in healthy controls (blue line) and MS patients (red line) over the selected range of thresholds. (bottom) Boxplots with the distribution of the mean values of the global flow coefficient at each threshold in both groups. IQR: inter-quartile range.

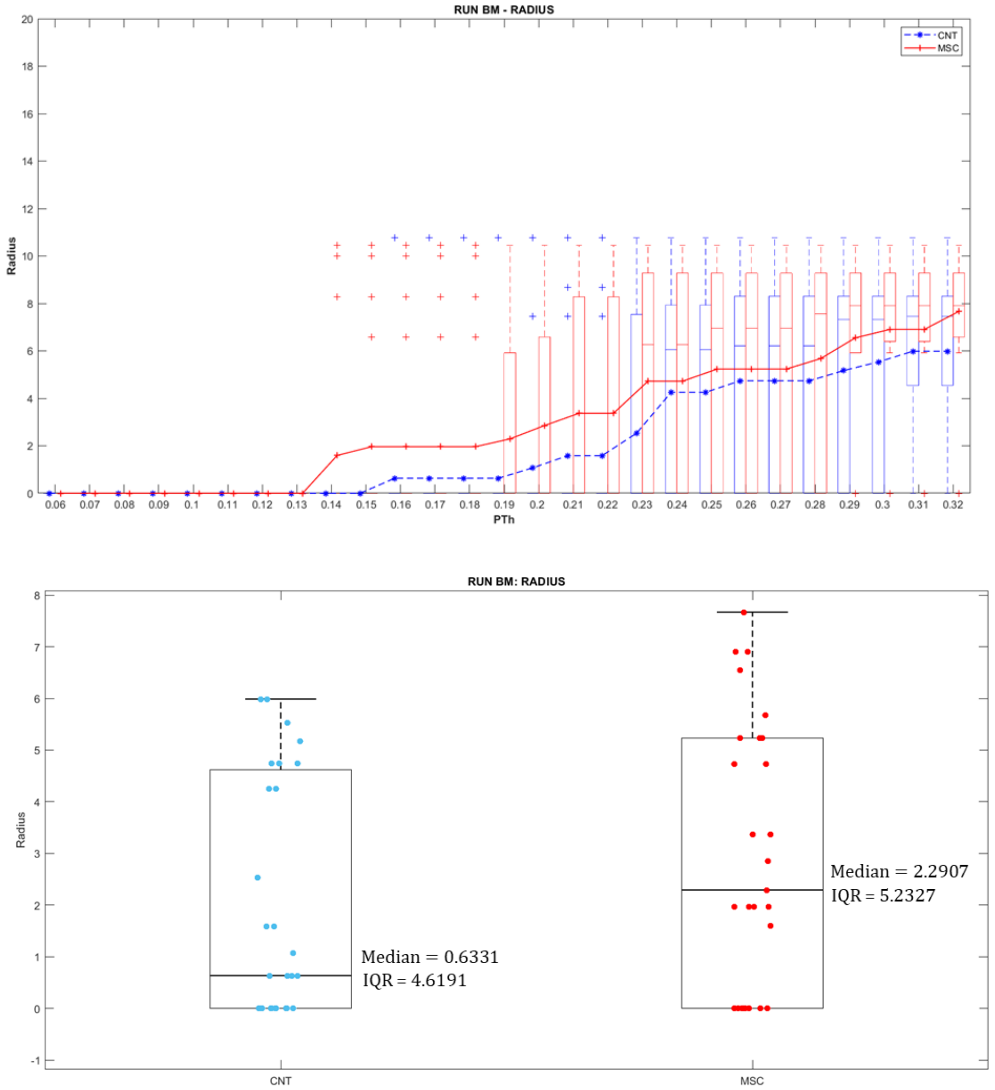

Figure 33- (top) Boxplot of the distribution of the **radius** values in healthy controls (blue line) and MS patients (red line) over the selected range of thresholds. (bottom) Box plots with the distribution of the mean values of the radius at each threshold in both groups. IQR: inter-quartile range.

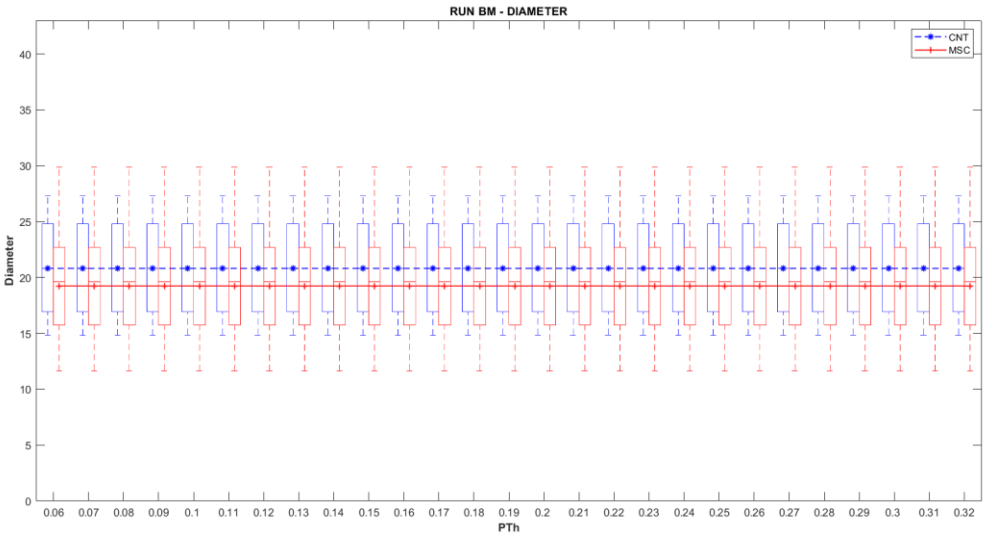

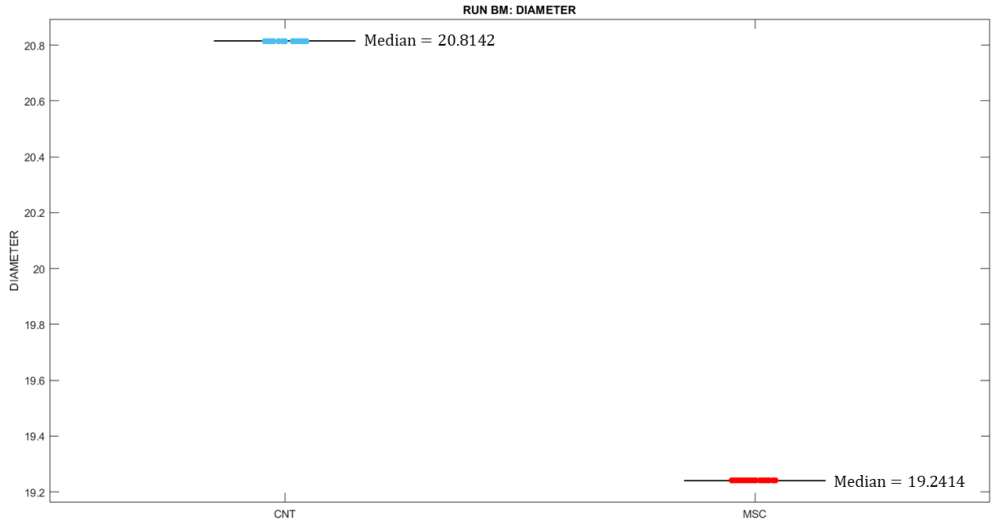

Figure 34- (top) Boxplot of the distribution of the **diameter** values in healthy controls (blue line) and MS patients (red line) over the selected range of thresholds. (bottom) Boxplots with the distribution of the mean values of the diameter at each threshold in both groups. IQR: inter-quartile range.

RUN RS

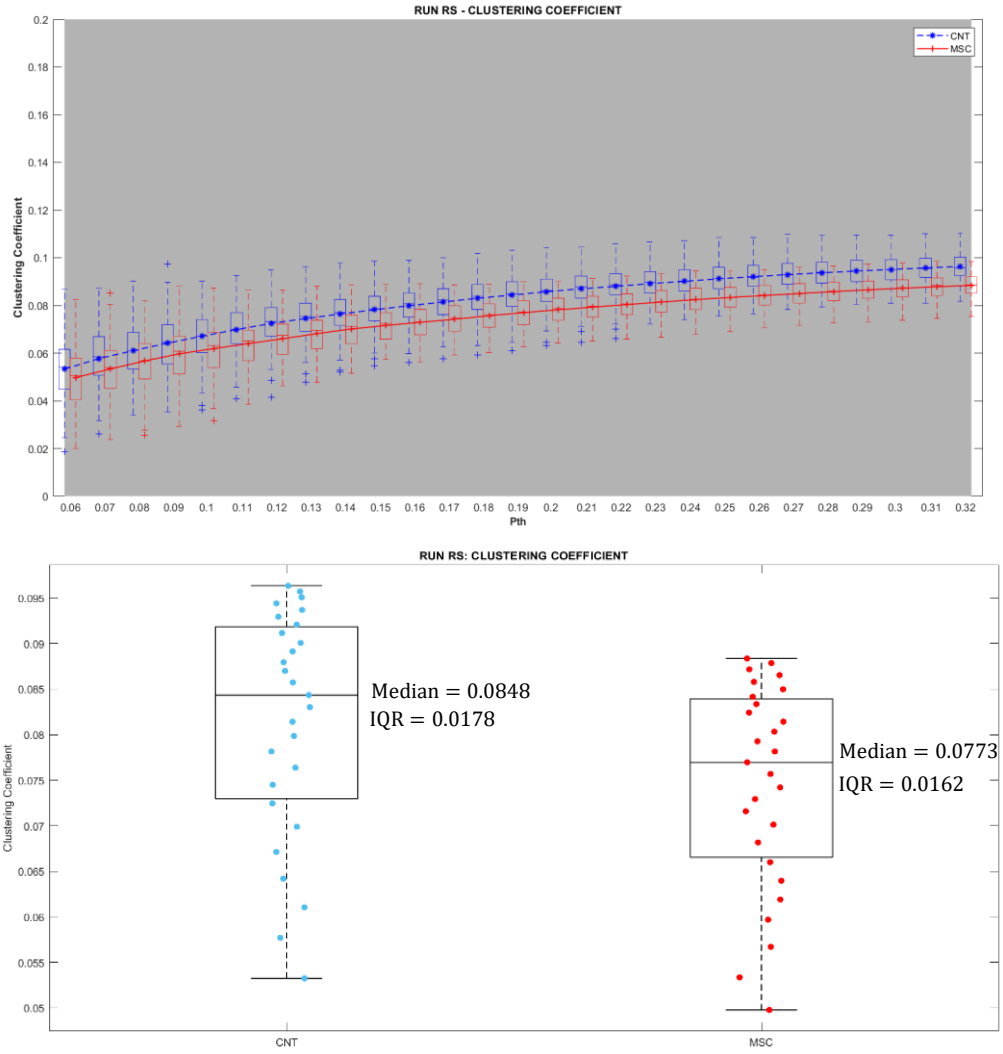

Figure 35- (top) Boxplot of the distribution of the **mean clustering coefficient** values in CNT (blue line) and MSC (red line) over the selected range of thresholds, shaded areas indicate the PTh's where between-group differences were statistically significant. (bottom) Boxplots with the distribution of the mean values of the mean clustering coefficient at each threshold in both groups. IQR: inter-quartile range.

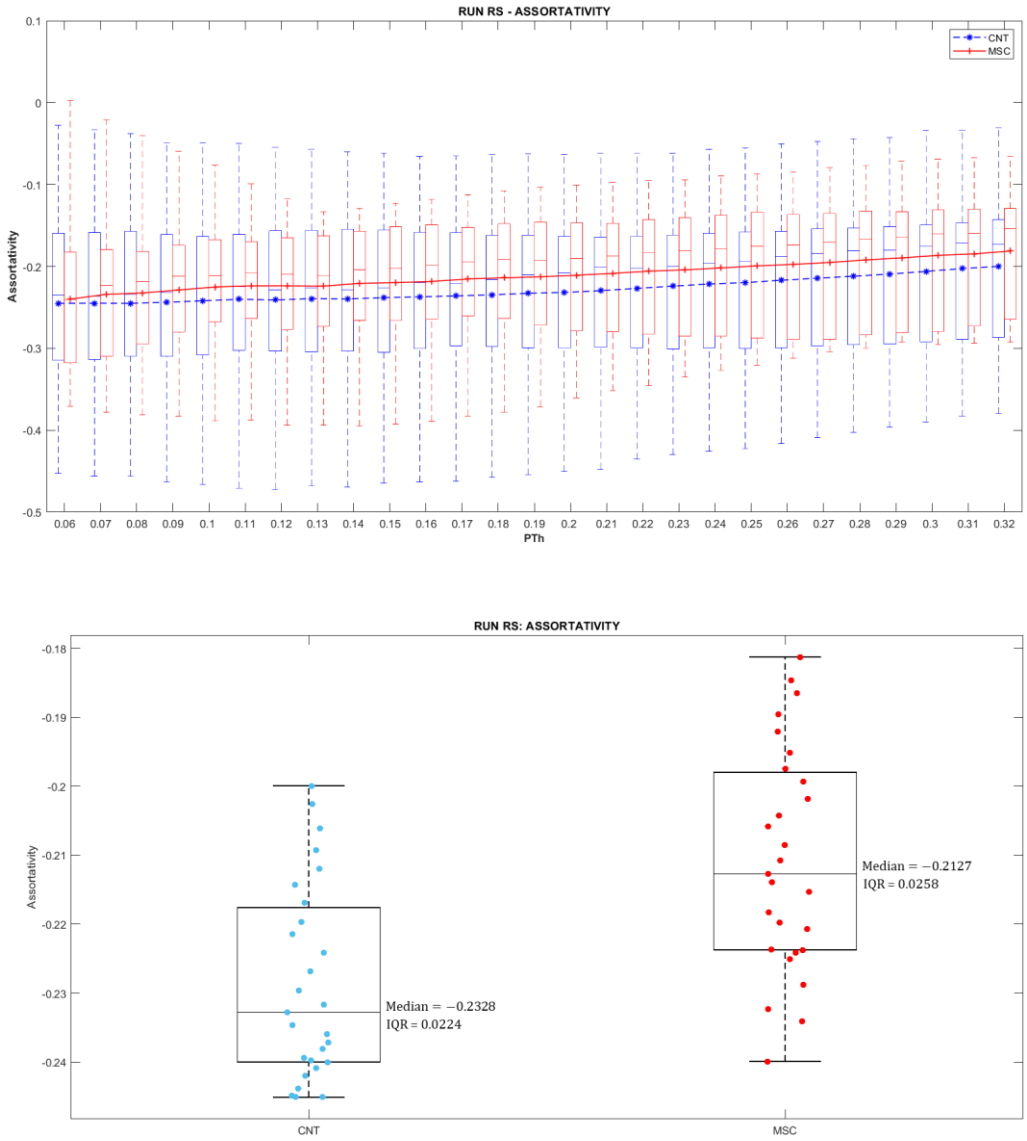

Figure 36- (top) Boxplot of the distribution of the **assortativity** values in healthy controls (blue line) and MS patients (red line) over the selected range of thresholds. (bottom) Boxplots with the distribution of the mean values of the assortativity at each threshold in both groups. IQR: inter-quartile range.

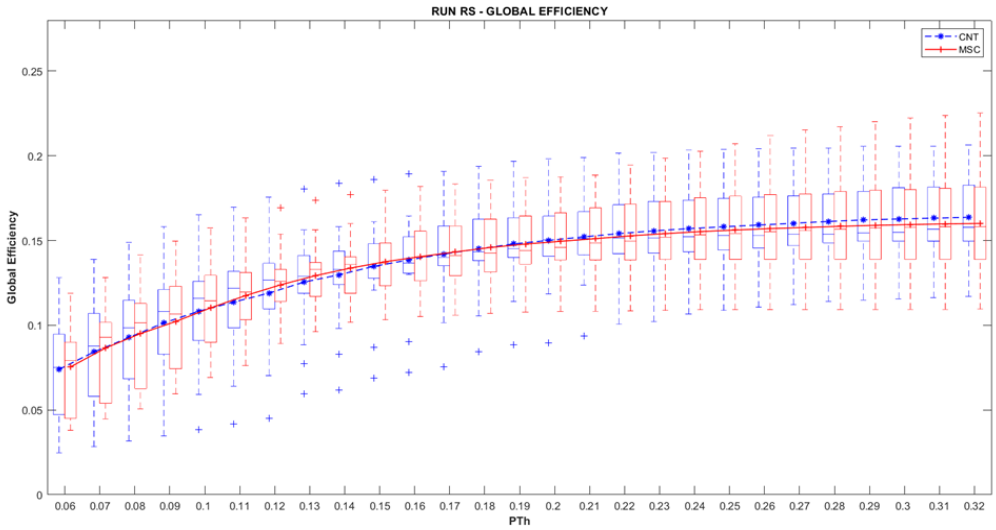

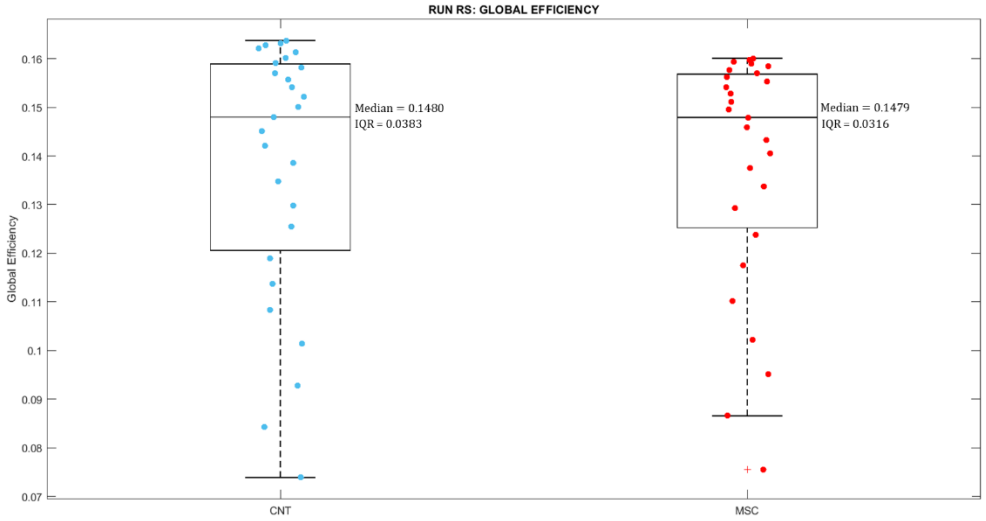

Figure 37- (top) Boxplot of the distribution of the **global efficiency** values in healthy controls (blue line) and MS patients (red line) over the selected range of thresholds. (bottom) Boxplots with the distribution of the mean values of the global efficiency at each threshold in both groups. IQR: inter-quartile range.

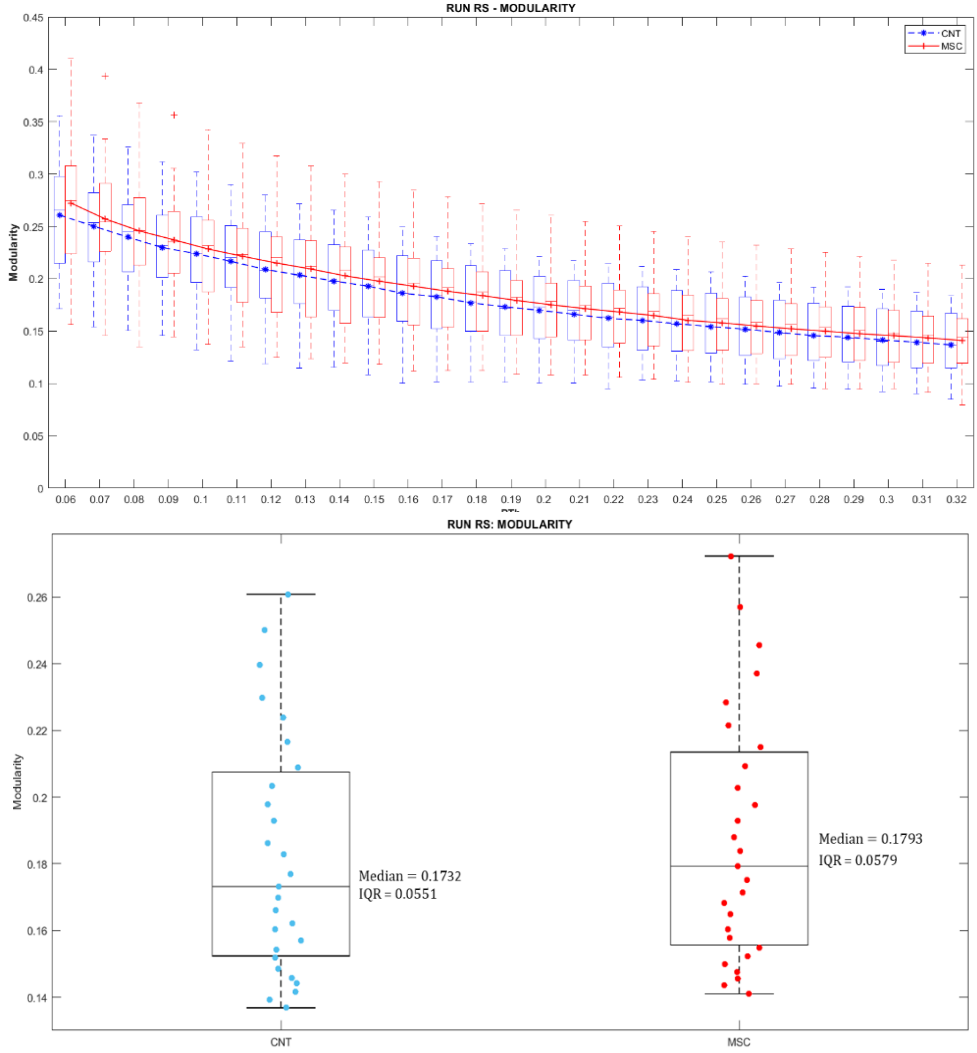

Figure 38- (top) Boxplot of the distribution of the **modularity** values in healthy controls (blue line) and MS patients (red line) over the selected range of thresholds. (bottom) Boxplots with distribution of the mean values of the global efficiency at each threshold in both groups. IQR: inter-quartile range.

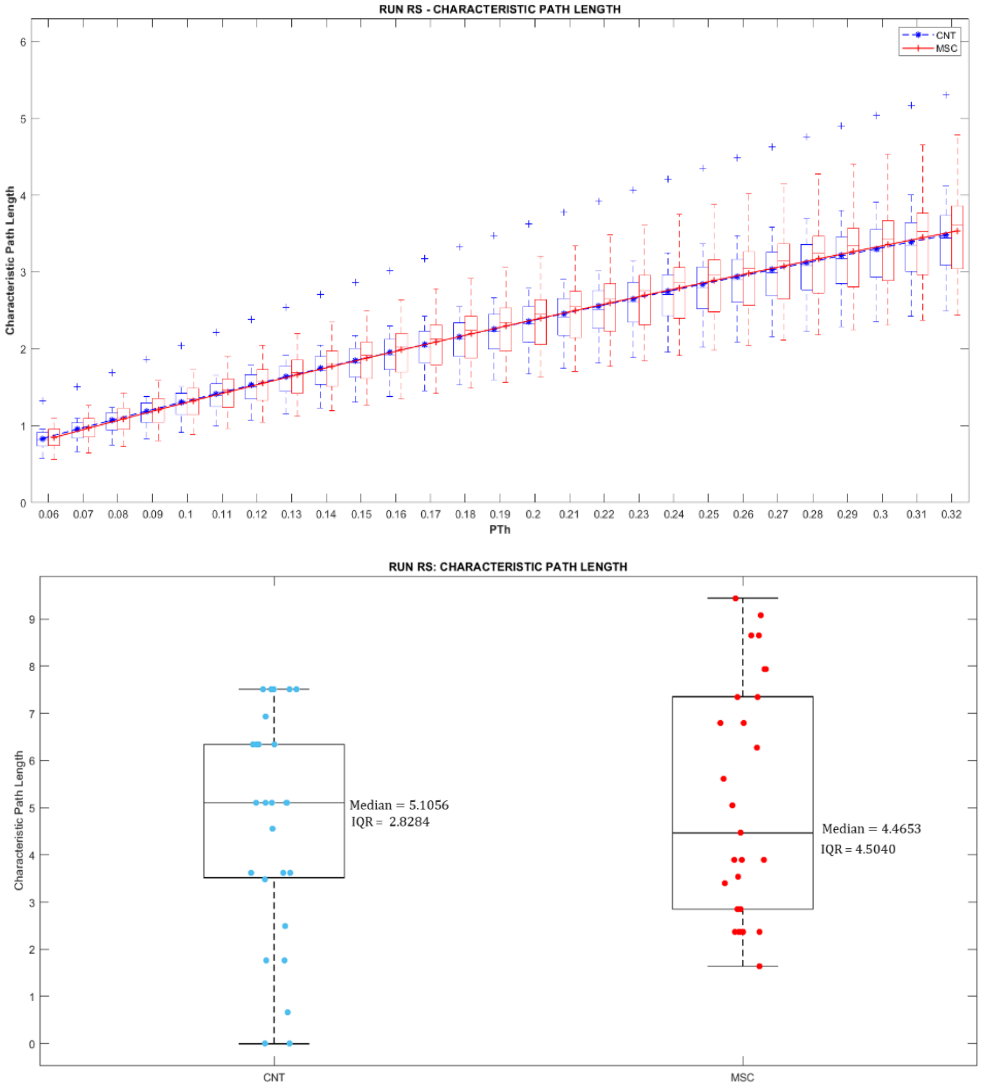

Figure 39- (top) Boxplot of the distribution of the **characteristic path length** values in healthy controls (blue line) and MS patients (red line) over the selected range of thresholds. (bottom) Boxplots with the distribution of the mean values of the characteristic path length at each threshold in both groups. IQR: inter-quartile range.

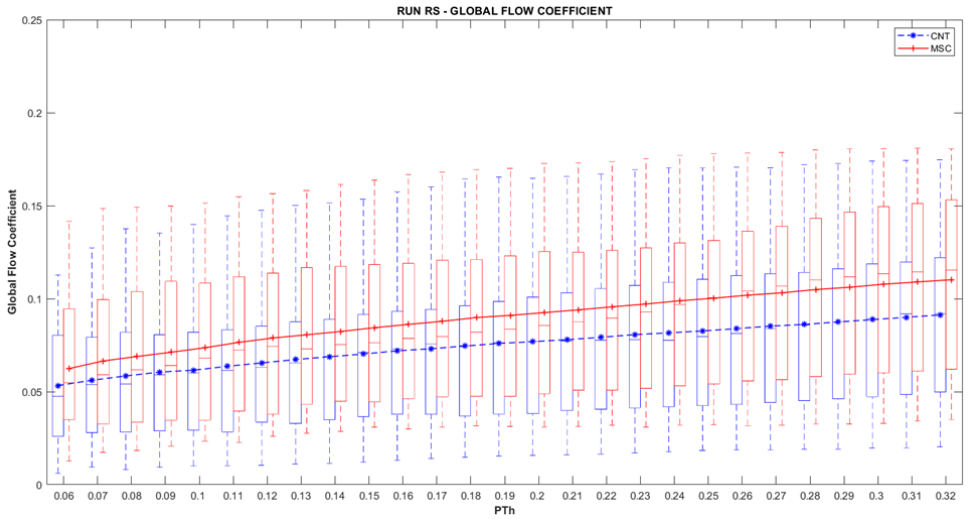

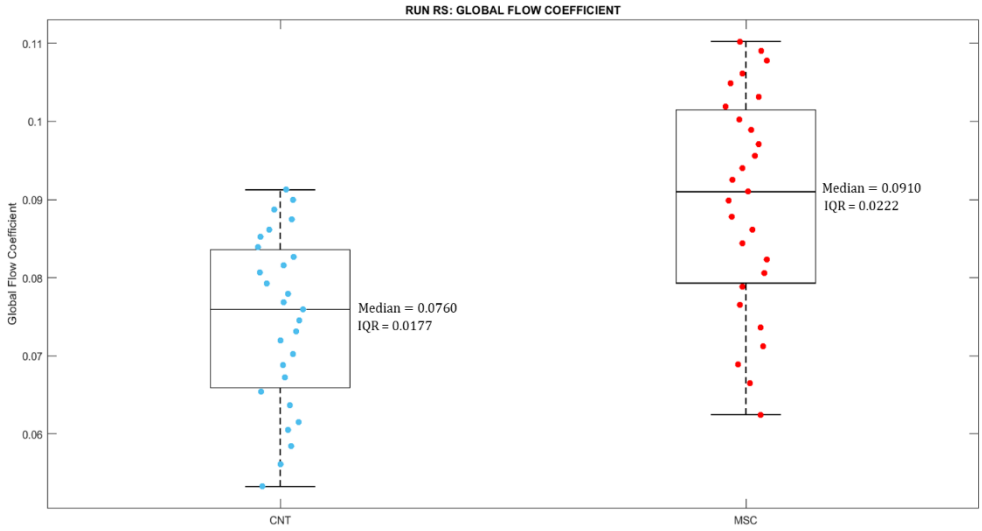

Figure 40- (top) Boxplot of the distribution of the **global flow coefficient** values in healthy controls (blue line) and MS patients (red line) over the selected range of thresholds. (bottom) Boxplots with the distribution of the mean values of the global flow coefficient at each threshold in both groups. IQR: inter-quartile range.

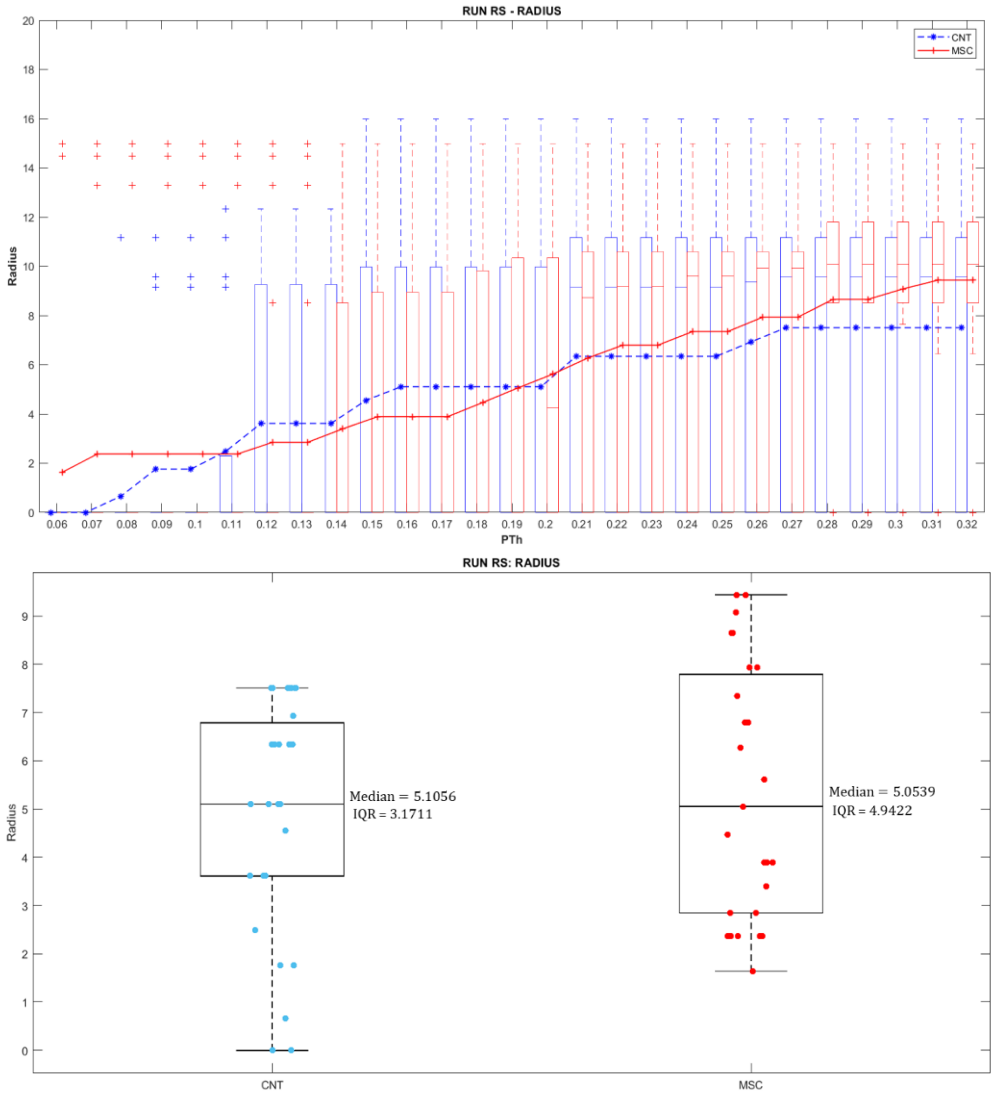

Figure 41- (top) Boxplot of the distribution of the **radius** values in healthy controls (blue line) and MS patients (red line) over the selected range of thresholds. (bottom) Boxplots with the distribution of the mean values of radius at each threshold in both groups. IQR: inter-quartile range.

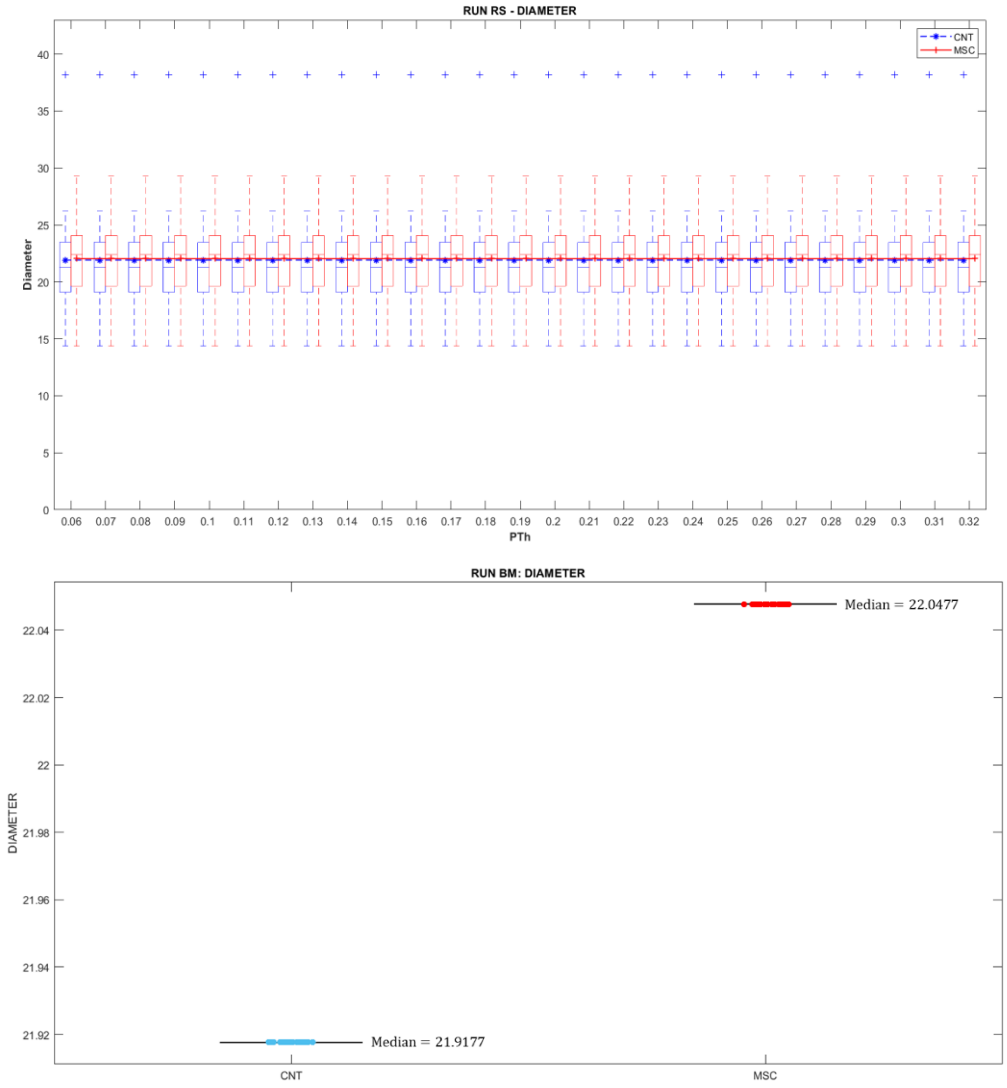

Figure 42- (top) Boxplot of the distribution of the **diameter** values in healthy controls (blue line) and MS patients (red line) over the selected range of thresholds. (bottom) Boxplots with the distribution of the mean values of the diameter at each threshold in both groups. IQR: inter-quartile range.

After performing the statistical test, only the mean clustering coefficient showed statistically significant differences between the two groups. Compared with healthy controls, MS patients displayed significantly lower values of mean clustering coefficient in every run, at several thresholds (shaded areas of figure 19, figure 27 and figure 35).

The clustering coefficient quantifies the number of connections that exist between the nearest neighbours of a node [31,35]. The mean clustering coefficient is the average of the clustering coefficients of all nodes, and lower values imply that the network is less interconnected, with a more random architecture.

The majority of MS studies using task-based or resting state paradigms claim that even in the early stages of the disease there is a general increase in modularity and

characteristic path length, and decreases in global efficiency, which entails that the network is more clustered, thought to reflect adaptive mechanisms for maintaining network function and compensate the structural damages (Welton et al.,[59]; Abidin et al., [61]).

Although in this case this was not found, these results are still valid since the patients in this study were diagnosed very recently, compared to the patients of the other studies, who despite having the same subtype of the disease, are in different stages of MS. Another factor that may be hindering the appearance of significant differences, is the fact that we are examining whole brain connectivity changes - although there are no immediate differences in the other connectivity measures, this does not mean that in a more specific and restricted network, where it is known that changes are occurring, these differences cannot arise.

It is interesting how during both tasks and resting state, the outcomes were the same regarding the measure that is shown to be significantly different between groups. Nevertheless, in resting state these differences were more consistent, as there were significant differences in all threshold values, which did not happen in the task runs. These results are in line with what we were expecting. In resting-state there is a relatively low fluctuation of the BOLD signal over time, the bold activity never oscillates brusquely, and therefore if there is any change in the value of the connectivity measurements, as all brain regions have a BOLD signal that is varying similarly, this change will be more likely to be detected. Therefore, physiologically it makes more sense for these differences to appear in a larger range of thresholds. On the other hand, under task conditions, the ROIs involved in the task will be more active, BOLD signal will deviate much more from baseline, and therefore the differences detected will be more specific. Precisely because they are more specific, it makes sense that on task any differences that may exist, are detected in a more restricted threshold range.

Figure 43 will provide a more intuitive understanding of this phenomenon.

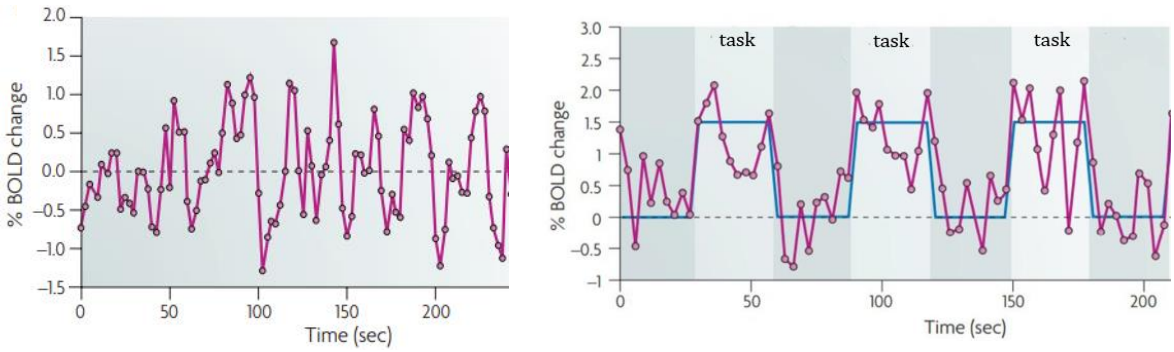

Figure 43- Comparison between the time course of the BOLD signal recorded during rest (left) and during task (right). The BOLD signal is represented by the purple line, the whiter areas are times when the task is being performed, and the grey darker areas are times when it is being rested (or baseline). (adapted from [82])

5.3.2. Local/nodal Connectivity measures

The thresholded matrices of each participant were used to extract the following local measures: total degree, in-degree, out-degree, total strength, in-strength, out-strength, subgraph centrality, K-coreness centrality, betweenness centrality, participation coefficient, pagerank centrality, local efficiency, node flow coefficient, total flow, and eccentricity.

For each of the 170 nodes (or ROIs), and for each participant of the two groups (CNT and MSC), the metrics mentioned above were calculated. Then, to simplify the analysis, the metric of each node was averaged for each group of participants, so there would only be a single metric value for each group and for each node. This reasoning was applied for each of the 27 thresholds (PTh's), so each node will have a value of the metric for each PTh. Summarizing, there will be 2 groups x 170 nodes x 27 PTh's values for every metric. These data were tested for normality using the KS test, available in MATLAB, and all returned as not normally distributed. Thus, statistical analysis using the Wilcoxon Rank Sum test was performed to find which metrics showed significant differences between groups (with a significance level at $p<0.05$) and, consequently, which nodes could be impacted by the disease.

It was only considered that a node's metric was statistically different between groups when, after the performance of the statistical test, it showed statistically significant differences in more than half of the number of thresholds. To demonstrate with an example, in the V1MT run, the left pre-central gyrus (node 1) showed that in one measure (total flow, i.e., the flow of information that passes through that node) the p-values were less than 0.05 in more than 14 PTh's, hence, we can consider that this node in particular is affected by MS, during the performance of this task. On the other hand, the right pre-central gyrus (node 91) showed no significant differences in any of the metrics since it did not have $p<0.05$ in more than half of the thresholds. For that reason, we can assume that this node may not be as affected by the disease.

Thus, to make it easier to identify which nodes showed significant differences in each metric, and also the number of times they showed statistical differences along the PTh's, bar plots for all the runs were constructed (figure 44) as well as a 3D representation of the mentioned nodes (figure 45), with the BrainNet Viewer toolbox for Matlab, where the diameter of each sphere is proportional to the number of measures that showed significant

differences. Each color present on the bars correspond to the regions indexed in table 6 (section 4.2.1), as shown in the 3D image.

With the knowledge of the significantly different local metrics of the nodes it will be possible to understand more about each node's role within the network and what might take place if it is compromised due to the structural damage induced by MS.

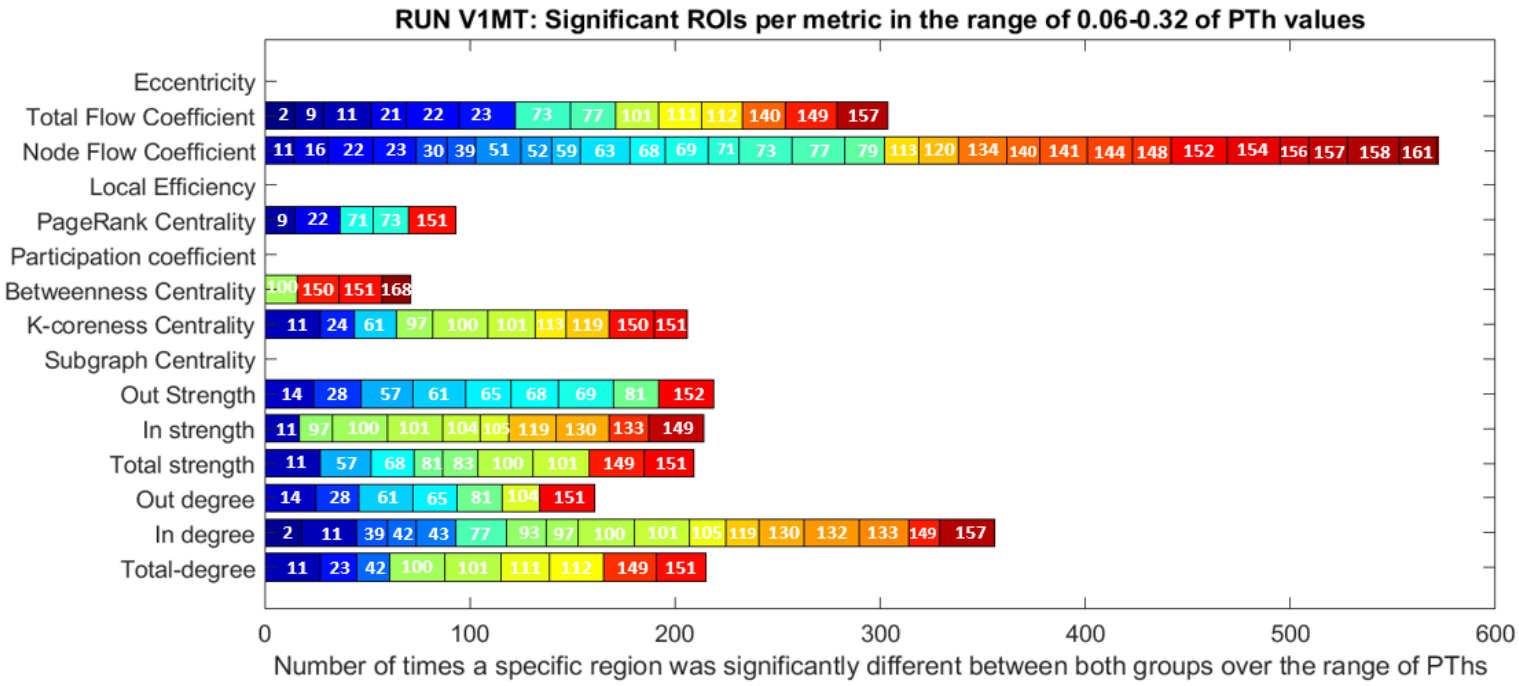

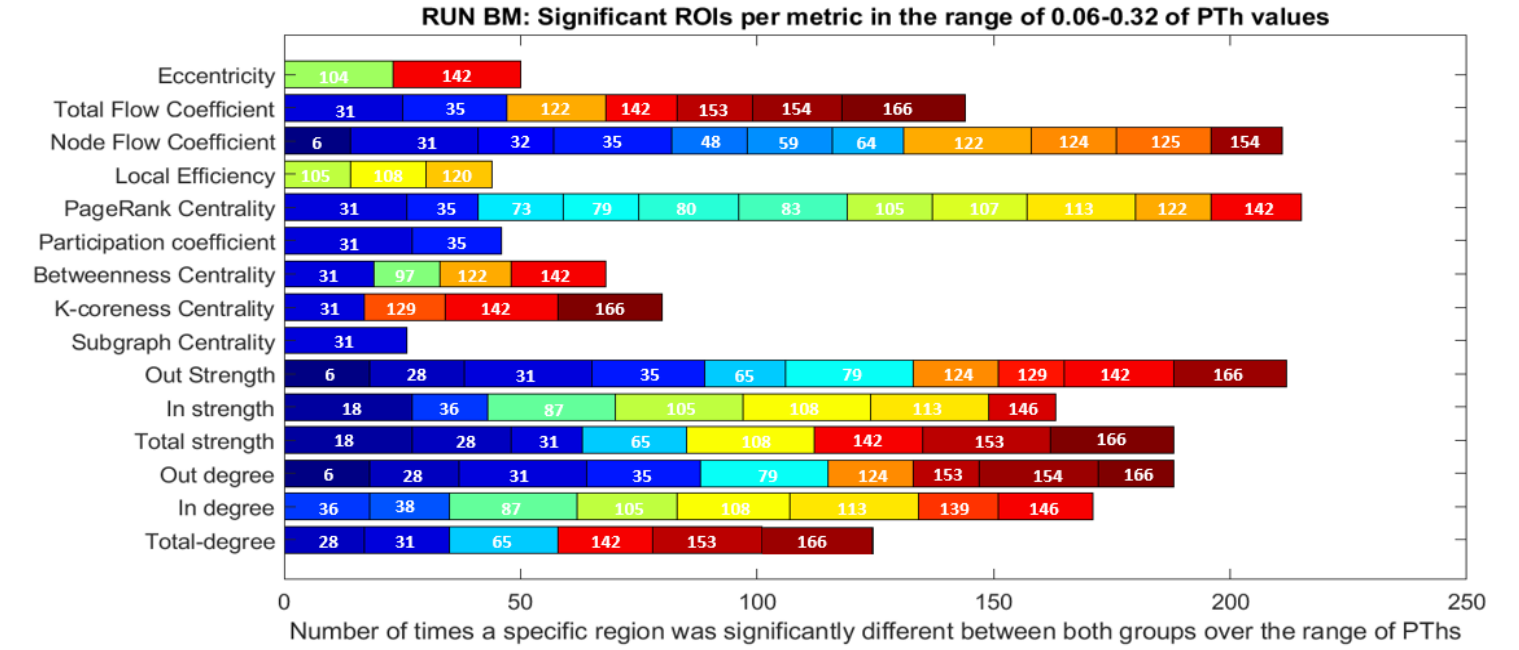

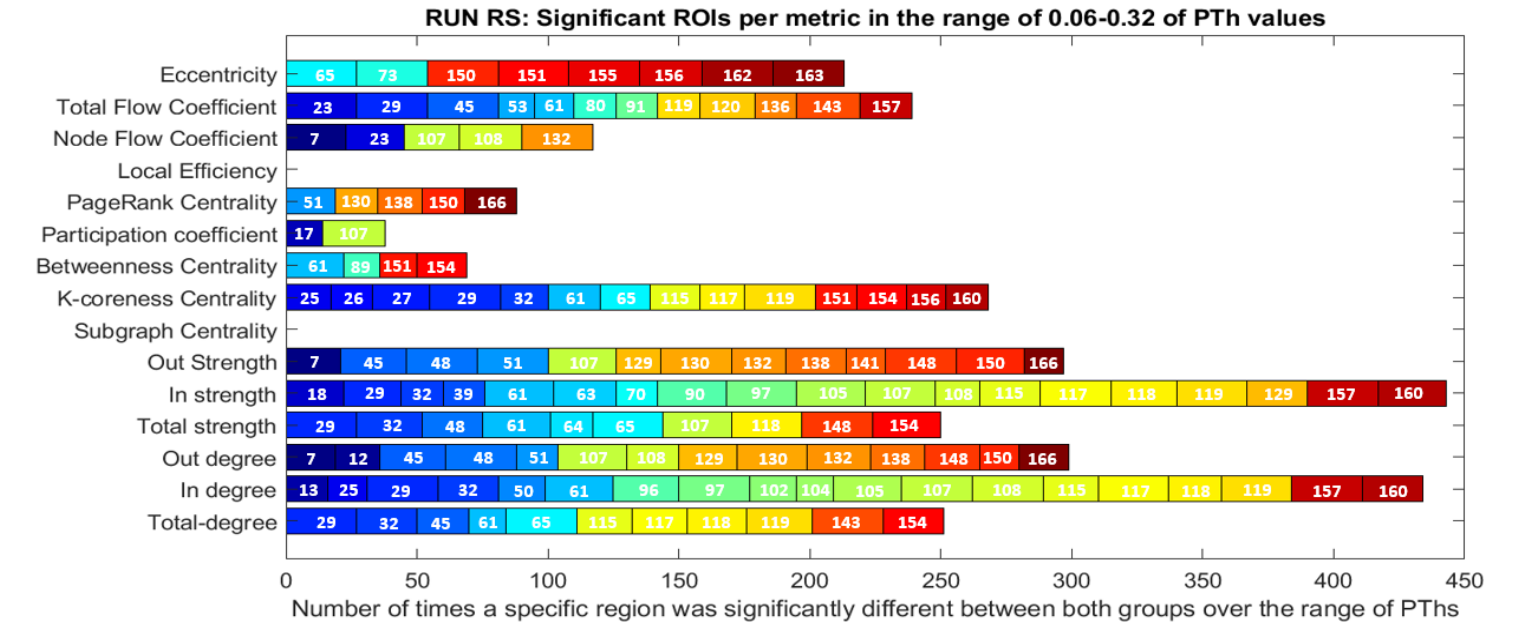

Figure 44- Bar plot of the number of times a specific region had a statistically significantly different metric between groups in more than half of the thresholds, in the V1MT run (top), BM run (middle), and RS run (bottom). The numbers correspond to the regions according to the table 6.

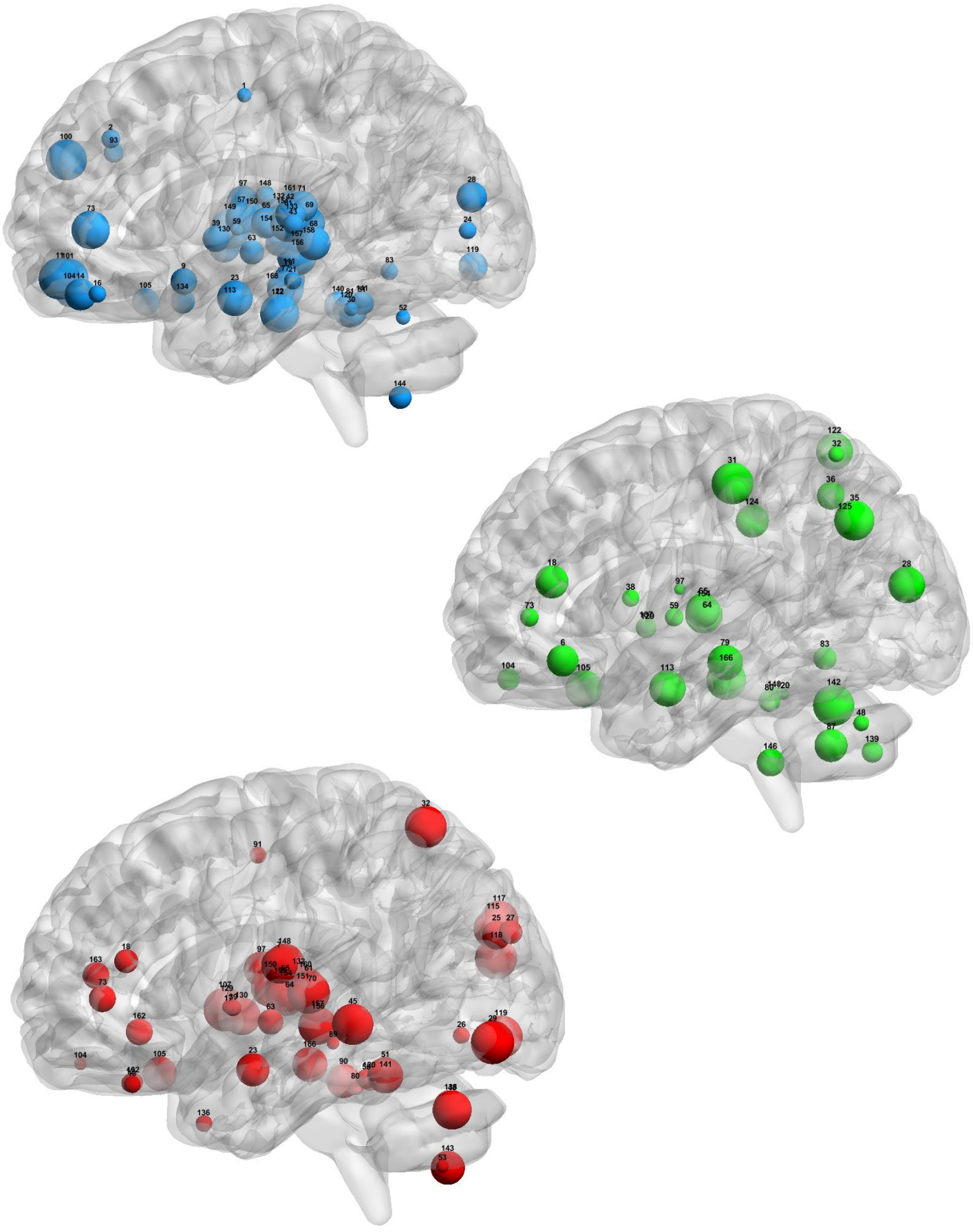

Figure 45- 3D representation of the regions mentioned in the Fig.44 in the V1MT run (above), BM run (middle), and RS run (below).

In the V1MT run, there were a total of 59 regions with local metrics which showed statistical differences between the MSC and CNT groups. The top three local measures where most ROIs had meaningful differences were in the node flow coefficient, in-degree, and the total flow coefficient. It is also worth noting that in local efficiency, eccentricity, and subgraph centrality no ROIs showed metrics with statistical differences between groups.

In the BM run, there were fewer regions with local metrics which showed statistical differences between the MSC and CNT groups, but still 35 regions present these significances. Node flow coefficient is once again one of the measures with more ROIs that showed differences, as well as out-strength and PageRank centrality.

In the RS run, a total of 56 regions showed local metrics with significant differences between groups. In-degree, in-strength and k-coreness centrality are the three nodal graph measures that presented the highest number of ROIs with statistical differences. On the other hand, local efficiency and subgraph centrality didn't show significant differences in any ROI.

More information about these regions and the local measures is listed in table 15 for the V1MT run, table 16 for the BM run, and table 17 for RS run in appendix II). The first column of each table represents the regions that showed metrics statistically different between groups in more than half of the thresholds. Each entry has the minimum p-value and corresponding PTh, plus the difference between the measure of the two groups (MSC-CNT). If the difference is positive, this means that in that region, the value of the measure is increased in the MSC group (represented in grey). On the contrary, if the difference is negative, the value of the measure is decreased in the MSC group (represented in white). These differences are also represented in matrix form with all local measures in the x-axis and the respective regions in which this measure is significantly different between groups in the y-axis.

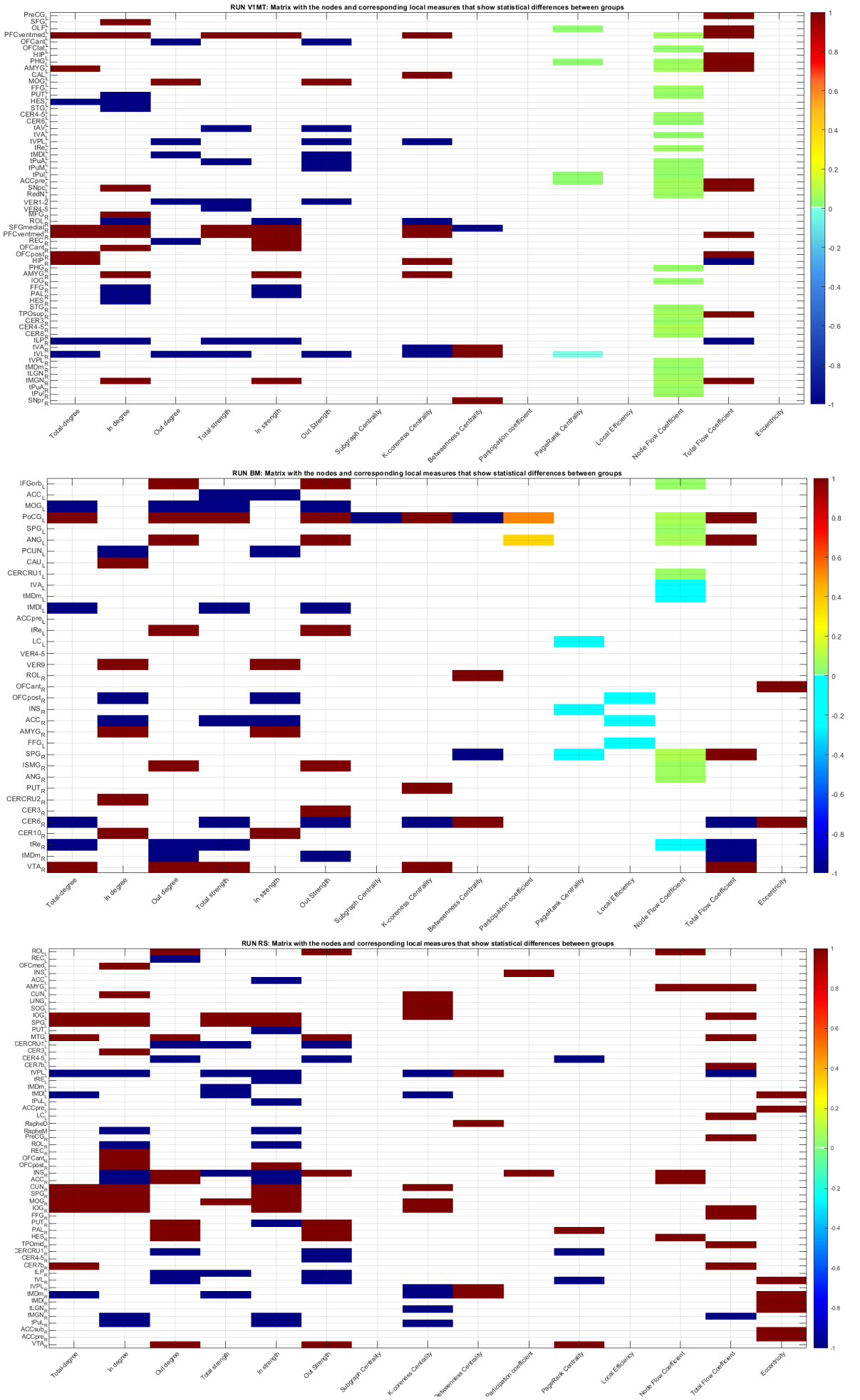

Figure 46- Matrix with the nodes and corresponding local measures that are statistically significantly different between groups in the V1MT run (top), BM run (middle) and RS run (bottom). The colorbar represents the results ranging from -1 (blue) to 1 (red) of the differences between the measure of the two groups (MSC-CNT). Hot colors represent a higher difference in the MS patients' group and cool/blue colors represent a higher difference in the healthy control group.

In all the three runs we could observe both an increase in the value of the connectivity measures in patients, as well as a decrease in connectivity in MS.

Overall, the brain regions seem to have a more increased value of the connectivity measures in the MS patients. As it can be seen from figure 46, in the less demanding tasks this is easier to notice, since there are more cells colored in hot colors than cool colors, while in the run BM it is more balanced. For the run V1MT in particular, it is evident that, in some measures (such as the node flow coefficient), all regions have the connectivity metrics with higher values in the MS patients. The node flow coefficient was also one of the measures that, in the BM run, had more regions with statistically different metrics. Node flow coefficient represents the capacity of the node to manage information flow [4]. Therefore, the higher the nodal flow coefficient, the higher is the node's capacity to conduct information from one region to another.

Few studies used flow coefficient in the research of between-group significant differences. Nonetheless, Azarmi et al., [4] reported significant differences between groups in this metric. This could suggest that these nodes may have gained the ability to drive the information in a more effortless way in the MSC group, to be able to perform the tasks in an efficient way as a compensatory mechanism for the damages in some specific regions caused by MS.

Noteworthy, in the BM run, compared to the less demanding task runs, V1MT and RS run, the number of regions with statistically significant connectivity measures is smaller. This might seem counterintuitive because since this task involves more brain regions it should be expected that more regions present more significantly different metrics between groups. However, by analyzing the width of the bars, it is noticeable that the number of times those regions show different metrics between groups for all of the threshold values is higher - the size of the bars is larger in the BM run than in the other runs, thus we can assume with more confidence that the calculated metrics are significantly different and can be markers for the analysis of the alterations in the brain regions, provoked by MS.

Pagerank centrality is one of the top 3 measures with more ROIs which showed significant differences in the connectivity metrics, in the BM run (eleven to be more precise). This measure quantifies the level of influence of a node inside a network. The undirected version of PageRank centrality known as eigenvector centrality, according to Ashtiani et al., [35], is useful in identifying brain hubs, which are typically altered in MS patients. Eight of the eleven ROIs with significant differences in the metric presented greater values of the metric in MSC, suggesting that these regions may be highly influential within the network

and interact with many other nodes. Left postcentral gyrus is the region with more potential to represent one hub, since it showed significant differences in other measures (total-degree, out-degree, total-strength, out-strength, k-coreness, participation coefficient, node and total flow coefficient).

In figure 45 (middle), something that does not happen in the other runs is that there are regions that belong to the parietal lobe with metrics presenting differences between groups. These regions are believed to be associated with functions that are recruited in this task, and that, curiously, always have higher values of the measures in the MS patients.

Finally, it's important to emphasize that even if we cannot identify a consistent pattern of differences between groups (for example, MS patients didn't show increased values in all measures), this does not imply that the data are meaningless. A group of patients with altered brain connectivity measures may reveal information such as the connections/regions that are maintained, if those connections or regions were not affected by MS, connections that are compensating and adapting to the disease due to e.g., neuroplasticity, loss of its function, and connections/nodes that are damaged and unable to compensate that showed decreased connectivity.

5.4. Cognitive and Neuropsychological Evaluation

Besides the physical disabilities, patients with Multiple Sclerosis also present evidence of cognitive dysfunction, even in the early stages of the disease [33], [68]. For this reason, identifying signs of cognitive deficits, and evaluating their relationship with brain connectivity might be a potential predictive marker of the progression of the disease.

Cognitive functions in MS can be evaluated through the neuropsychological tests explained in section 4.1.1. Thus, our main goal was to analyze the relationship between the scores of these tests for the MS patients' group and the connectivity values that we obtained. Therefore, both parametric and non-parametric statistics were used depending on whether the data distribution was considered to be normal. Since the EDSS scores are not normally distributed, Spearman's rank correlation analysis was performed between the F-values of every pairwise connection within the network and the clinical scores. However, in the case of MFIS, SDMT, CVLT, and RME tests, Pearson's correlation was the one chosen due to their normal distribution. In all these analyses, a correlation was considered significant at $p<0.05$ with no correction for multiple comparisons, since after FDR correction was applied, none of the connections remained statistically significant.

The functional connectivity and its correlation with neuropsychological evaluations was explored for all the runs (V1MT, BM and RS), and each results' subsection will display:

- Three matrices: (1) the p-values of the statistically significant ($p<0.05$) correlations, (2) the Pearson's coefficient or Spearman -values ranging from -1 to 1, for those connections in the first matrix, and (3) the connections that were different between groups (section 5.2) and had simultaneously a significant correlation with the neuropsychological test.
- A figure with boxplots, each one denoting the distribution of the Spearman or Pearson correlations coefficients of the connections shown to be different between MSC and CNT, in the V1MT, BM, and RS runs. This way, we will be able to conclude whether there were a greater number of positive or negative correlations to eventually help reach some conclusions.

During the interpretation of the results, it is important to keep in mind that different tests give information on different domains, and that not always a higher score means better results. It is also worth noting that we refer to the V1MT and RS runs as the least demanding

runs, and to the BM run as the most demanding run. When we restrict ourselves to task runs, the BM run is associated with a more complex task than the V1MT run.

5.4.1. Expanded Disability Status Scale (EDSS)

RUN V1MT

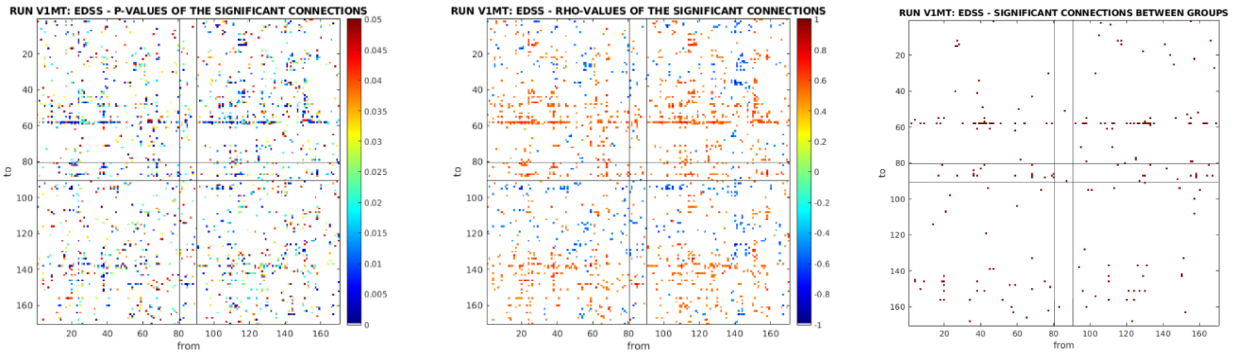

Figure 47- Results after performing the non-parametric Spearman's test for the EDSS scores. (Left) p-values of the significant correlations ($p < 0.05$). The colorbar represents p-values. (Middle) Spearman ρ-values ranging from -1 to 1, for those connections with significant correlations. The colorbar represents Spearman -values. (Right) Connections among those which were previously considered to be different between groups and at the same time have significant correlation between the F-values and the test scores.

F-values and EDSS scores were correlated in 202 connections already known to be significantly different between groups. In this case, there is a higher prevalence for positive correlations (negative correlation in 23 connections, and positive in 179). The three connections with stronger correlations were $PHG_R(112) \rightarrow tLP_L(58)$, rho of 0.8516 with higher F-values in CNT, $LING_L(26) \rightarrow OFCpost_L(15)$, rho of 0.7871 with higher F-values in CNT and $tVLP_R(151) \rightarrow STG_R(133)$, rho of 0.7738 with higher F-values in MSC.

RUN BM

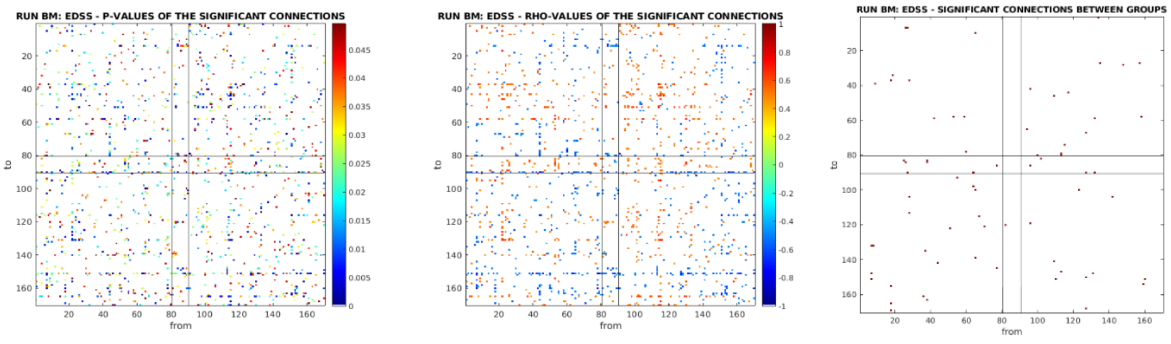

Figure 48- Results after performing the non-parametric Spearman's test for the EDSS scores. (Left) p-values of the significant correlations ($p < 0.05$). The colorbar represents p-values. (Middle) Spearman ρ-values ranging from -1 to 1, for those connections with significant correlations. The colorbar represents Spearman ρ-values. (Right) Connections among those which were previously considered to be different between groups and at the same time have significant correlation between the F-values and the test scores.

For the run BM, we observed that 36 of the 70 connections with between-groups differences were negatively correlated with EDSS. Two of the connections with the strongest correlations (negative) were $tMDm_L(64) \rightarrow RapheM(90)$ and $ROL_L(7) \rightarrow tVLP_R(151)$ with higher values in CNT with rho values of -0.7682 and -0.7504 respectively. A third connection $SOG_R(117) \rightarrow TPOsup_R(44)$ instead presented a positive correlation with a rho of 0.7737 with higher values in MSC.

RUN RS

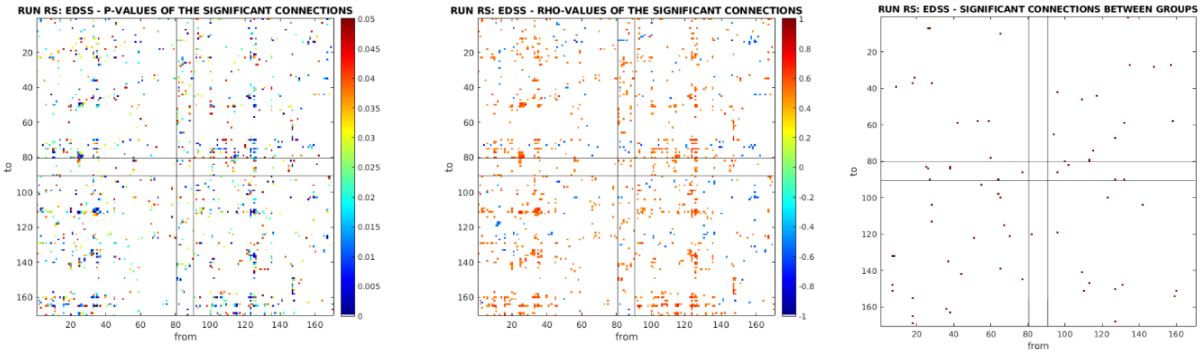

Figure 49- Results after performing the non-parametric Spearman's test for the EDSS scores. (Left) p-values of the significant correlations ($p < 0.05$). The colorbar represents p-values. (Middle) Spearman ρ-values ranging from -1 to 1, for those connections with significant correlations. The colorbar represents Spearman ρ-values. (Right) Connections among those which were previously considered to be different between groups and at the same time have significant correlation between the F-values and the test scores.

F-values and EDSS scores were positively correlated in 26 connections and negatively correlated in 16 connections, among those with differences between MSC and CNT. $PCL_L(64) \rightarrow TPOmid_L(90)$ and $OFCpost_R(7) \rightarrow MCC_R(151)$ were the connections with higher positive correlation coefficient rho=0.6492 and rho=0.6048, with higher F-values in MSC. For the negative correlations, the highest was in the connection $tPuM_R(159) \rightarrow ACCpre_L(73)$, with an rho value of -0.6037 and higher F-values in CNT.

EDSS: What should be expected and what was obtained

Previous studies suggest that there may not exist an association between FC and clinical scores after multiple comparisons' correction: Huang and colleagues [74] noticed no significant associations between alterations in rs-FC function and EDSS scores. They concluded that a possible explanation can be due to the sample size of their study (only 37 RRMS patients), because this is not the general rule.

In RRMS patients undergoing resting state condition, correlations between FC values and EDSS in specific brain networks such as the sensorimotor (SMN) were found to be majoritarily negative, i.e., lower rs-FC associated with higher disability (Sjøgård et al. [69]). Similar to the aforementioned but focusing now on the frontoparietal areas and auditory network, the same results were found regarding the values of the correlations (Høgestøl et al., [70]). On the other hand, a positive correlation between FC of the bi-frontal pair of regions and EDSS was reported by Tommasin et al., [60], suggesting that these positive correlations could be indications of maladaptive compensatory mechanisms.

Although the existent studies generally don't adopt whole brain networks, Tahedl et al., [53] infers that, often, decreased FC corresponds to increased EDSS (physical disability).

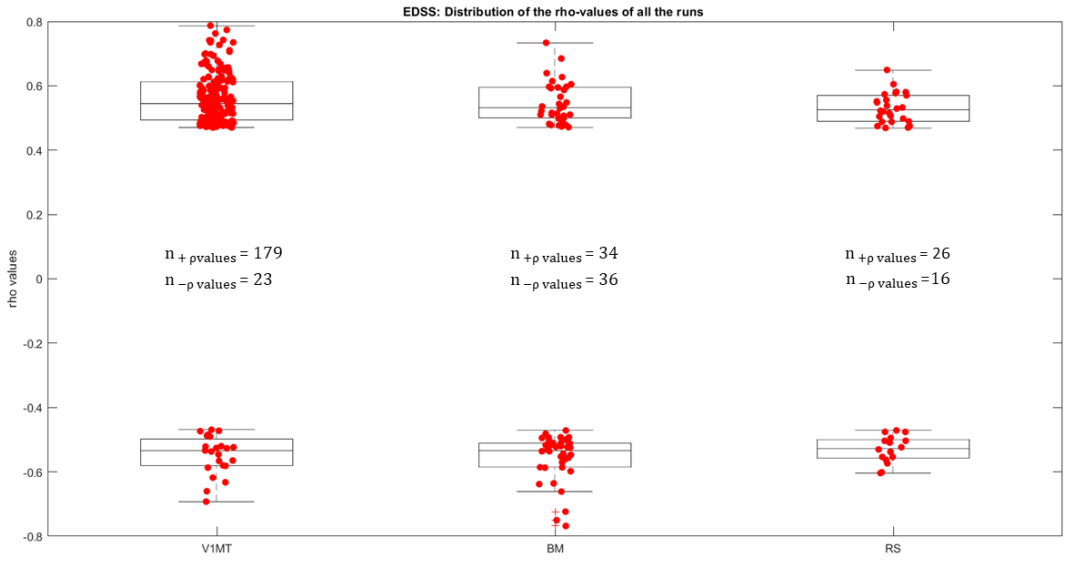

Figure 50- Boxplots with the distribution of the ρ values for the V1MT, BM and RS run. Each figure has three boxplots, each divided into two, positive values represented in the above, and negative represented in the boxplot below. $\boldsymbol{n_{+\rho values}}$ is the number of positive correlations and $\boldsymbol{n_{-\rho values}}$ the number of negative correlations.

The results from the correlations between FC and EDSS show that 88.61%, 48.57% and 61.90% of the correlation coefficients were positive in the V1MT, BM and RS runs, respectively. This means that in less demanding runs (V1MT and RS), an increase in FC can be explained by increases in the EDSS (and disability). Even though in the BM task there is a slight prevalence of negative values, the number of positive and negative values is relatively the same. Nevertheless, the connection with the strongest correlation in run BM is within the visual cortex ($SOG_R \rightarrow TPOsup_R$) and seems to have a positive correlation with the EDSS data and higher F-values in the MSC, i.e., increases in the FC of these connections in the MS patients may be related to a higher EDSS, and, thus, to a higher disability.

Another interesting fact is that in resting state there were less significant correlations of FC changes with EDSS scores, compared to task conditions. In this particular case the number of significant correlations was much higher in the run V1MT, which was not expected, since we were waiting to see more correlations, whether positive or negative, in the most demanding task (run BM).

In conclusion, we were able to distinguish a pattern of prevalence of positive correlations in the less demanding conditions (run V1MT and RS). These positive correlations could be an indicator of maladaptive compensatory mechanisms, which in turn could lead to worse disability. On the other hand, in the most demanding task (run BM), a balance between positive and negative correlations was observed.

5.4.2. Modified Fatigue Impact Scale (MFIS)

RUN V1MT

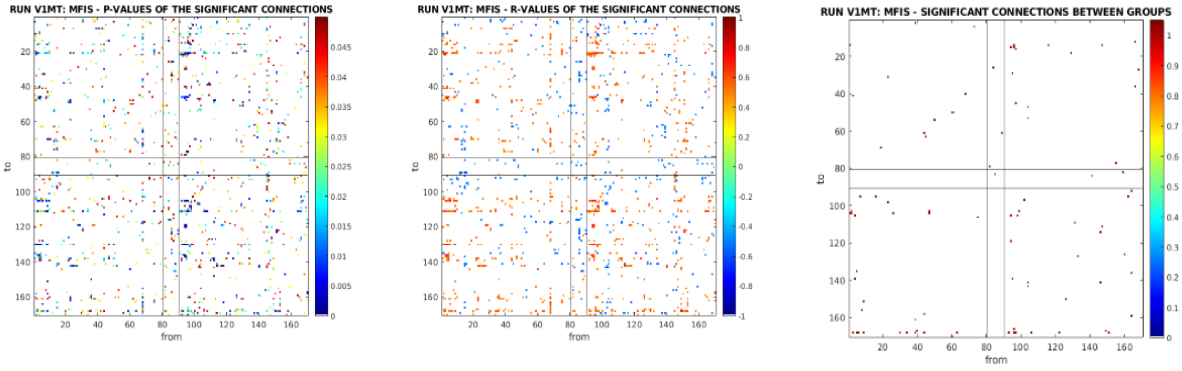

Figure 51- Results after performing the Pearson's correlation test for the MFIS scores. (Left) p-values of the significant correlations ($p < 0.05$). The colorbar represents p-values. (Middle) Pearson r-values ranging from -1 to 1, for those connections with significant correlations. The colorbar represents Pearson r-values. (Right) Connections among those which were previously considered to be different between groups and at the same time have significant correlation between the F-values and the test scores.

F-values and MFIS were correlated in 88 connections, among those with differences between MSC and CNT. We observed that in 65 connections the correlations were positive and in 23 connections the correlations were negative. Of the three correlations we identified as the strongest, all of them have positive correlations and higher F-values in the CNT: $IFGoperc_R(94) \rightarrow OFCpost_R$ (105) with a r-value of 0.7228; $IFGoperc_R(94) \rightarrow IOG_R(119)$ with a r-value of 0.6822 and $IFGorb_R(96) \rightarrow OFCpost_L(15)$ with a r-value of 0.6471.

RUN BM

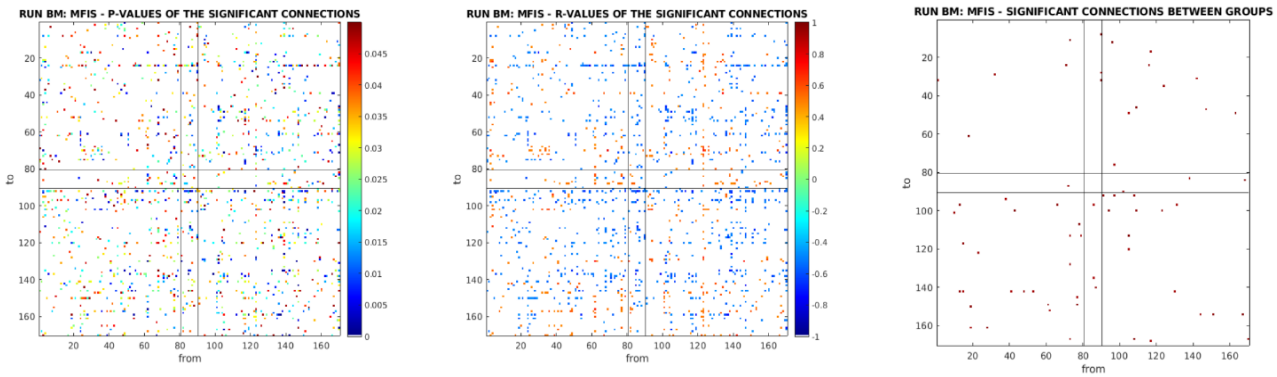

Figure 52- Results after performing the Pearson's correlation test for the MFIS scores. (Left) p-values of the significant correlations ($p < 0.05$). The colorbar represents p-values. (Middle) Pearson r-values ranging from -1 to 1, for those connections with significant correlations. The colorbar represents Pearson r-values. (Right) Connections among those which were previously considered to be different between groups and at the same time have significant correlation between the F-values and the test scores.

F-values and MFIS scores were positively correlated in 25 of 65 connections with between-groups differences and negatively correlated in 40 other connections. Two of the connections with the strongest correlation were $OFCpost_R(105) \rightarrow CERCRU2_L(49)$ and $CAU_L(38) \rightarrow IFGoperc_R(94)$ which have higher values in CNT with r-values of -0.6836 and 0.6480 respectively. The third connection with the strongest correlation was $CER6_R(142) \rightarrow PoCG_L(31)$ which presented an r-value of -0.6150 with higher values in MSC.

RUN RS

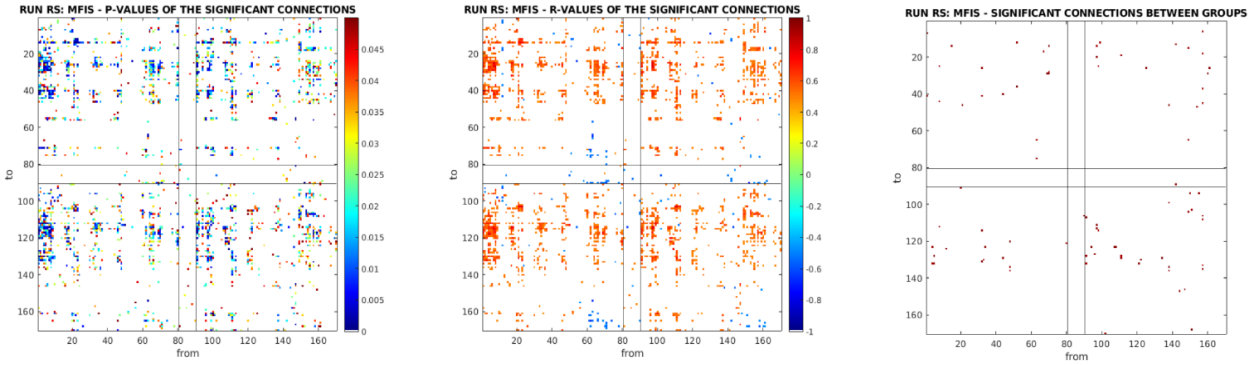

Figure 53- Results after performing the Pearson's correlation test for the MFIS scores. (Left) p-values of the significant correlations ($p < 0.05$). The colorbar represents p-values. (Middle) Pearson r-values ranging from -1 to 1, for those connections with significant correlations. The colorbar represents Pearson r-values. (Right) Connections among those which were previously considered to be different between groups and at the same time have significant correlation between the F-values and the test scores.

F-values and MFIS were correlated in 83 connections with between-groups differences, and in most cases the correlations were positive. The strongest correlations were found in $tRE_L(63) \rightarrow tMDI_L(65)$, $IFGopercA_R(98) \rightarrow IOG_R(114)$, and $ROL_R(8) \rightarrow MTG_L(25)$, with r-values equal to -0.6970, 0.6919 and 0.6856 respectively, all with higher F-values in CNT.

MFIS: What should be expected and what was obtained

Fatigue in MS is one of the most troublesome symptoms that significantly interferes with patients' quality of life.

Several studies show widespread alterations in FC that vary with fatigue. For example, Stefancin et al., [71] found in patients with RRMS positive correlations between fatigue and rs-FC of the basal ganglia to the medial prefrontal cortex, precuneus, and posterior cingulate gyrus and negative correlations between the connectivity of the insula and posterior cingulate and cognitive fatigue scores. The insula is associated with

perception, motor control, and self-awareness. The posterior cingulate gyrus is a region of the DMN that, in previous studies with RRMS patients, revealed negative correlations with MFIS results [69]. During the execution of a task, it has also been shown that MS patients affected by fatigue often show an increase in FC in some cortical and subcortical areas compared to CNT (Filippi et al., [72]).

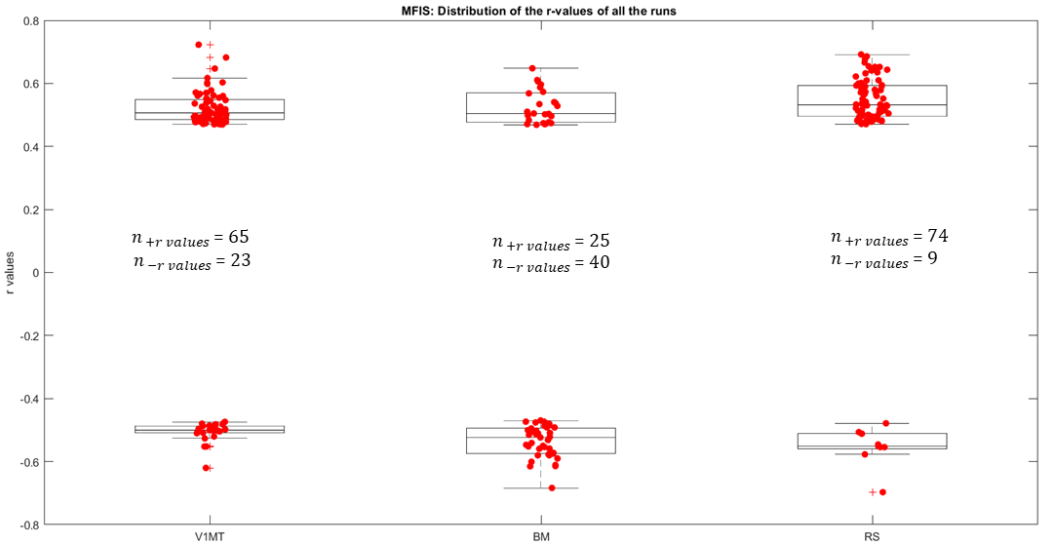

Figure 54- Boxplots with the distribution of the $\boldsymbol{r}$ values for the run V1MT, BM and RS. Each figure has three boxplots, each divided into two, positive values represented in the above, and negative represented in the boxplot below. $\boldsymbol{n_{+rvalues}}$ is the number of positive correlations and $\boldsymbol{n_{-rvalues}}$ the number of negative correlations.

The results of the correlations between FC and MFIS show that 57.53%, 31.94% and 84.81% of the correlation coefficients were positive in the V1MT, BM and RS runs. In the BM run, there were more connections with a negative correlation of FC with MFIS, possibly underlying an efficient compensatory mechanism, where reorganization of the brain led to an increase in FC, as a way to fight fatigue.

It is interesting to note that, from the group of the 3 connections with the strongest correlation in the run BM, the one with the highest connectivity values in the MSC ($CER6_R(142) \rightarrow PoCG_L(31)$) is directly involved in the task and has a negative correlation with the MFIS data. This connection is constituted by the right lobule VI of cerebellar hemisphere ($CER6_R$) which in this particular case is responsible for motor processing and visual working memory [73], and by the left Postcentral gyrus ($PoCG_L$), which is responsible for proprioception. Thus, it reinforces the idea that an increase in FC in the areas involved in the task allows the patients to perform a task at "normal" levels, without worsening fatigue.

Again, the outcomes of the less demanding tasks have a different pattern from the run BM. This pattern consists of a prevalence of positive correlations, that indicates that higher scores of fatigue are accompanied by higher values of FC. A possible explanation for these results may be the inefficient (maladaptive) compensatory mechanisms, and accumulation of fatigue as a result of higher energetic expenditure to increase FC.

However, there is a need for further investigation since the processes that induce fatigue in MS are still barely understood [74]. In fact, fatigue is a particular case, which occurs naturally if a person expends more energy or not. Hence, it is easy to imagine that a MS patient recruits more of a certain network or reorganizes this network and consequently increases his functional connectivity, leading to more fatigue/tiredness. At first it may seem like a maladaptive mechanism because it leads to a worse score in MFIS, but if this happens to accomplish beneficial task performance, it is also not correct to infer that it is an inefficient mechanism. This implies that, increases in FC are neither purely efficient (adaptative) nor purely inefficient (maladaptive), but rather a mix of the two [53]. It is adaptive in the sense that task performance improves, whereas it is maladaptive from the point of view of energy cost.

Although it is not fully possible to dissociate adaptative from maladaptive mechanisms, the interpretation of the results will be less ambiguous in task runs than in resting-state. This is due to the intrinsic limitation of resting-state of not having a performance reference, i.e., there is not a specific goal to reach during rest. Having a performance reference, allows to distinguish with more certainty the two mechanisms.

5.4.3. Symbol Digit Modalities Test (SDMT)

RUN V1MT

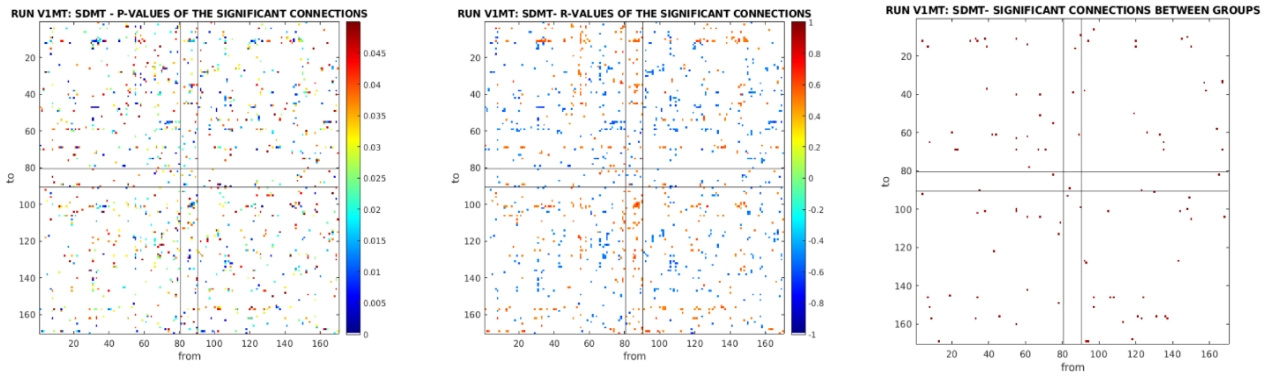

Figure 55- Results after performing the Pearson's correlation test for the SDMT scores. (Left) p-values of the significant correlations ($p < 0.05$). The colorbar represents p-values. (Middle) Pearson r-values ranging from -1 to 1, for those connections with significant correlations. The colorbar represents Pearson r-values. (Right) Connections among those which were previously considered to be different between groups and at the same time have significant correlation between the F-values and the test scores.

F-values and SDMT were positively correlated in 49 connections and negatively correlated in 52. The strongest positive correlation was in $MTG_R(135) \rightarrow tPuM_L(69)$, with an r-value of 0.7222 and highest F-values in CNT; the negative correlations were in the $RapheD(89) \rightarrow tVLP_L(61)$ with an r-value of -0.7230 and higher F-values in CNT, and in $SFG_R(92) \rightarrow CAU_L(38)$ with an r-value of -0.6900 and highest F-values in MSC.

RUN BM

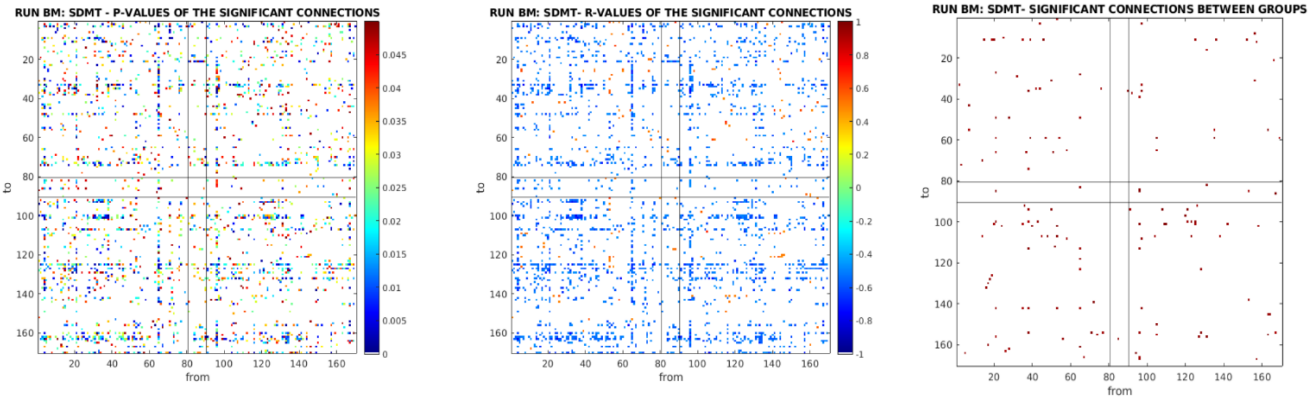

Figure 56- Results after performing the Pearson's correlation test for the SDMT scores. (Left) p-values of the significant correlations ($p < 0.05$). The colorbar represents p-values. (Middle) Pearson r-values ranging from -1 to 1, for those connections with significant correlations. The colorbar represents Pearson r-values. (Right) Connections among those which were previously considered to be different between groups and at the same time have significant correlation between the F-values and the test scores

Correlations between the F-values and SDMT were positive in 2 connections, and negative in 139, among those with differences between MSC and CNT. In this case, the strongest correlations were all negative, with an r of -0.7252, -0.7105 and -0.7230, belonging respectively to $CAU_L(38) \rightarrow SFGmedial_R(100)$, $ANG_L(14) \rightarrow PFCventmed_L(107)$ with highest F-values in CNT and to $OFCant_L(35) \rightarrow INS_R(11)$ with highest F-values in MSC.

RUN RS

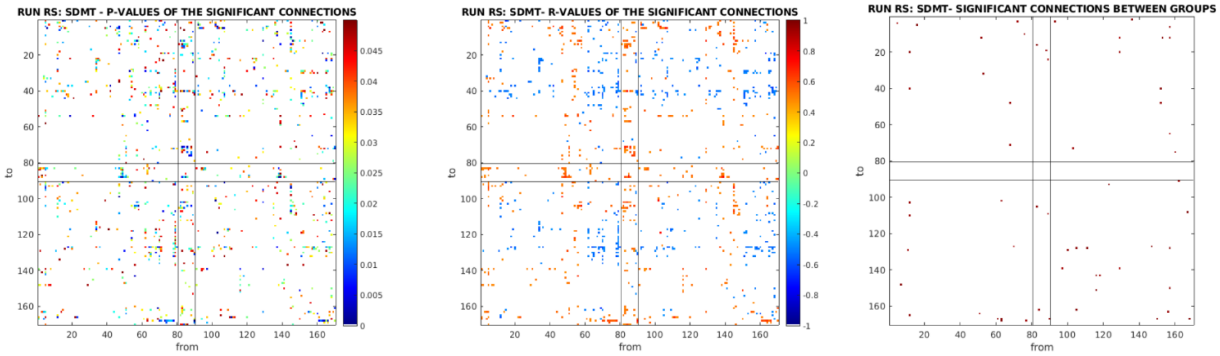

Figure 57- Results after performing the Pearson's correlation test for the SDMT scores. (Left) p-values of the significant correlations ($p < 0.05$). The colorbar represents p-values. (Middle) Pearson r-values ranging from -1 to 1, for those connections with significant correlations. The colorbar represents Pearson r-values. (Right) Connections among those which were previously considered to be different between groups and at the same time have significant correlation between the F-values and the test scores.

From the correlations between the F-values and SDMT, in the RS run, 30 connections showed positive correlations and 29 connections showed negative ones. The strongest correlations were found in $PUT_R(129) \rightarrow REC_L(12)$, $OFCant_R(104) \rightarrow CERCRU2_R(139)$, and $ROL_R(97) \rightarrow CERCRU2_R(139)$, with r-values equal to 0.6880, 0.6383 and 0.6309 respectively, all with higher F-values in CNT.

SDMT: What should be expected and what was obtained

The cognitive domain that is mostly affected in all MS phenotypes is processing speed (PS), often assessed by SDMT [75].

SDMT also has correlations with FC, however not many studies attempted to correlate it with functional connectivity from task-based fMRI. To our knowledge, there are also few studies focusing this analysis on the whole brain. In fact, only one study assessed the relationship of PS of the whole brain with rs-FC and concluded that FC increases correlated with a decrease in PS, i.e., increases in FC justifies lower SDMT scores, meaning lower PS (negative correlation).

Apart from whole brain studies, Zhang et al., [75] reported some main findings, showing that in RRMS patients, a higher rs-FC within the DMN particularly between medial prefrontal and frontal pole regions, seemed to improve the performance in the SDMT test (positive correlations).

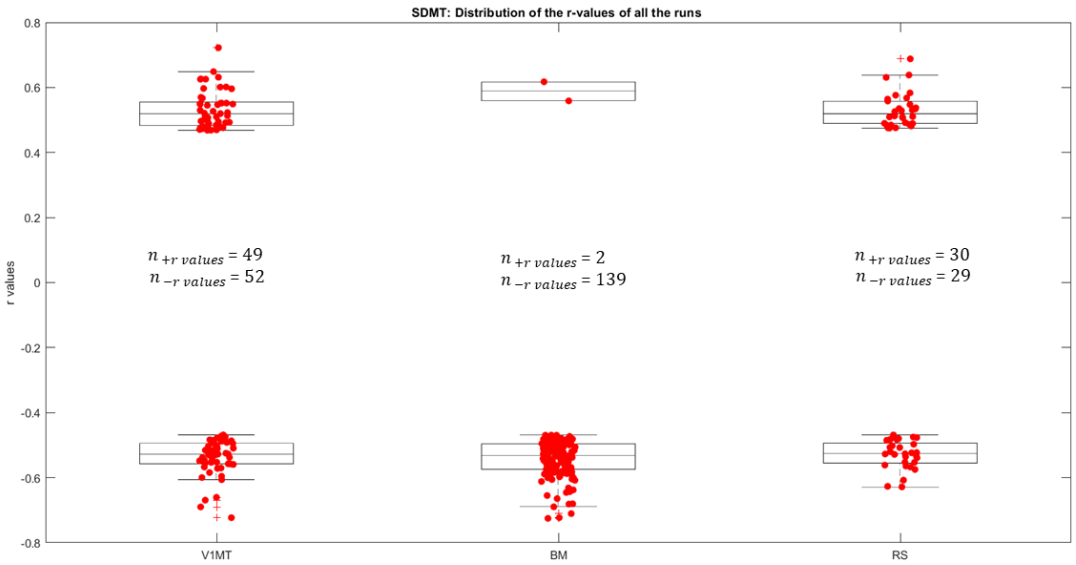

Figure 58- Boxplots with the distribution of the $\boldsymbol{r}$ values for the run V1MT, BM and RS. Each figure has three boxplots, each divided into two, positive values represented in the above, and negative represented in the boxplot below. $\boldsymbol{n_{+rvalues}}$ is the number of positive correlations and $\boldsymbol{n_{-rvalues}}$ the number of negative correlations.

The results of the correlations between FC and SDMT show that 48.51%, 1.42% and 50.85% of the correlation coefficients were positive in the V1MT, BM and RS runs, respectively. The correlations found between FC and SDMT are inversely correlated in the run BM, where almost all correlations are negative (only two correlations are positive). This matches the concept that an increase in FC is associated with a decrease in processing speed, which may be an indicator of a maladaptive mechanism that eventually leads to cognitive impairment.

In the BM run it is clear to observe that there is a consistency for negative correlations, unlike the less demanding runs that seem to have a very balanced number of positive and negative correlations.

Further investigation is needed to understand the meaning of the previous results. Longitudinal analysis is the key to explaining if these number of negative correlations in the run BM could be an indication that a person in the future may develop cognitive deficits: if the patient, with the progression of the disease, performs worse on the test, and if previously their functional connectivity was increased relative to the healthy control group, it could corroborate that there was a compensatory mechanism going on, that at some point stopped occurring, and that led to a lower test result.

5.4.4. California Verbal Learning Test (CVLT)

RUN V1MT

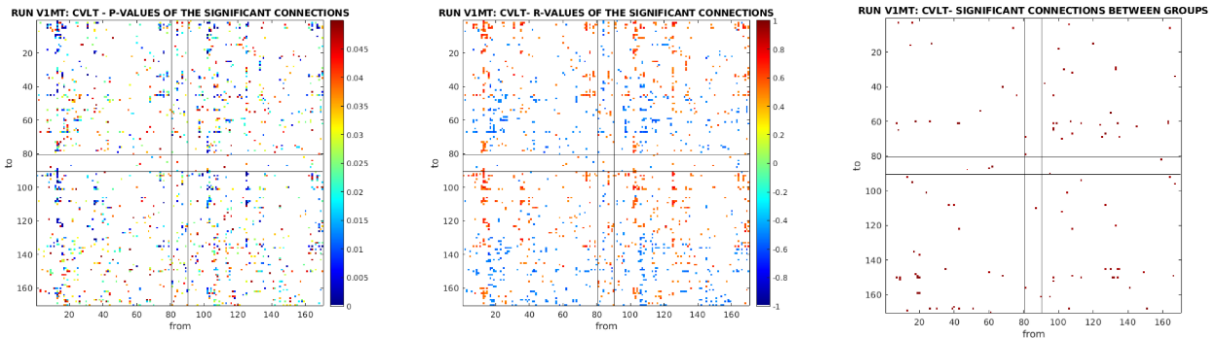

Figure 59- Results after performing the Pearson's correlation test for the CVLT scores. (Left) p-values of the significant correlations ($p < 0.05$). The colorbar represents p-values. (Middle) Pearson r-values ranging from -1 to 1, for those connections with significant correlations. The colorbar represents Pearson r-values. (Right) Connections among those which were previously considered to be different between groups and at the same time have significant correlation between the F-values and the test scores.

F-values and CVLT showed positive correlations in 48 connections and negative correlations in 56 connections. Of these, the 3 connections with stronger correlations, all of them positive, were $OFCpost_R(105) \rightarrow PFCventmed_R(101)$ with an r-value of 0.7671 and higher F-values in CNT; $ACCsup_L(74) \rightarrow IFGorb_L(6)$ with an r-value of 0.7373 and higher F-values in the MSC group and $tVL_L(60) \rightarrow tVA_R(147)$ with an r-value of 0.7004 and higher values in the CNT group.

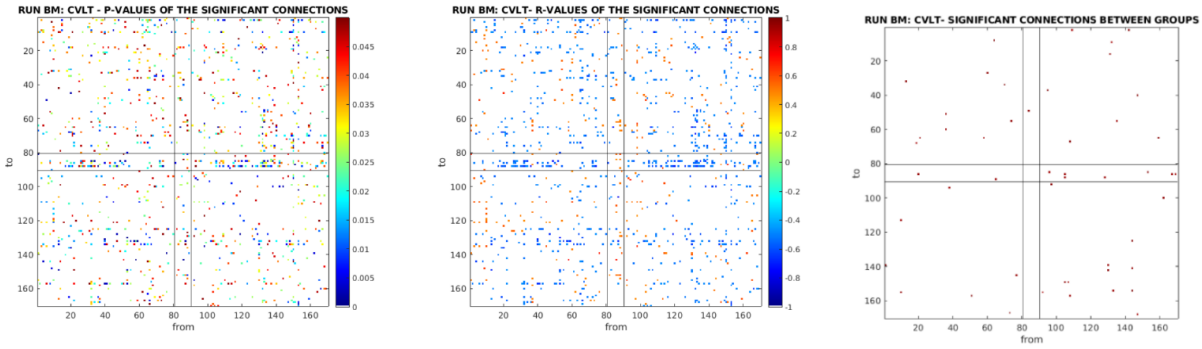

Figure 60- Results after performing the Pearson's correlation test for the CVLT scores. (Left) p-values of the significant correlations ($p < 0.05$). The colorbar represents p-values. (Middle) Pearson r-values ranging from -1 to 1, for those connections with significant correlations. The colorbar represents Pearson r-values. (Right) Connections among those which were previously considered to be different between groups and at the same time have significant correlation between the F-values and the test scores.

F-values and CVLT were negatively correlated in 35 of the 49 connections, with differences between MSC and CNT. Two of the three connections with the strongest correlations $SFG_R(92) \rightarrow tMDl_R(155)$ (r-value of 0.6507) and $MCC_L(19) \rightarrow tPuA_L(68)$(r-value of -0.6387) were found to have higher F-values in the CNT. The third connection with the strongest correlation was$LC\ (132) \rightarrow PreCG_L(1)$ (r-value of -0.6136) that had higher F values in MSC.

RUN RS

Figure 61- Results after performing the Pearson's correlation test for the CVLT scores. (Left) p-values of the significant correlations ($p < 0.05$). The colorbar represents p-values. (Middle) Pearson r-values ranging from -1 to 1, for those connections with significant correlations. The colorbar represents Pearson r-values. (Right) Connections among those which were previously considered to be different between groups and at the same time have significant correlation between the F-values and the test scores.

F-values and CVLT showed correlations in 44 connections among those with differences between groups (24 negative, 20 positive). Focusing on the 3 strongest correlations, the strongest positive correlation was in $tIL_R(152) \rightarrow ACCsub_R(162)$ (r-value of 0.6601) with superior F-values in the CNT and the negative correlations, both with superior F-values in the MSC, were found in $HES_L(42) \rightarrow PreCG_R(91)$ (r-value of -0.6611) and in $tVLP_L(61) \rightarrow tVA_R(149)$ (r-value of -0.5985).

CVLT: What should be expected and what was obtained

CVLT is a test that assesses short-term and long-term free recall and recognition, i.e., the ability to quickly learn new information and recall it at a later time. Sousa et al.[76] and Stegen et al., [77] showed that this memory was impaired in MS. As a result, if this cognitive component is impaired, MS patients perform poorly on this test, achieving lower scores than the healthy control group.

To our knowledge, few studies have attempted to correlate functional connectivity with the CVLT test on RRMS patients. The ones that are available are during resting state, never while performing a task.

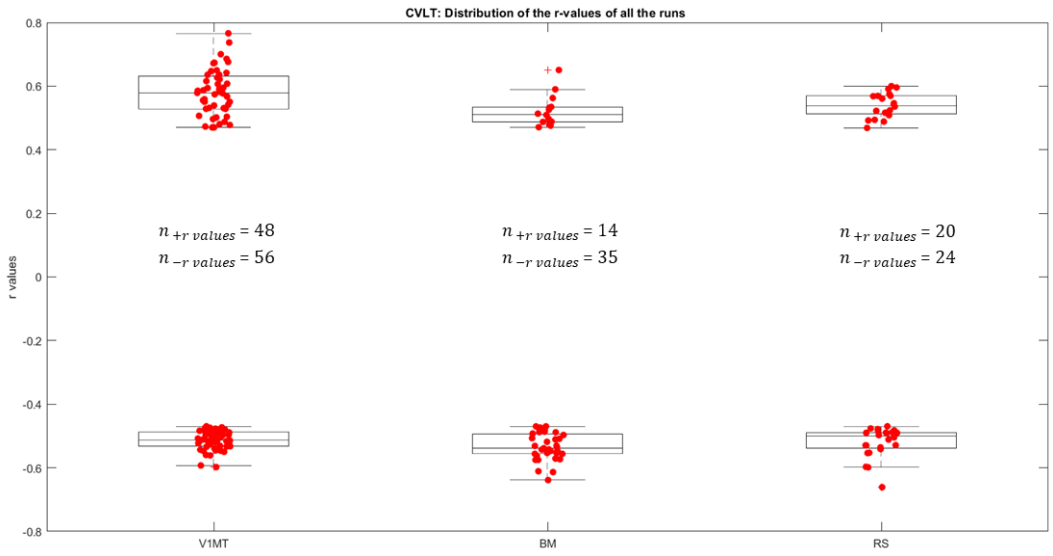

Figure 62- Boxplots with the distribution of the $\boldsymbol{r}$ values for the run V1MT, BM and RS. Each figure has three boxplots, each divided into two, positive values represented in the above, and negative represented in the boxplot below. $\boldsymbol{n_{+rvalues}}$ is the number of positive correlations and $\boldsymbol{n_{-rvalues}}$ the number of negative correlations.

The results of the correlations between FC and CVLT show that 46.15%, 28.57% and 45.45% of the correlation coefficients were positive in the V1MT, BM and RS runs,

respectively. This means that in all the runs there is a prevalence for negative correlations. However, in the BM run this difference between positive and negative correlations is more evident, unlike the less demanding runs, where the positive and negative correlations are very balanced.

In BM run, one of the connections with the strongest and most significant correlation ($LC \rightarrow PreCG_L$) seems to have a negative correlation with the CVLT data and higher F-values in the MSC. This connection arises from the locus coeruleus, a region involved in many neurodegenerative diseases. It is one of the ascending pathways of the LC thought to be involved in functions, such as behavioral flexibility, wakefulness, formation and retrieval of episodic and emotional memories (etc.,), but more important in cognitive control.

Again, it can highlight the idea that there is an increase of FC in the areas involved in the task, to allow the patient to perform a task at "normal" levels. One the other hand, these compensatory mechanisms may not be efficient enough, resulting in worse scores (maladaptive compensatory mechanism).

5.4.5. Brief Visuospatial Memory Test (BVMT)

RUN V1MT

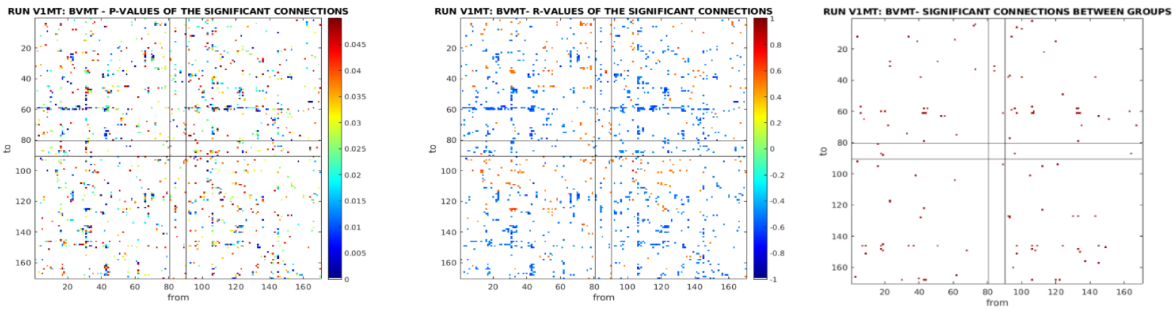

Figure 63- Results after performing the Pearson's correlation test for the BVMT scores. (Left) p-values of the significant correlations ($p < 0.05$). The colorbar represents p-values. (Middle) Pearson r-values ranging from -1 to 1, for those connections with significant correlations. The colorbar represents Pearson r-values. (Right) Connections among those which were previously considered to be different between groups and at the same time have significant correlation between the F-values and the test scores.

F-values and BVMT showed correlations in 118 connections shown to be different between MSC and CNT, 103 having negative correlations and 15 having positive correlations. The stronger correlation was for $SFG_R(92) \rightarrow CAU_L(38)$, with r-value of -0.7356 and highest F-values in MSC. The other two second strongest correlations had highest F-values in the CNT: $CER9_R(145) \rightarrow tMGN_R(157)$, with an r of -0.6991, and $IFGOperc_L(4) \rightarrow SFG_R(92)$, with an r of -0.6971.

RUN BM

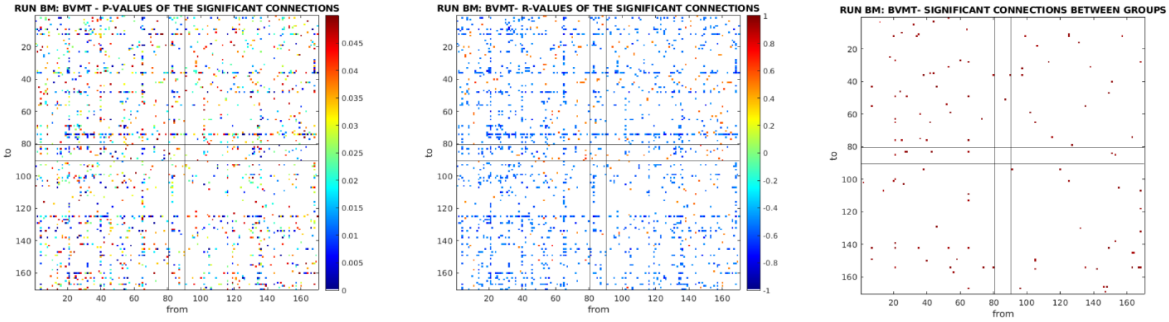

Figure 64- Results after performing the Pearson's correlation test for the BVMT scores. (Left) p-values of the significant correlations (p < 0.05). The colorbar represents p-values. (Middle) Pearson r-values ranging from -1 to 1, for those connections with significant correlations. The colorbar represents Pearson r-values. (Right) Connections among those which were previously considered to be different between groups and at the same time have significant correlation between the F-values and the test scores.

F-values and BVMT were correlated in 112 connections, with negative correlations in 101 and positive in 11. When searching for the strongest correlations, all of them showed to be negative, but only the $tMGN_R(157) \rightarrow REC_L(12)$ (r of -0.7519) showed to have higher F-values in MSC, unlike the $OFClat_R(106) \rightarrow ACC_L(18)$ (r of -0.6735) and $OFCant_L(14) \rightarrow INS_R(107)$ (r of -0.6614) that showed to have higher F-values in CNT.

RUN RS

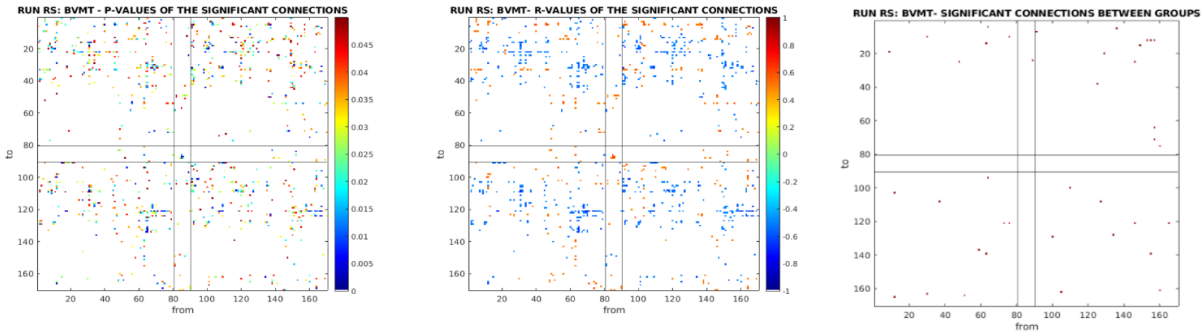

Figure 65- Results after performing the Pearson's correlation test for the BVMT scores. (Left) p-values of the significant correlations (p < 0.05). The colorbar represents p-values. (Middle) Pearson r-values ranging from -1 to 1, for those connections with significant correlations. The colorbar represents Pearson r-values. (Right) Connections among those which were previously considered to be different between groups and at the same time have significant correlation between the F-values and the test scores.

There were 38 connections with correlation between their F-values and BVMT data, 12 showed positive correlations and 26 negative correlations. Of the three that were identified as the strongest, all of them show to have negative correlations. $RapheD(89) \rightarrow CAL_L(24)$ with an r-value of -0.6544 and $tPUL_R(170) \rightarrow Nacc_L(75)$ with an r of -0.6321, both with higher F-values in the CNT, and finally $ACCpre_L(73) \rightarrow PoCG_R(121)$ with an r of -0.6262 and higher F-values in the MSC.

BVMT: What should be expected and what was obtained

As explained earlier, BVMT measures cognitive performance in the form of visuospatial learning and memory. It is similar to the CVLT test to the extent that it also assesses long-term memory. In Sousa et al., [73] it was shown that the MS group performed significantly worse than the CNT group in BVMT.

More in line with the emerging topic, Zhang J et al., [75] noticed that PPMS patients showed increased rs-FC between the cerebellar lobule VIIb and right precentral gyrus, correlating with worse long-term memory measured by BVMT. Veréb D et.al., [78] also found altered connectivity correlated with BVMT. They used a visual attention task in RRMS patients, and their results were: higher connectivity between visual/attention-related networks and DMN correlating with worse BVMT scores (r = −0.48) and lower connectivity within Dorsal Attention Networks (DAN) correlating with worse BVMT scores (r= 0.53).

One other interesting fact is that BVMT and SDMT found to be highly correlated in a positive way. This means that with a decrease in FC, should be accompanied by a decrease in processing speed (decrease in SDMT), and the predominance for positive or negative correlations between FC and BVMT scores should be similar to what was found for SDMT.

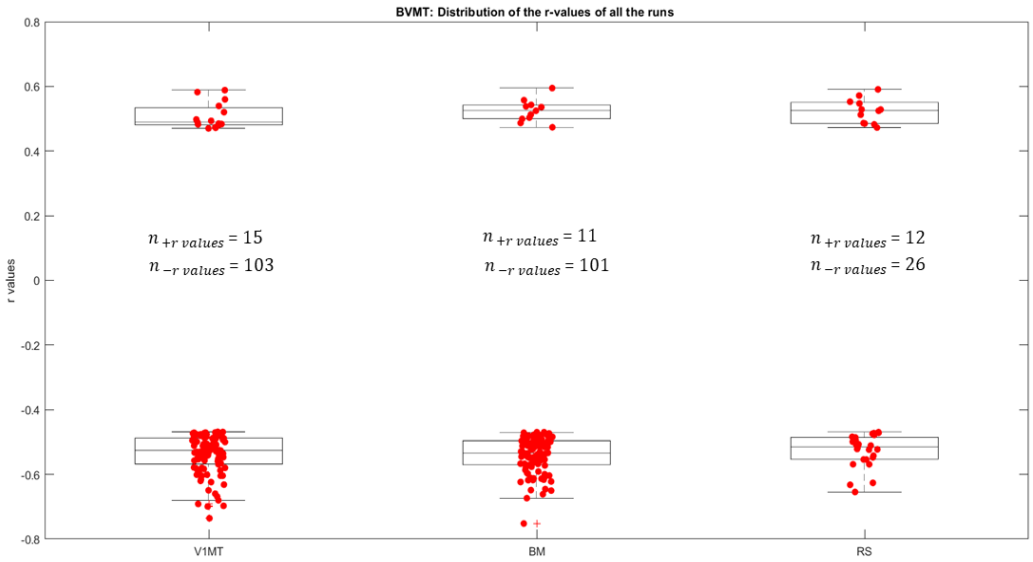

Figure 66- Boxplots with the distribution of the $\boldsymbol{r}$ values for the run V1MT, BM and RS. Each figure has three boxplots, each divided into two, positive values represented in the above, and negative represented in the boxplot below. $\boldsymbol{n_{+rvalues}}$ is the number of positive correlations and $\boldsymbol{n_{-rvalues}}$ the number of negative correlations.

The results of the correlations between FC and BVMT show that 12.71%, 9.82% and 31.58% of the correlation coefficients were positive in the V1MT, BM and RS runs, respectively. The predominance of negative correlations between FC and BVMT in all the

runs are in line with the SDMT scores, as expected. Here, a decrease in BVMT scores is associated with lower processing speed.

Regarding the relationship between BVMT and SDMT, as some changes in the FC of some connections have been reported, we explored if the connections that were shown to have a strongest correlation between FC and BVMT scores, were in accordance with what has already been seen in previous studies. For all runs, we focused on the connections that were shown to have FC increases in the MSC group, since a general increase in brain FC is associated with the phenomenon of neuroplasticity.

For the task runs, the results were coherent with Veréb D et.al., [54]. In the V1MT run, $SFG_R \rightarrow tVPL_L$ appeared to have a negative correlation with the BVMT data, meaning that increases in the FC of these connections may lead to lower test scores. In the BM run, $OFCant_L \rightarrow INS_R$, a connection known to be involved in elaborate attentional and working memory processing [79], shows to correlate inversely with BVMT data. Again, the influence of maladaptive phenomenon in cognitive performance has to be taken into account.

For the RS run, the connection found to have the highest increase of FC in MSC shows a negative correlation with the BVMT scores. This connection is not the same as in Zhang J et.al., [75] , which was already expected since the patients were not at the same stage of the disease (PPMS patients instead of RRMS patients). However, it involves regions that are involved in the test, namely the left Anterior cingulate & paracingulate gyri $(ACCpre_L)$ which are regions with central roles in theories of attention and cognitive control [79], and the right Postcentral gyrus ($PoCG_L$), that is included in the DMN. This demonstrates that even when the recruited network is smaller, differences in the connectivity of the connections involved in the task are already observed and may indicate maladaptive mechanisms.

5.4.6. Reading the mind in the eyes (RME)

RUN V1MT

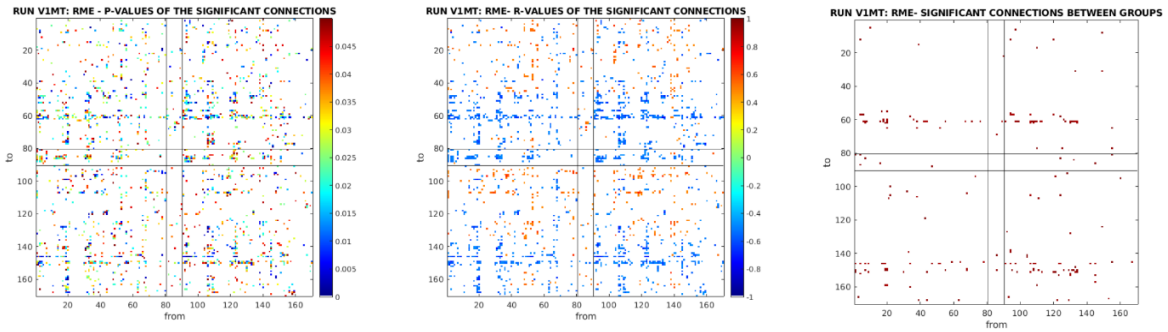

Figure 67- Results after performing the Pearson's correlation test for the RME scores. (Left) p-values of the significant correlations (p < 0.05). The colorbar represents p-values. (Middle) Pearson r-values ranging from -1 to 1, for those connections with significant correlations. The colorbar represents Pearson r-values. (Right) Connections among those which were previously considered to be different between groups and at the same time have significant correlation between the F-values and the test scores.

Of all the 183 significant correlations between FC and RME, 18 were positive. The strongest correlations were found in $STG_R(133) \rightarrow CAU_L(61)$, $SMG_R(124) \rightarrow CER10_R(146)$ and $SMG_L(34) \rightarrow CER10_R(146)$, with r-values equal to -0.8037, -0.7338 and -0.7266 respectively, all with higher F-values in CNT.

RUN BM

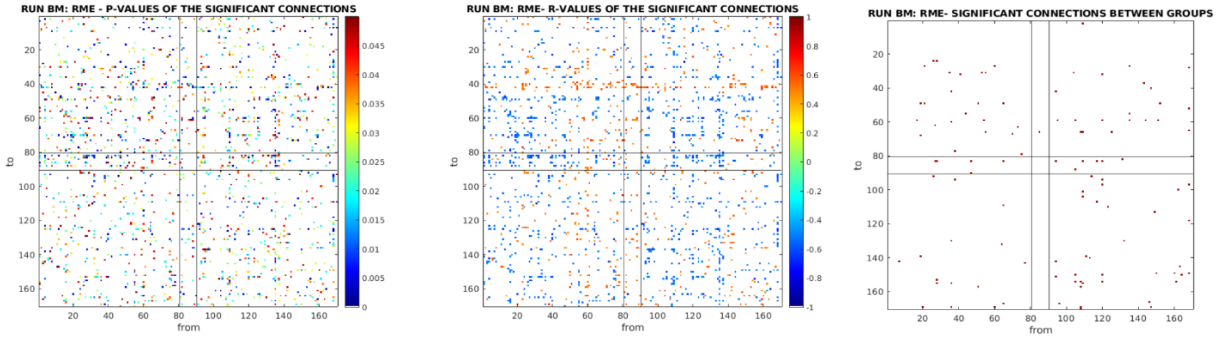

Figure 68- Results after performing the Pearson's correlation test for the RME scores. (Left) p-values of the significant correlations (p < 0.05). The colorbar represents p-values. (Middle) Pearson r-values ranging from -1 to 1, for those connections with significant correlations. The colorbar represents Pearson r-values. (Right) Connections among those which were previously considered to be different between groups and at the same time have significant correlation between the F-values and the test scores.

FC and RME were negatively correlated in 82 connections and positively correlated in 25 (total of 107 correlations). The highest positive correlations were in $IFGoperc_R(94) \rightarrow CAU_L(42)$, with an r of 0.7199 and higher F-values in CNT, and in $OFcant_R(104) \rightarrow PoCG_L(31)$, with an r of 0.6905, and higher F-values in MSC. The strongest negative correlation was in the $PCUN_L(36) \rightarrow tVL_L(60)$ with an r of -0.483 and higher F-values in CNT.

RUN RS

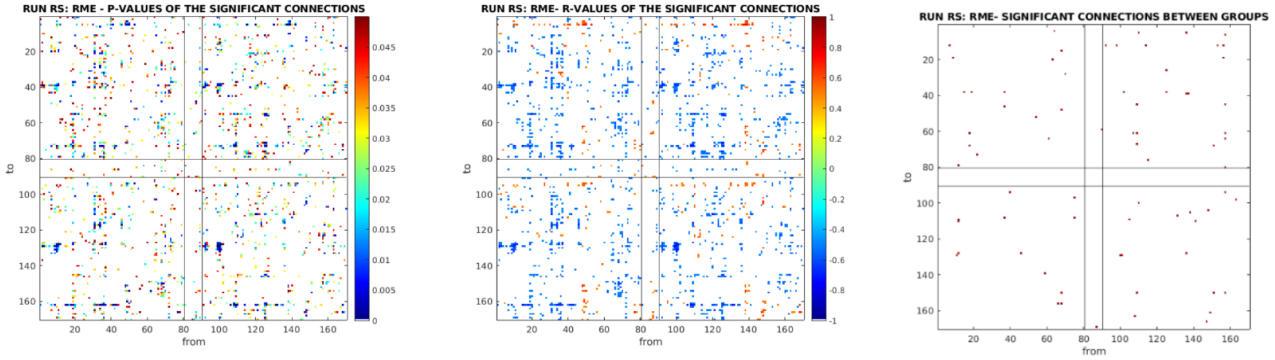

Figure 69- Results after performing the Pearson's correlation test for the RME scores. (Left) p-values of the significant correlations ($p < 0.05$). The colorbar represents p-values. (Middle) Pearson r-values ranging from -1 to 1, for those connections with significant correlations. The colorbar represents Pearson r-values. (Right) Connections among those which were previously considered to be different between groups and at the same time have significant correlation between F-values and the test scores.

From the connections previously identified to be different between groups, 73 showed correlations between their F-values and RME results. Thus, the strongest correlations were $tAV_R\,(147) \rightarrow VTA_R(166)$, with an r of 0.7280, $SFGmedial_R(100) \rightarrow PUT_R(129)$, with an r of -0.6964, both with highest F-values in MSC and $tLP_R(148) \rightarrow OFCant_R(104)$ with an r of 0.6944 and highest values in CNT.

RME: What should be expected and what was obtained

The RME is the most commonly used test to assess theory of mind decoding. In studies with only RRMS patients, social cognitive deficits, including impairment in predicting other's emotions states, were found to be affected by MS [80].

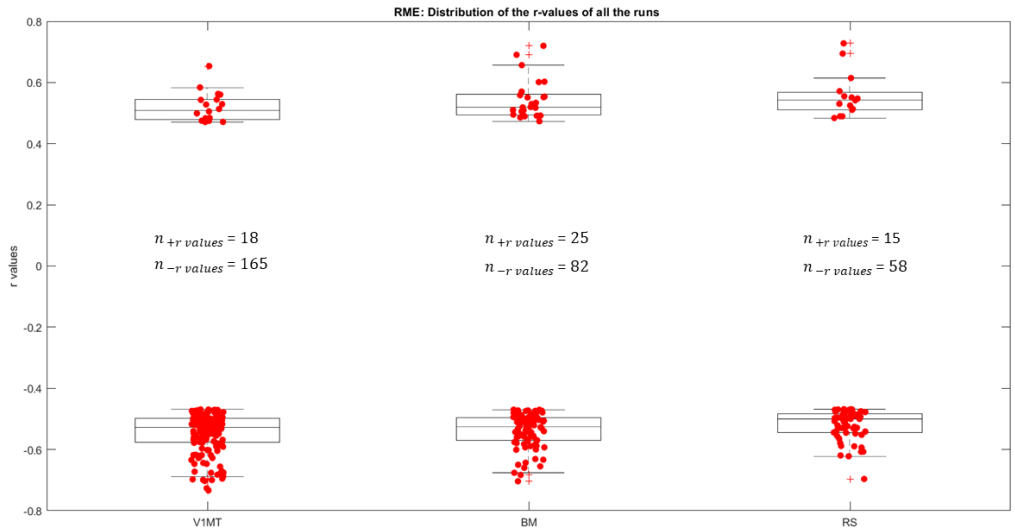

Figure 70- Boxplots with the distribution of the $\boldsymbol{r}$ values for the run V1MT, BM and RS. Each figure has three boxplots, each divided into two, positive values represented in the above, and negative represented in the boxplot below. $\boldsymbol{n_{+rvalues}}$ is the number of positive correlations and $\boldsymbol{n_{-rvalues}}$ the number of negative correlations.

The results of the correlations between FC and RME show that 9.84%, 23.36% and 20.55% of the correlation coefficients were positive in the V1MT, BM and RS runs, respectively, which is the same as saying that the correlations were mostly negative in all the runs.

Previous studies reported that impairment in social cognition in MS is likely to be multifactorial, dependent on non-specific factors such as fatigue, as well as specific factors such as abnormalities in the regions involved in social cognition. Not many studies have yet investigated the effect of fatigue as a potential mediator on social cognition performance in MS, although Bora et al., [80] pointed out that MS-related fatigue is associated with reduced performance on vigilance assessment tasks. This was indeed true for the V1MT, and RS runs, where a prevalence of positive correlations indicated that with increasing functional connectivity, fatigue levels would increase. Meanwhile, during the RME test increased functional connectivity was followed by worse test scores. This may mean that as the person feels more tired/has more fatigue, the performance of the test will turn out worse. The same cannot be said for the BM run, i.e., fatigue levels do not indicate a possible explanation for the test results. Nevertheless, from the group of the 3 connections with the strongest correlation values in the run BM, $OFcant_R \rightarrow PoCG_L$ has a negative correlation with the RME data and higher FC values in the MS patients' group. As expected, this connection is constituted by regions involved in the performance of the test. Right Anterior Orbital gyrus ($OFcant_R$) is associated with intellectual and emotional expression; left Postcentral gyrus ($PoCG_L$) is related to proprioception. This shows that an increase in FC contributes to worse scores in the RME test, which suggest, again, possible maladaptive neuroplasticity.

In the RS run, in addition to the possible relationship with fatigue levels, one of the connections with strongest correlations that has a negative correlation with RME data and higher FC values in the MS patients' group, is involved in the performance of the test. It is constituted by the right Thalamus-Anteroventral Nucleus (tAV_R) which plays a role in the modulation of alertness, and by the right ventral tegmental area (VTA_R), which is best known for its robust dopaminergic projections to forebrain regions and their critical role in cognition [81]. This could also be evidence of maladaptive compensatory mechanisms, where a higher FC (especially in the areas involved in the task), leads to poor cognitive performance.

Finally, it is important to take into consideration the compensatory mechanisms in cognitive performance even if they are not efficient, as a way of combating pathological processes, in this case structural damage provoked by MS.

Final considerations

From the boxplots, it is clear that the run tasks showed overall more connections with correlations than the RS run. Interestingly, in all of the neuropsychological tests, except the BVMT, the number of correlations was higher in the V1MT run than in the BM run. This was unexpected, because the BM run is a more complex task, that also includes decision making and theoretically involves more brain regions in information exchange. At first sight, there is not a "crystal clear" explanation for why this happen, therefore is necessary to explore in a deeper level. Regarding, this reinforces the importance of task-fMRI, as it proves that if we recruit a specific network, we may find connections that are altered, and not identified in the resting state.

The correlations of connectivity with the EDSS and MFIS tests seem to follow a tendency. The results of the more complex run are the inverse of the results of the less complex runs. As an example, if in the BM run there is a predominance for negative correlations, then in the other two runs, a predominance for positive correlations will be observed. In the correlations of connectivity with cognitive tests SDMT, CVLT, BVMT and RME we no longer verify the inverse correlations as in the previously mentioned results, but we still notice a difference between the BM run and the others.

Further studies are needed to understand if these results on the BM run will change during disease progression, and if at this stage these results would already be indicators of developing cognitive deficits.

It should not be neglected that in all runs there are both positive and negative correlations, i.e., although there may be a very high prevalence of one type of correlation, e.g., positive suggesting a prevalence of an adaptative mechanism (in the case of the SDMT, BVMT, CVLT and RME test), there are still negative correlations, which are also informative. Ideally in the future, in each of the connections we should evaluate between positive/negative correlation of the tests' scores and FC and increases or decreases in connectivity as a way to find out where an efficient compensation is being employed, and if this can serve as a guide to an intervention like cognitive training or remyelination.

6. Limitations

This study has several limitations that should be taken into consideration when analyzing the results.

In the actual data acquisition process, the constraints of a relatively small number of participants might lead to some imprecise results and interpretations, possibly due to poor statistical power. In this sense, increasing the amount of available data (for example, with the addition of new participants) can make the conclusions of the study more convincing.

The calculation of functional connectivity was performed via bivariate GCA not the multivariate algorithm. The limitation with using a bivariate approach to Granger causality, is that the prediction model doesn't include more than two variables in the autoregressive model, increasing the number of false/spurious connections. However, with the proportional thresholding approach these spurious connections should be compensated.

The calculation of the connectivity measures was done across 27 thresholds. Thus, when we say that a measurement was increased in patients, as it is an average value, for example there is a risk that the values are increased in 14 thresholds and decreased in 13 thresholds (although very unlikely). However, it is a risk that we take by choosing the optimal threshold and trying to preserve the strongest connections.

The interpretation of the neuropsychological tests with the F-values was made based on all the correlation values, so if for a run, most of the correlations were negative, it is inferred that there was a tendency for the test results in that run to have a negative correlation with the F-values. In the future, connectivity should be measured during test performance and each significant correlation must be studied.

Finally, to validate the source of the functional compensatory mechanisms, future research focusing on the relationship between structural damage and functional connectivity, as well as longitudinal studies to verify the previous results, should be considered.

7. General conclusions

The main goal of this project was to understand if changes in directed functional connectivity in patients during task and resting-state fMRI could be due to Multiple Sclerosis, and if the calculation of graph theory connectivity measures could be useful in the investigation and better understanding of the disease. Lastly, we wanted to investigate if the relationship between brain connectivity and cognitive and neuropsychological tests could bring some insight into the disease.

As said previously, our study did not comply with our a priori assumptions (section 1.2). Our results were not able to support the hypothesis of brain neuroplasticity in the early phases of MS when the analysis is made from a whole-brain point of view. We observed slight decreases of FC in MS patients, which suggests that patients may have not yet developed these compensatory mechanisms, due to the short time that has passed since the onset of the disease.

However, we were able to prove that it is advantageous to work in task conditions in fMRI since more specific differences in FC were detected in the V1MT and BM runs, than in the RS run.

Regarding the analysis of the global connectivity measures, it revealed loss of functional integrity, however, it was not very informative to explain the mechanisms that generally occur to compensate for the disconnections provoked by MS. This further corroborates the results obtained, showing that these mechanisms have not yet been developed.

We studied the possibility of changes occurring within the brain network at a more local/nodal level through local/nodal graph measures. Moreover, we found that some nodes had different roles in early MS, with overall increased values of the connectivity measures in MS patients. An additional result in the BM run was that pagerank centrality proved to be one of the measures with most ROIs showing significant differences between groups, already reported by other studies to be altered in MS patients, and ROIs in the parietal lobule were detected, which did not happen in the other runs. The results of the correlations of FC with the scores of neuropsychological tests are also important and useful for what may be happening in MS (adaptive or maladaptive mechanisms) depending on each paradigm. Interesting patterns were found that may provide useful information: in the correlations of connectivity with EDSS and MFIS tests the results of the BM run are the inverse of the results

of the less complex runs, and in the correlations of connectivity with the remaining tests we no longer verify this, but we still evidence a difference between the BM run and the others.

This thesis opens paths for many research fronts, not only to improve the identification of potentially useful candidate biomarkers for the disease but also to allow the identification of novel treatment options, such as targeted intervention.

References

[1] M. M. Goldenberg, "DISEASE OVERVIEW Multiple Sclerosis Review," 2012.

[2] C. Walton *et al.*, "Rising prevalence of multiple sclerosis worldwide: Insights from the Atlas of MS, third edition," *Multiple Sclerosis Journal*, vol. 26, no. 14, pp. 1816–1821, Dec. 2020, doi: 10.1177/1352458520970841.

[3] A. Feinstein, J. Freeman, and A. C. Lo, "Treatment of progressive multiple sclerosis: What works, what does not, and what is needed," *The Lancet Neurology*, vol. 14, no. 2. Lancet Publishing Group, pp. 194–207, 2015. doi: 10.1016/S1474-4422(14)70231-5.

[4] F. Azarmi, S. N. Miri Ashtiani, A. Shalbaf, H. Behnam, and M. R. Daliri, "Granger causality analysis in combination with directed network measures for classification of MS patients and healthy controls using task-related fMRI," *Computers in Biology and Medicine*, vol. 115, Dec. 2019, doi: 10.1016/j.compbiomed.2019.103495.

[5] N. Ghasemi, S. Razavi, and E. Nikzad, "Multiple Sclerosis: Pathogenesis, Symptoms, Diagnoses and Cell-Based Therapy Citation: Ghasemi N, Razavi Sh, Nikzad E. Multiple sclerosis: pathogenesis, symptoms, diagnoses and cell-based therapy."

[6] N. Garg and T. W. Smith, "An update on immunopathogenesis, diagnosis, and treatment of multiple sclerosis," *Brain and Behavior*, vol. 5, no. 9, Sep. 2015, doi: 10.1002/brb3.362.

[7] R. Dobson and G. Giovannoni, "Multiple sclerosis – a review," *European Journal of Neurology*, vol. 26, no. 1. Blackwell Publishing Ltd, pp. 27–40, Jan. 01, 2019. doi: 10.1111/ene.13819.

[8] S. Ömerhoca, S. Yazici Akkaş, and N. Kale Içen, "Multiple sclerosis: Diagnosis and differential diagnosis," *Noropsikiyatri Arsivi*, vol. 55. Turkish Neuropsychiatric Society, pp. S1–S9, Sep. 01, 2018. doi: 10.29399/NPA.23418.

[9] A. J. Thompson *et al.*, "Diagnosis of multiple sclerosis: 2017 revisions of the McDonald criteria," *The Lancet Neurology*, vol. 17, no. 2. Lancet Publishing Group, pp. 162–173, Feb. 01, 2018. doi: 10.1016/S1474-4422(17)30470-2.

[10] S. Meyer-Moock, Y. S. Feng, M. Maeurer, F. W. Dippel, and T. Kohlmann, "Systematic literature review and validity evaluation of the Expanded Disability Status Scale (EDSS) and the Multiple Sclerosis Functional Composite (MSFC) in patients with multiple sclerosis," *BMC Neurology*, vol. 14, no. 1, Mar. 2014, doi: 10.1186/1471-2377-14-58.

[11] M. John F. Kurtzke, "Rating neurologic impairment in multiple sclerosis: An expanded disability status scale (EDSS)," *NEUROLOGY (Cleveland)*, pp. 1444–1452, 1983.

[12] N. Kashou, "A Practical Guide to an fMRI Experiment," in *Advanced Brain Neuroimaging Topics in Health and Disease - Methods and Applications*, InTech, 2014. doi: 10.5772/58260.

[13] M. A. Lindquist and T. D. Wager, "Principles of functional Magnetic Resonance Imaging."

[14] N. K. Logothetis and B. A. Wandell, "Interpreting the BOLD signal," *Annual Review of Physiology*, vol. 66. pp. 735–769, 2004. doi: 10.1146/annurev.physiol.66.082602.092845.

[15] N. K. Logothetis, "What we can do and what we cannot do with fMRI," *Nature*, vol. 453, no. 7197. Nature Publishing Group, pp. 869–878, Jun. 12, 2008. doi: 10.1038/nature06976.

[16] S. Ogawat *et al.*, “Intrinsic signal changes accompanying sensory stimulation: Functional brain mapping with magnetic resonance imaging (cerebral blood flow/blood oxygenation/visual cortex/positron emission tomography/magnetic susceptibility),” 1992.

[17] K. Uludaˇ, D. J. Dubowitz, and R. B. Buxton, “BASIC PRINCIPLES O F FUNCTIONAL MRI INTRODUCTION TO FUNCTIONAL MAGNETIC RESONANCE IMAGING.”

[18] J. C. W. Siero, A. Bhogal, and J. M. Jansma, “Blood oxygenation level-dependent/functional magnetic resonance imaging: Underpinnings, practice, and perspectives,” *PET Clinics*, vol. 8, no. 3. pp. 329–344, Jul. 2013. doi: 10.1016/j.cpet.2013.04.003.

[19] J. V. Duarte, “The role of long-range neural oscillatory synchrony as a mechanism underlying in perceptual coherence,” 2016.

[20] E. Sbardella, N. Petsas, F. Tona, and P. Pantano, “Resting-state fMRI in MS: General concepts and brief overview of its application,” *BioMed Research International*, vol. 2015. Hindawi Limited, 2015. doi: 10.1155/2015/212693.

[21] J. E. Chen, J. R. Polimeni, S. Bollmann, and G. H. Glover, “On the analysis of rapidly sampled fMRI data,” *Neuroimage*, vol. 188, pp. 807–820, Mar. 2019, doi: 10.1016/j.neuroimage.2019.02.008.

[22] Alexandre Nuno de Morais Sayal Abreu Campos, “BRAIN CONNECTIVITY ANALYSIS FOR REAL TIME FMRI NEUROFEEDBACK EXPERIMENTS,” IBILI, Coimbra, 2016.

[23] R. Abreu and J. V. Duarte, “Quantitative Assessment of the Impact of Geometric Distortions and Their Correction on fMRI Data Analyses,” *Frontiers in Neuroscience*, vol. 15, Mar. 2021, doi: 10.3389/fnins.2021.642808.

[24] João Valente Duarte, “The role of long-range neural oscillatory synchrony as a mechanism underlying in perceptual coherence,” Universidade de Coimbra, 2016.

[25] J. Faber, P. C. Antoneli, G. Via, N. S. Araújo, D. J. L. L. Pinheiro, and E. Cavalheiro, “Critical elements for connectivity analysis of brain networks.”

[26] E. Bullmore and O. Sporns, “Complex brain networks: Graph theoretical analysis of structural and functional systems,” *Nature Reviews Neuroscience*, vol. 10, no. 3. pp. 186–198, Mar. 2009. doi: 10.1038/nrn2575.

[27] V. Fleischer *et al.*, “Graph Theoretical Framework of Brain Networks in Multiple Sclerosis: A Review of Concepts,” *Neuroscience*, vol. 403. Elsevier Ltd, pp. 35–53, Apr. 01, 2019. doi: 10.1016/j.neuroscience.2017.10.033.

[28] F. v. Farahani, W. Karwowski, and N. R. Lighthall, “Application of graph theory for identifying connectivity patterns in human brain networks: A systematic review,” *Frontiers in Neuroscience*, vol. 13, no. JUN. Frontiers Media S.A., 2019. doi: 10.3389/fnins.2019.00585.

[29] L. Barnett and A. K. Seth, “The MVGC multivariate Granger causality toolbox: A new approach to Granger-causal inference,” *Journal of Neuroscience Methods*, vol. 223, pp. 50–68, Feb. 2014, doi: 10.1016/j.jneumeth.2013.10.018.

[30] Q. K. Telesford, S. L. Simpson, J. H. Burdette, S. Hayasaka, and P. J. Laurienti, “The Brain as a Complex System: Using Network Science as a Tool for Understanding the Brain,” *Brain Connectivity*, vol. 1, no. 4. pp. 295–308, Oct. 01, 2011. doi: 10.1089/brain.2011.0055.

[31] M. Rubinov and O. Sporns, “Complex network measures of brain connectivity: Uses and interpretations,” *Neuroimage*, vol. 52, no. 3, pp. 1059–1069, Sep. 2010, doi: 10.1016/j.neuroimage.2009.10.003.

[32] M. A. Rocca, P. Valsasina, A. Meani, A. Falini, G. Comi, and M. Filippi, "Impaired functional integration in multiple sclerosis: a graph theory study," *Brain Structure and Function*, vol. 221, no. 1, pp. 115–131, Jan. 2016, doi: 10.1007/s00429-014-0896-4.

[33] S. N. Miri Ashtiani, H. Behnam, M. R. Daliri, G. A. Hossein-Zadeh, and M. Mehrpour, "Analysis of brain functional connectivity network in MS patients constructed by modular structure of sparse weights from cognitive task-related fMRI," *Australasian Physical and Engineering Sciences in Medicine*, vol. 42, no. 4, pp. 921–938, Dec. 2019, doi: 10.1007/s13246-019-00790-1.

[34] J. Liu *et al.*, "Complex Brain Network Analysis and Its Applications to Brain Disorders: A Survey," *Complexity*, vol. 2017. Hindawi Limited, 2017. doi: 10.1155/2017/8362741.

[35] S. N. Miri Ashtiani *et al.*, "Altered topological properties of brain networks in the early MS patients revealed by cognitive task-related fMRI and graph theory," *Biomedical Signal Processing and Control*, vol. 40, pp. 385–395, Feb. 2018, doi: 10.1016/j.bspc.2017.10.006.

[36] M. Mijalkov, E. Kakaei, J. B. Pereira, E. Westman, and G. Volpe, "BRAPH: A graph theory software for the analysis of brain connectivity," *PLoS ONE*, vol. 12, no. 8, Aug. 2017, doi: 10.1371/journal.pone.0178798.

[37] Alan Shaw, "Understanding The Concepts of Eigenvector Centrality And Pagerank," Jul. 13, 2019.

[38] S. Dalai, Jadavpur University, Institute of Electrical and Electronics Engineers, Institute of Electrical and Electronics Engineers. Kolkata Section., and IEEE Signal Processing Society. Kolkata Chapter., *Proceedings of 2018 IEEE Applied Signal Processing Conference (ASPCON) : Dec 7-9, 2018, venue: Jadavpur University Main Campus, Kolkata, India*.

[39] A. Ceccarelli, R. Bakshi, and M. Neema, "MRI in multiple sclerosis: A review of the current literature," *Current Opinion in Neurology*, vol. 25, no. 4. pp. 402–409, Aug. 2012. doi: 10.1097/WCO.0b013e328354f63f.

[40] M. Filippi and F. Agosta, "Imaging biomarkers in multiple sclerosis," *Journal of Magnetic Resonance Imaging*, vol. 31, no. 4. John Wiley and Sons Inc., pp. 770–788, 2010. doi: 10.1002/jmri.22102.

[41] M. Filippi and M. A. Rocca, "MR imaging of multiple sclerosis," *Radiology*, vol. 259, no. 3. pp. 659–681, Jun. 2011. doi: 10.1148/radiol.11101362.

[42] R. Bakshi *et al.*, "MRI in multiple sclerosis: current status and future prospects," *The Lancet Neurology*, vol. 7, no. 7. pp. 615–625, Jul. 2008. doi: 10.1016/S1474-4422(08)70137-6.

[43] D. García-Lorenzo, S. Francis, S. Narayanan, D. L. Arnold, and D. L. Collins, "Review of automatic segmentation methods of multiple sclerosis white matter lesions on conventional magnetic resonance imaging," *Medical Image Analysis*, vol. 17, no. 1. pp. 1–18, Jan. 2013. doi: 10.1016/j.media.2012.09.004.

[44] M. A. Rocca, M. M. Schoonheim, P. Valsasina, J. J. G. Geurts, and M. Filippi, "Task- and resting-state fMRI studies in multiple sclerosis: From regions to systems and time-varying analysis. Current status and future perspective," *NeuroImage: Clinical*, vol. 35, p. 103076, 2022, doi: 10.1016/j.nicl.2022.103076.

[45] A. Droby *et al.*, "Changes in brain functional connectivity patterns are driven by an individual lesion in MS: a resting-state fMRI study," *Brain Imaging and Behavior*, vol. 10, no. 4, pp. 1117–1126, Dec. 2016, doi: 10.1007/s11682-015-9476-3.

[46] K. A. Meijer, Q. van Geest, A. J. C. Eijlers, J. J. G. Geurts, M. M. Schoonheim, and H. E. Hulst, "Is impaired information processing speed a matter of structural or functional damage in MS?," *NeuroImage: Clinical*, vol. 20, pp. 844–850, Jan. 2018, doi: 10.1016/j.nicl.2018.09.021.

[47] B. Audoin *et al.*, "Compensatory cortical activation observed by fMRI during a cognitive task at the earliest stage of MS," *Human Brain Mapping*, vol. 20, no. 2, pp. 51–58, Oct. 2003, doi: 10.1002/hbm.10128.

[48] C. Mainero *et al.*, "fMRI evidence of brain reorganization during attention and memory tasks in multiple sclerosis," *Neuroimage*, vol. 21, no. 3, pp. 858–867, Mar. 2004, doi: 10.1016/j.neuroimage.2003.10.004.

[49] W. Staffen *et al.*, "Cognitive function and fMRI in patients with multiple sclerosis: evidence for compensatory cortical activation during an attention task."

[50] B. Basile *et al.*, "Functional connectivity changes within specific networks parallel the clinical evolution of multiple sclerosis," *Multiple Sclerosis Journal*, vol. 20, no. 8, pp. 1050–1057, 2014, doi: 10.1177/1352458513515082.

[51] P. Preziosa *et al.*, "Progression of regional atrophy in the left hemisphere contributes to clinical and cognitive deterioration in multiple sclerosis: A 5-year study," *Human Brain Mapping*, vol. 38, no. 11, pp. 5648–5665, Nov. 2017, doi: 10.1002/hbm.23755.

[52] O. Agcaoglu, R. Miller, A. R. Mayer, K. Hugdahl, and V. D. Calhoun, "Lateralization of resting state networks and relationship to age and gender," *Neuroimage*, vol. 104, pp. 310–325, Jan. 2015, doi: 10.1016/j.neuroimage.2014.09.001.

[53] M. Tahedl, S. M. Levine, M. W. Greenlee, R. Weissert, and J. v. Schwarzbach, "Functional connectivity in multiple sclerosis: Recent findings and future directions," *Frontiers in Neurology*, vol. 9, no. OCT. Frontiers Media S.A., Oct. 11, 2018. doi: 10.3389/fneur.2018.00828.

[54] D. Veréb *et al.*, "Altered brain network function during attention-modulated visual processing in multiple sclerosis," *Multiple Sclerosis Journal*, vol. 27, no. 9, pp. 1341–1349, Aug. 2021, doi: 10.1177/1352458520958360.

[55] A. Charil *et al.*, "Statistical mapping analysis of lesion location and neurological disability in multiple sclerosis: Application to 452 patient data sets," *Neuroimage*, vol. 19, no. 3, pp. 532–544, Jul. 2003, doi: 10.1016/S1053-8119(03)00117-4.

[56] M. Filippi *et al.*, "Does hemispheric dominance influence brain lesion distribution in multiple sclerosis?," 1995.

[57] E. M. Pool, A. K. Rehme, S. B. Eickhoff, G. R. Fink, and C. Grefkes, "Functional resting-state connectivity of the human motor network: Differences between right- and left-handers," *Neuroimage*, vol. 109, pp. 298–306, Apr. 2015, doi: 10.1016/j.neuroimage.2015.01.034.

[58] N. Shu *et al.*, "Disrupted topological organization of structural and functional brain connectomes in clinically isolated syndrome and multiple sclerosis," *Scientific Reports*, vol. 6, Jul. 2016, doi: 10.1038/srep29383.

[59] T. Welton, C. S. Constantinescu, D. P. Auer, and R. A. DIneen, "Graph Theoretic Analysis of Brain Connectomics in Multiple Sclerosis: Reliability and Relationship with Cognition," *Brain Connectivity*, vol. 10, no. 2, pp. 95–104, Mar. 2020, doi: 10.1089/brain.2019.0717.

[60] S. Tommasin *et al.*, "Multi-scale resting state functional reorganization in response to multiple sclerosis damage," *Neuroradiology*, vol. 62, no. 6, pp. 693–704, Jun. 2020, doi: 10.1007/s00234-020-02393-0.

[61] A. Z. Abidin, U. Chockanathan, A. M. DSouza, M. Inglese, and A. Wismüller, "Using large-scale Granger causality to study changes in brain network properties in the Clinically Isolated Syndrome (CIS) stage of multiple sclerosis," in *Medical Imaging 2017: Biomedical Applications in Molecular, Structural, and Functional Imaging*, Mar. 2017, vol. 10137, p. 101371B. doi: 10.1117/12.2254395.

[62] M. M. Schoonheim, K. A. Meijer, and J. J. G. Geurts, "Network collapse and cognitive impairment in multiple sclerosis," *Frontiers in Neurology*, vol. 6, no. MAR, 2015, doi: 10.3389/fneur.2015.00082.

[63] R. Abreu *et al.*, "Optimizing EEG Source Reconstruction with Concurrent fMRI-Derived Spatial Priors," *Brain Topography*, vol. 35, no. 3, pp. 282–301, May 2022, doi: 10.1007/s10548-022-00891-3.

[64] A. C. Huk, R. F. Dougherty, and D. J. Heeger, "Retinotopy and Functional Subdivision of Human Areas MT and MST," 2002.

[65] J. F. Soares *et al.*, "On the optimal strategy for tackling head motion in fMRI data," in *BIOSIGNALS 2021 - 14th International Conference on Bio-Inspired Systems and Signal Processing; Part of the 14th International Joint Conference on Biomedical Engineering Systems and Technologies, BIOSTEC 2021*, 2021, pp. 306–313. doi: 10.5220/0010327803060313.

[66] E. T. Rolls, C. C. Huang, C. P. Lin, J. Feng, and M. Joliot, "Automated anatomical labelling atlas 3," *Neuroimage*, vol. 206, Feb. 2020, doi: 10.1016/j.neuroimage.2019.116189.

[67] A. Fornito, A. Zalesky, and E. Bullmore, "Fundamentals of Brain Network Analysis," 2016.

[68] M. Oset, M. Stasiolek, and M. Matysiak, "Cognitive Dysfunction in the Early Stages of Multiple Sclerosis—How Much and How Important?," *Current Neurology and Neuroscience Reports*, vol. 20, no. 7. Springer, Jul. 01, 2020. doi: 10.1007/s11910-020-01045-3.

[69] M. Sjøgård *et al.*, "Brain dysconnectivity relates to disability and cognitive impairment in multiple sclerosis," *Human Brain Mapping*, vol. 42, no. 3, pp. 626–643, Feb. 2021, doi: 10.1002/hbm.25247.

[70] E. A. Høgestøl *et al.*, "Functional connectivity in multiple sclerosis modelled as connectome stability: A 5-year follow-up study," *Multiple Sclerosis Journal*, vol. 28, no. 4, pp. 532–540, Apr. 2022, doi: 10.1177/13524585211030212.

[71] P. Stefancin, S. T. Govindarajan, L. Krupp, L. Charvet, and T. Q. Duong, "Resting-State Functional Connectivity Networks Associated with Fatigue in Multiple Sclerosis with Early Age Onset," 2019.

[72] M. Filippi *et al.*, "Functional magnetic resonance imaging correlates of fatigue in multiple sclerosis," *Neuroimage*, vol. 15, no. 3, pp. 559–567, 2002, doi: 10.1006/nimg.2001.1011.

[73] H. Li *et al.*, "Functional parcellation of the right cerebellar lobule VI in children with normal or impaired reading," *Neuropsychologia*, vol. 148, Nov. 2020, doi: 10.1016/j.neuropsychologia.2020.107630.

[74] Z. M. Manjaly *et al.*, "Pathophysiological and cognitive mechanisms of fatigue in multiple sclerosis," *Journal of Neurology, Neurosurgery and Psychiatry*, vol. 90, no. 6. BMJ Publishing Group, pp. 642–651, Jun. 01, 2019. doi: 10.1136/jnnp-2018-320050.

[75] J. Zhang, R. Cortese, N. de Stefano, and A. Giorgio, "Structural and Functional Connectivity Substrates of Cognitive Impairment in Multiple Sclerosis," *Frontiers in Neurology*, vol. 12. Frontiers Media S.A., Jul. 08, 2021. doi: 10.3389/fneur.2021.671894.

[76] C. Sousa *et al.*, "Validation of the brief international cognitive assessment for multiple sclerosis (BICAMS) in the Portuguese population with multiple sclerosis 11 Medical and Health Sciences 1109 Neurosciences," *BMC Neurology*, vol. 18, no. 1, Oct. 2018, doi: 10.1186/s12883-018-1175-4.

[77] S. Stegen *et al.*, "Validity of the California verbal learning test-II in multiple sclerosis," *Clinical Neuropsychologist*, vol. 24, no. 2, pp. 189–202, Feb. 2010, doi: 10.1080/13854040903266910.

[78] D. Veréb *et al.*, "Functional Connectivity Lateralisation Shift of Resting State Networks is Linked to Visuospatial Memory and White Matter Microstructure in Relapsing–Remitting Multiple Sclerosis," *Brain Topography*, vol. 35, no. 2, pp. 268–275, Mar. 2022, doi: 10.1007/s10548-021-00881-x.

[79] M. Tops and M. A. S. Boksem, "A potential role of the inferior frontal gyrus and anterior insula in cognitive control, brain rhythms, and event-related potentials," *Frontiers in Psychology*, vol. 2, no. NOV, 2011, doi: 10.3389/fpsyg.2011.00330.

[80] E. Bora, S. Özakbaş, D. Velakoulis, and M. Walterfang, "Social Cognition in Multiple Sclerosis: a Meta-Analysis," *Neuropsychology Review*, vol. 26, no. 2. Springer New York LLC, pp. 160–172, Jun. 01, 2016. doi: 10.1007/s11065-016-9320-6.

[81] C. Bouarab, B. Thompson, and A. M. Polter, "VTA GABA Neurons at the Interface of Stress and Reward," *Frontiers in Neural Circuits*, vol. 13. Frontiers Media S.A., Dec. 05, 2019. doi: 10.3389/fncir.2019.00078.

[82] M. D. Fox and M. E. Raichle, "Spontaneous fluctuations in brain activity observed with functional magnetic resonance imaging," *Nature Reviews Neuroscience*, vol. 8, no. 9. pp. 700–711, Sep. 2007. doi: 10.1038/nrn2201.

8. Appendix

I. Global Connectivity measures – Results

Table 103- **(RUN V1MT)** Mean values of each global connectivity measure and standard deviation for each PTh (0.06-0.32) in each group (CNT and MSC). Additionally, p-values from the Wilcoxon rank sum test performed to assess which measures were significantly different between groups ($p<0.05$) are also represented in the table.

Characteristic Path Length					Radius					Diameter					Mean Clustering Coefficient				
	PTh	CNT	MSC	p-value		PTh	CNT	MSC	p-value		PTh	CNT	MSC	p-value		PTh	CNT	MSC	p-value
	0.06	0.95±0.17	0.95±0.14	0.9605		0.06	1.76±4.96	0.71±3.03	0.4968		0.06	24.25±4.89	23.86±4.81	0.6799		0.06	0.044±0.011	0.046±0.011	0.0514
	0.07	1.09±0.20	1.09±0.16	0.9605		0.07	1.76±4.96	0.71±3.03	0.4968		0.07	24.25±4.89	23.86±4.81	0.6799		0.07	0.046±0.010	0.048±0.011	0.1528
	0.08	1.22±0.23	1.22±0.18	0.9605		0.08	2.39±5.40	0.71±3.03	0.2691		0.08	24.25±4.89	23.86±4.81	0.6799		0.08	0.048±0.009	0.050±0.010	0.1573
	0.09	1.36±0.25	1.36±0.20	0.9342		0.09	3.22±6.05	0.71±3.03	0.1289		0.09	24.25±4.89	23.86±4.81	0.6799		0.09	0.051±0.009	0.051±0.009	0.5755
	0.10	1.49±0.28	1.49±0.21	0.9080		0.10	3.85±6.25	1.92±4.45	0.3128		0.10	24.25±4.89	23.86±4.81	0.6799		0.10	0.054±0.008	0.052±0.008	0.8986
	0.11	1.62±0.30	1.62±0.23	0.9080		0.11	3.85±6.25	1.92±4.45	0.3128		0.11	24.25±4.89	23.86±4.81	0.6799		0.11	0.055±0.008	0.053±0.008	0.9573
	0.12	1.74±0.32	1.75±0.24	0.9080		0.12	6.13±6.84	1.92±4.45	0.0509		0.12	24.25±4.89	23.86±4.81	0.6799		0.12	0.056±0.008	0.055±0.008	0.93536
	0.13	1.87±0.35	1.87±0.26	0.8819		0.13	7.26±7.34	2.76±5.38	0.0546		0.13	24.25±4.89	23.86±4.81	0.6799		0.13	0.057±0.007	0.056±0.007	0.9205
	0.14	1.99±0.37	1.99±0.27	0.8819		0.14	8.64±6.91	4.02±5.96	0.0549		0.14	24.25±4.89	23.86±4.81	0.6799		0.14	0.058±0.007	0.057±0.007	0.4984
	0.15	2.11±0.40	2.12±0.29	0.8559		0.15	8.64±6.91	5.70±6.72	0.2594		0.15	24.25±4.89	23.86±4.81	0.6799		0.15	0.060±0.007	0.058±0.007	0.1485
	0.16	2.23±0.42	2.24±0.30	0.8301		0.16	8.64±6.91	5.70±6.72	0.2594		0.16	24.25±4.89	23.86±4.81	0.6799		0.16	0.061±0.006	0.058±0.007	0.0228
	0.17	2.35±0.44	2.36±0.31	0.8045		0.17	8.64±6.91	6.99±6.62	0.4843		0.17	24.25±4.89	23.86±4.81	0.6799		0.17	0.062±0.006	0.059±0.006	0.0049
	0.18	2.48±0.46	2.48±0.33	0.8045		0.18	8.64±6.91	6.99±6.62	0.4843		0.18	24.25±4.89	23.86±4.81	0.6799		0.18	0.063±0.006	0.060±0.006	0.0003
	0.19	2.59±0.49	2.60±0.34	0.8045		0.19	9.16±6.55	6.99±6.62	0.4065		0.19	24.25±4.89	23.86±4.81	0.6799		0.19	0.064±0.006	0.060±0.006	2.994e-5
	0.20	2.70±0.51	2.72±0.35	0.8045		0.20	9.16±6.55	7.63±6.46	0.5669		0.20	24.25±4.89	23.86±4.81	0.6799		0.20	0.065±0.006	0.061±0.006	2.974e-7
	0.21	2.82±0.53	2.83±0.37	0.8045		0.21	9.89±6.14	8.35±6.29	0.5816		0.21	24.25±4.89	23.86±4.81	0.6799		0.21	0.065±0.005	0.061±0.005	1.034e-8
	0.22	2.93±0.55	2.94±0.38	0.8045		0.22	9.89±6.14	8.95±5.95	0.7019		0.22	24.25±4.89	23.86±4.81	0.6799		0.22	0.066±0.005	0.062±0.005	2.464e-11
	0.23	3.04±0.58	3.06±0.39	0.8301		0.23	10.43±5.59	8.95±5.95	0.6420		0.23	24.25±4.89	23.86±4.81	0.6799		0.23	0.066±0.005	0.062±0.005	1.642e-13
	0.24	3.15±0.60	3.17±0.40	0.8301		0.24	11.04±4.91	8.95±5.95	0.5620		0.24	24.25±4.89	23.86±4.81	0.6799		0.24	0.067±0.005	0.062±0.005	2.959e-15
	0.25	3.26±0.62	3.28±0.42	0.8301		0.25	11.04±4.91	8.95±5.95	0.5620		0.25	24.25±4.89	23.86±4.81	0.6799		0.25	0.068±0.005	0.063±0.005	6.514e-18
	0.26	3.37±0.64	3.39±0.43	0.7791		0.26	11.04±4.91	9.46±5.51	0.6314		0.26	24.25±4.89	23.86±4.81	0.6799		0.26	0.069±0.005	0.063±0.005	3.571e-20
	0.27	3.48±0.66	3.50±0.44	0.7791		0.27	11.04±4.91	10.03±4.98	0.7039		0.27	24.25±4.89	23.86±4.81	0.6799		0.27	0.069±0.005	0.063±0.004	4.208e-22
	0.28	3.58±0.68	3.61±0.45	0.7791		0.28	11.04±4.91	10.03±4.98	0.7039		0.28	24.25±4.89	23.86±4.81	0.6799		0.28	0.069±0.005	0.063±0.004	3.1912e-24
	0.29	3.69±0.71	3.71±0.46	0.7791		0.29	11.04±4.91	10.03±4.98	0.7039		0.29	24.25±4.89	23.86±4.81	0.6799		0.29	0.070±0.005	0.063±0.004	8.832e-27
	0.30	3.79±0.73	3.82±0.47	0.7791		0.30	11.04±4.91	10.03±4.98	0.7039		0.30	24.25±4.89	23.86±4.81	0.6799		0.30	0.070±0.004	0.063±0.004	2.956e-29
	0.31	3.89±0.75	3.92±0.49	0.7791		0.31	11.0±4.91	10.03±4.98	0.7039		0.31	24.25±4.89	23.86±4.81	0.6799		0.31	0.070±0.004	0.064±0.004	3.5579e-32
	0.32	3.99±0.77	4.03±0.50	0.7539		0.32	11.04±4.91	10.03±4.98	0.7039		0.32	24.25±4.89	23.86±4.81	0.6799		0.32	0.070±0.004	0.064±0.004	4.8863e-34

* continues in next page

odularity	PTh	CNT	MSC	p-value	Global Effiency	PTh	CNT	MSC	p-value	Global Flow Coefficient	PTh	CNT	MSC	p-value	Assortativity	PTh	CNT	MSC	p-value
	0.06	0.258±0.044	0.278±0.059	0.181		0.06	0.083±0.023	0.091±0.024	0.255		0.06	0.079±0.040	0.099±0.036	0.151		0.06	-0.216 ±0.114	-0.203±0.097	0.656
	0.07	0.243±0.044	0.267±0.054	0.142		0.07	0.093±0.021	0.100±0.024	0.283		0.07	0.083±0.042	0.104±0.037	0.133		0.07	-0.216±0.117	-0.197±0.098	0.520
	0.08	0.233±0.043	0.256±0.055	0.125		0.08	0.101±0.021	0.107±0.023	0.419		0.08	0.086±0.041	0.108±0.038	0.102		0.08	-0.207±0.114	-0.193±0.100	0.609
	0.09	0.224±0.044	0.246±0.051	0.117		0.09	0.108±0.022	0.113±0.022	0.656		0.09	0.088±0.042	0.111±0.039	0.109		0.09	-0.205±0.114	-0.189±0.097	0.564
	0.10	0.216±0.041	0.235±0.050	0.216		0.10	0.113±0.021	0.118±0.022	0.656		0.10	0.090±0.042	0.114±0.040	0.096		0.10	-0.201±0.113	-0.184±0.097	0.542
	0.11	0.208±0.040	0.228±0.048	0.216		0.11	0.118±0.022	0.122±0.022	0.754		0.11	0.092±0.042	0.116±0.040	0.096		0.11	-0.197±0.114	-0.179±0.095	0.656
	0.12	0.202±0.038	0.220±0.048	0.204		0.12	0.122±0.021	0.125±0.021	0.882		0.12	0.094±0.042	0.119±0.040	0.089		0.12	-0.193±0.114	-0.175±0.093	0.729
	0.13	0.195±0.038	0.216±0.045	0.133		0.13	0.126±0.021	0.127±0.020	0.987		0.13	0.096±0.041	0.120±0.040	0.083		0.13	-0.191±0.112	-0.170±0.091	0.609
	0.14	0.192±0.037	0.211±0.042	0.204		0.14	0.129±0.022	0.129±0.020	0.856		0.14	0.098±0.041	0.122±0.040	0.083		0.14	-0.189±0.112	-0.166±0.090	0.586
	0.15	0.186±0.035	0.205±0.043	0.216		0.15	0.131±0.022	0.131±0.020	0.779		0.15	0.100±0.041	0.124±0.040	0.067		0.15	-0.185±0.112	-0.161±0.087	0.478
	0.16	0.180±0.036	0.201±0.041	0.096		0.16	0.133±0.023	0.132±0.020	0.754		0.16	0.101±0.041	0.126±0.040	0.077		0.16	-0.182±0.111	-0.158±0.087	0.520
	0.17	0.177±0.034	0.197±0.039	0.109		0.17	0.134±0.023	0.133±0.020	0.729		0.17	0.102±0.042	0.127±0.040	0.083		0.17	-0.179±0.108	-0.154±0.086	0.520
	0.18	0173±0.034	0.192±0.039	0.133		0.18	0.136±0.024	0.134±0.020	0.609		0.18	0.104±0.041	0.129±0.040	0.096		0.18	-0.177±0.108	-0.151±0.086	0.478
	0.19	0.168±0.034	0.188±0.038	0.089		0.19	0.137±0.024	0.134±0.020	0.586		0.19	0.106±0.041	0.130±0.040	0.089		0.19	-0.176±0.108	-0.146±0.086	0.438
	0.20	0.165±0.034	0.184±0.037	0.109		0.20	0.138±0.025	0.135±0.020	0.564		0.20	0.107±0.041	0.132±0.040	0.077		0.20	-0.174±0.108	-0.144±0.085	0.419
	0.21	0.161±0.033	0.181±0.036	0.117		0.21	0.138±0.025	0.135±0.020	0.499		0.21	0.108±0.041	0.133±0.040	0.077		0.21	-0.172±0.106	-0.140±0.084	0.438
	0.22	0.158±0.034	0.178±0.035	0.102		0.22	0.139±0.025	0.135±0.020	0.458		0.22	0.110±0.041	0.135±0.039	0.072		0.22	-0.169±0.104	-0.138±0.083	0.400
	0.23	0.155±0.034	0.175±0.035	0.125		0.23	0.140±0.026	0.135±0.021	0.478		0.23	0.111±0.041	0.136±0.039	0.067		0.23	-0.166±0.104	-0.134±0.083	0.382
	0.24	0.153±0.034	0.172±0.034	0.142		0.24	0.140±0.026	0.135±0.021	0.438		0.24	0.113±0.041	0.137±0.039	0.062		0.24	-0.163±0.103	-0.132±0.082	0.382
	0.25	0.151±0.034	0.170±0.033	0.151		0.25	0.140±0.026	0.136±0.021	0.458		0.25	0.114±0.041	0.139±0.039	0.072		0.25	-0.161±0.102	-0.129±0.081	0.382
	0.26	0.148±0.033	0.168±0.034	0.102		0.26	0.141±0.026	0.136±0.021	0.458		0.26	0.115±0.041	0.140±0.038	0.072		0.26	-0.157±0.102	-0.126±0.080	0.382
	0.27	0.146±0.033	0.164±0.032	0.125		0.27	0.141±0.026	0.136±0.021	0.458		0.27	0.117±0.041	0.142±0.038	0.062		0.27	-0.155±0.101	-0.123±0.079	0.382
	0.28	0.144±0.032	0.162±0.033	0.102		0.28	0.141±0.026	0.136±0.021	0.458		0.28	0.118±0.041	0.143±0.038	0.054		0.28	-0.153±0.100	-0.121±0.078	0.382
	0.29	0.141±0.032	0.160±0.032	0.083		0.29	0.141±0.027	0.136±0.021	0.458		0.29	0.119±0.041	0.144±0.037	0.058		0.29	-0.151±0.099	-0.118±0.077	0.382
	0.30	0.139±0.032	0.157±0.031	0.125		0.30	0.141±0.027	0.136±0.021	0.458		0.30	0.120±0.041	0.145±0.037	0.054		0.30	-0.148±0.098	-0.115±0.076	0.400
	0.31	0.138±0.032	0.156±0.031	0.117		0.31	0.141±0.027	0.136±0.021	0.438		0.31	0.121±0.041	0.146±0.037	0.058		0.31	-0.146±0.098	-0.113±0.075	0.400
	0.32	0.136±0.031	0.154±0.031	0.102		0.32	0.141±0.027	0.136±0.021	0.438		0.32	0.122±0.041	0.147±0.037	0.058		0.32	-0.142±0.097	-0.111±0.074	0.400

Table 11- **(RUN BM)** Mean values of each global connectivity measure and standard deviation for each PTh (0.06-0.32) in each group (CNT and MSC). Additionally, p-values from the Wilcoxon rank sum test performed to assess which measures were significantly different between groups ($p<0.05$) are also represented in the table.

Characteristic Path Length					Radius					Diameter					Mean Clustering Coefficient				
	PTh	CNT	MSC	p-value		PTh	CNT	MSC	p-value		PTh	CNT	MSC	p-value		PTh	CNT	MSC	p-value
	0.06	0. 729 ±0.104	0.729±0.145	0.830		0.06	0	0	NaN		0.06	20.81± 4.13	19.24± 4.78	0.31		0.06	0.080±0.024	0.073±0.5	0.2259
	0.07	0. 829 ±0.118	0.831±0.163	0.882		0.07	0	0	NaN		0.07	20.81± 4.13	19.24± 4.78	0.31		0.07	0.085±0.023	0.079±0.024	0.0783
	0.08	0. 926 ±0.131	0.931±0.180	0.882		0.08	0	0	NaN		0.08	20.81± 4.13	19.24± 4.78	0.31		0.08	0.087±0.023	0.081±0.024	0.1307
	0.09	1.201 ±0.145	1.028 ±0.197	0.856		0.09	0	0	NaN		0.09	20.81± 4.13	19.24± 4.78	0.31		0.09	0.089±0.022	0.085±0.023	0.1350
	0.10	1.113 ±0.158	1.123±0.213	0.805		0.10	0	0	NaN		0.10	20.81± 4.13	19.24± 4.78	0.31		0.10	0.091±0.020	0.087±0.022	0.1731
	0.11	1.204 ±0.170	1.216±0.228	0.754		0.11	0	0	NaN		0.11	20.81± 4.13	19.24± 4.78	0.31		0.11	0.092±0.020	0.090±0.022	0.1823
	0.12	1.293 ±0.182	1.308±0.243	0.704		0.12	0	0	NaN		0.12	20.81± 4.13	19.24± 4.78	0.31		0.12	0.0950.019	0.092±0.021	0.1302
	0.13	1.380 ±0.194	1.398±0.258	0.704		0.13	0	0	NaN		0.13	20.81± 4.13	19.24± 4.78	0.31		0.13	0.098±0.019	0.094±0.020	0.1058
	0.14	1.466 ±0206	1.486±0.273	0.680		0.14	0	1.595±3.692	0,089		0.14	20.81± 4.13	19.24± 4.78	0.31		0.14	0.101±0.019	0.096±0.020	0.0627
	0.15	1.551 ±0.217	1.574±0.287	0.632		0.15	0	1.962±3.848	0.055		0.15	20.81± 4.13	19.24± 4.78	0.31		0.15	0.102±0.019	0.098±0.019	0.0791
	0.16	1.635 ±0.228	1.660±0.301	0.609		0.16	0.633±2.610	1.962±3.848	0.222		0.16	20.81± 4.13	19.24± 4.78	0.31		0.16	0.105±0.018	0.101±0.018	0.0308
	0.17	1.717 ±0.238	1.745±0.314	0.609		0.17	0.633±2.610	1.962±3.848	0.222		0.17	20.81± 4.13	19.24± 4.78	0.31		0.17	0.107±0.018	0.103±0.018	0.0315
	0.18	1.798±0.249	1.829±0.328	0.632		0.18	0.633±2.610	1.962±3.848	0.222		0.18	20.81± 4.13	19.24± 4.78	0.31		0.18	0.109±0.017	0.105±0.017	0.0234
	0.19	1.878 ±0.260	1.912±0.341	0.632		0.19	0.633±2.610	2.291±3.923	0.125		0.19	20.81± 4.13	19.24± 4.78	0.31		0.19	0.112±0.017	0.108±0.016	0.0203
	0.20	1.958±0.280	1.994±0.354	0.632		0.20	1.072±3.083	2.852±4.282	0.171		0.20	20.81± 4.13	19.24± 4.78	0.31		0.20	0.113±0.016	0.109±0.016	0.0203
	0.21	2.036 ±0.290	2.075±0.366	0.609		0.21	1.582±3.572	3.370±4.476	0.207		0.21	20.81± 4.13	19.24± 4.78	0.31		0.21	0.116±0.016	0.111±0.016	0.0043
	0.22	2.113 ±0.300	2.155±0.379	0.609		0.22	1.582±3.572	3.370±4.476	0.207		0.22	20.81± 4.13	19.24± 4.78	0.31		0.22	0.118±0.016	0.113±0.015	0.0024
	0.23	2.190±0.310	2.235±0.392	0.609		0.23	2.530±4.091	4.726±4.496	0.159		0.23	20.81± 4.13	19.24± 4.78	0.31		0.23	0.121±0.016	0.115±0.015	0.0007
	0.24	2.266 ±0.320	2.313±0.404	0.609		0.24	4.253±4.262	4.726±4.496	0.665		0.24	20.81± 4.13	19.24± 4.78	0.31		0.24	0.122±0.015	0.116±0.015	0.0002
	0.25	2.1341 ±0.330	2.391±0.416	0.609		0.25	4.253±4.262	5.233±4.446	0.419		0.25	20.81± 4.13	19.24± 4.78	0.31		0.25	0.124±0.015	0.118±0.015	4.2923e-5
	0.26	2.415 ±0.228	2.468±0.428	0.656		0.26	4.741±4.219	5.233±4.446	0.609		0.26	20.81± 4.13	19.24± 4.78	0.31		0.26	0.126±0.015	0.120±0.015	1.4723e-5
	0.27	2.488 ±0.340	2.544±0.440	0.632		0.27	4.741±4.219	5.233±4.446	0.609		0.27	20.81± 4.13	19.24± 4.78	0.31		0.27	0.127±0.014	0.121±0.014	1.039e-5
	0.28	2.561 ±0.349	2.619±0,451	0.632		0.28	4.741±4.219	5.678±4.290	0.426		0.28	20.81± 4.13	19.24± 4.78	0.31		0.28	0.129±0.014	0.122±0.014	3.6434e-6
	0.29	2.633 ±0.359	2.694±0.463	0.632		0.29	5.173±4.077	6.550±3.791	0.263		0.29	20.81± 4.13	19.24± 4.78	0.31		0.29	0.132±0.014	0.124±0.014	3.0979e-7
	0.30	2.704 ±0.368	2.768±0.474	0.656		0.30	5.534±3.856	6.905±3.423	0.232		0.30	20.81± 4.13	19.24± 4.78	0.31		0.30	0.133±0.013	0.126±0.014	2.6913e-7
	0.31	2.775 ± 0.378	2.842±0.485	0.656		0.31	5.985±3.608	6.905±3.423	0.328		0.31	20.81± 4.13	19.24± 4.78	0.31		0.31	0.135±0.013	0.127±0.013	2.3782e-7
	0.32	2.845±0.387	2.915±0.496	0.656		0.32	5.985±3.608	7.667±2.350	0.181		0.32	20.81± 4.13	19.24± 4.78	0.31		0.32	0.136±0.013	0.128±0.013	7.8220e-8

* continues in next page

Modularity	PTh	CNT	MSC	p-value	Global Effiency	PTh	CNT	MSC	p-value	Global Flow Coefficient	PTh	CNT	MSC	p-value	Assortativity	PTh	CNT	MSC	p-value
	0.06	0.318±0.064	0.313±0.038	0.438		0.06	0.081±0.023	0.084±0.030	0.882		0.06	0.061±0.026	0.072±0.028	0.419		0.06	-0.165±0.124	-0.169±0.113	0.987
	0.07	0.295±0.063	0.290±0.034	0.564		0.07	0.095±0.023	0.097±0.031	0.632		0.07	0.066±0.025	0.076±0.027	0.419		0.07	-0.159±0.121	-0.161±0.114	0.934
	0.08	0.276±0.056	0.274±0.031	0.680		0.08	0.107±0.022	0.108±0.030	0.609		0.08	0.070±0.025	0.079±0.028	0.586		0.08	-0.149±0.122	-0.150±0.117	0.882
	0.09	0.264±0.050	0.258±0.030	0.419		0.09	0.115±0.024	0.117±0.030	0.656		0.09	0.073±0.025	0.082±0.028	0.704		0.09	-0.143±0.118	-0.145±0.113	0.882
	0.10	0.249±0.045	0.246±0.025	0.632		0.10	0.124±0.025	0.126±0.029	0.478		0.10	0.077±0.025	0.084±0.026	0.704		0.10	-0.136±0.117	-0.139±0.111	0.856
	0.11	0.236±0.039	0.238±0.025	0.934		0.11	0.132±0.025	0.133±0.028	0.542		0.11	0.080±0.025	0.088±0.026	0.729		0.11	-0.131±0.115	-0.136±0.109	0.754
	0.12	0.224±0.036	0.228±0.023	0.805		0.12	0.138±0.025	0.140±0.028	0.542		0.12	0.082±0.025	0.089±0.026	0.656		0.12	-0.128±0.114	-0.136±0.105	0.680
	0.13	0.215±0.033	0.220±0.022	0.656		0.13	0.143±0.024	0.146±0.027	0.609		0.13	0.084±0.025	0.092±0.025	0.586		0.13	-0.126±0.113	-0.133±0.101	0.754
	0.14	0.208±0.031	0.213±0.022	0.632		0.14	0.148±0.025	0.150±0.027	0.632		0.14	0.085±0.025	0.093±0.023	0.542		0.14	-0.122±0.113	-0.131±0.099	0.729
	0.15	0.200±0.029	0.206±0.022	0.632		0.15	0.152±0.025	0.155±0.027	0.656		0.15	0.086±0.025	0.095±0.022	0.520		0.15	-0.117±0.111	-0.130±0.099	0.704
	0.16	0.195±0.028	0.200±0.021	0.609		0.16	0.156±0.025	0.159±0.026	0.729		0.16	0.088±0.025	0.096±0.022	0.542		0.16	-0.114±0.111	-0.128±0.097	0.564
	0.17	0.188±0.028	0.195±0.021	0.542		0.17	0.160±0.025	0.162±0.026	0.680		0.17	0.089±0.024	0.097±0.021	0.541		0.17	-0.112±0.111	-0.127±0.094	0.478
	0.18	0.182±0.026	0.191±0.021	0.499		0.18	0.163±0.024	0.165±0.026	0.680		0.18	0.090±0.025	0.098±0.021	0.586		0.18	-0.111±0.111	-0.127±0.094	0.542
	0.19	0.178±0.025	0.185±0.020	0.542		0.19	0.166±0.024	0.168±0.026	0.704		0.19	0.091±0.025	0.099±0.021	0.564		0.19	-0.109±0.109	-0.126±0.093	0.609
	0.20	0.173±0.024	0.181±0.020	0.542		0.20	0.169±0.023	0.170±0.026	0.754		0.20	0.092±0.025	0.099±0.020	0.520		0.20	-0.108±0.110	-0.124±0.092	0.609
	0.21	0.170±0.024	0.177±0.020	0.704		0.21	0.172±0.022	0.172±0.026	0.729		0.21	0.093±0.025	0.101±0.020	0.499		0.21	-0.106±0.110	-0.123±0.092	0.564
	0.22	0.166±0.023	0.174±0.019	0.520		0.22	0.174±0.022	0.174±0.026	0.754		0.22	0.094±0.026	0.101±0.020	0.632		0.22	-0.105±0.110	-0.121±0.092	0.564
	0.23	0.162±0.023	0.172±0.019	0.364		0.23	0.176±0.022	0.176±0.026	0.779		0.23	0.095±0.026	0.102±0.020	0.586		0.23	-0.104±0.111	-0.120±0.092	0.542
	0.24	0.159±0.022	0.169±0.019	0.269		0.24	0.178±0.022	0.177±0.026	0.754		0.24	0.096±0.026	0.103±0.019	0.520		0.24	-0.105±0.111	-0.119±0.091	0.609
	0.25	0.156±0.022	0.166±0.019	0.255		0.25	0.180±0.022	0.179±0.026	0.779		0.25	0.097±0.026	0.104±0.019	0.419		0.25	-0.104±0.110	-0.119±0.090	0.542
	0.26	0.153±0.021	0.164±0.019	0.283		0.26	0.182±0.022	0.180±0.027	0.729		0.26	0.098±0.027	0.104±0.020	0.564		0.26	-0.104±0.109	-0.119±0.090	0.542
	0.27	0.150±0.021	0.161±0.018	0.241		0.27	0.183±0.022	0.181±0.027	0.680		0.27	0.099±0.027	0.105±0.020	0.564		0.27	-0.104±0.109	-0.119±0.090	0.564
	0.28	0.148±0.021	0.158±0.018	0.204		0.28	0.185±0.022	0.182±0.027	0.609		0.28	0.100±0.027	0.105±0.020	0.564		0.28	-0.104±0.108	-0.119±0.090	0.609
	0.29	0.145±0.021	0.156±0.018	0.204		0.29	0.186±0.023	0.183±0.027	0.586		0.29	0.100±0.027	0.105±0.020	0.586		0.29	-0.105±0.107	-0.116±0.090	0.704
	0.30	0.143±0.021	0.153±0.018	0.204		0.30	0.187±0.023	0.184±0.027	0.586		0.30	0.101±0.028	0.106±0.021	0.564		0.30	-0.106±0.105	-0.114±0.089	0.856
	0.31	0.140±0.020	0.152±0.018	0.171		0.31	0.188±0.022	0.185±0.027	0.609		0.31	0.102±0.028	0.106±0.021	0.656		0.31	-0.105±0.104	-0.113±0.088	0.856
	0.32	0.138±0.021	0.149±0.018	0.161		0.32	0.189±0.022	0.185±0.027	0.586		0.32	0.103±0.027	0.107±0.021	0.805		0.32	-0.105±0.104	-0.112±0.087	0.830

Table 8.12- **(RUN RS)** Mean values of each global connectivity measure and standard deviation for each PTh (0.06-0.32) in each group (CNT and MSC). Additionally, p-values from the Wilcoxon rank sum test performed to assess which measures were significantly different between groups ($p<0.05$) are also represented in the table.

Characteristic Path Length					Radius					Diameter					Mean Clustering Coefficient				
	PTh	CNT	MSC	p-value		PTh	CNT	MSC	p-value		PTh	CNT	MSC	p-value		PTh	CNT	MSC	p-value
	0.06	0.83±0.16	0.85±0.14	0.520		0.06	0	1.64±4.76	0.176		0.06	21.25± 5.17	22.43 ± 3.90	0.314		0.06	0.0.54±0.012	0.051±0.02	0.0088
	0.07	0.96±0.19	0.97±0.16	0.542		0.07	0	2.37±5.47	0.089		0.07	21.25± 5.17	22.43 ± 3.90	0.314		0.07	0.058±0.012	0.054±0.012	0.0007
	0.08	1.07±0.21	1.09±0.18	0.542		0.08	0.66±2.71	2.37±5.47	0.296		0.08	21.25± 5.17	22.43 ± 3.90	0.314		0.08	0.061±0.012	0.057±0.011	0.0009
	0.09	1.19±0.23	1.21±0.20	0.564		0.09	1.76±3.94	2.37±5.47	0.900		0.09	21.25± 5.17	22.43 ± 3.90	0.314		0.09	0.064±0.012	0.061±0.011	0.0005
	0.10	1.30±0.25	1.33±0.22	0.564		0.10	1.76±3.94	2.37±5.47	0.900		0.10	21.25± 5.17	22.43 ± 3.90	0.314		0.10	0.067±0.011	0.063±0.010	1.4722e-5
	0.11	1.42±0.27	1.44±0.24	0.564		0.11	2.48±4.66	2.37±5.47	0.850		0.11	21.25± 5.17	22.43 ± 3.90	0.314		0.11	0.070±0.010	0.065±0.009	1.6956e-7
	0.12	1.53±0.29	1.55±0.26	0.564		0.12	3.61±5.13	2.85±5.62	0.605		0.12	21.25± 5.17	22.43 ± 3.90	0.314		0.12	0.073±0.010	0.067±0.009	1.8415e-9
	0.13	1.64±0.31	1.66±0.28	0.564		0.13	3.61±5.13	2.85±5.62	0.605		0.13	21.25± 5.17	22.43 ± 3.90	0.314		0.13	0.075±0.009	0.070±0.009	1.5212e-9
	0.14	1.74±0.33	1.77±0.29	0.586		0.14	3.61±5.13	3.39±5.80	0.873		0.14	21.25± 5.17	22.43 ± 3.90	0.314		0.14	0.077±0.009	0.071±0.008	1.0448e-10
	0.15	1.85±0.35	1.88±0.31	0.586		0.15	4.55±5.84	3.89±5.88	0.718		0.15	21.25± 5.17	22.43 ± 3.90	0.314		0.15	0.079±0.009	0.072±0.007	2.005e-12
	0.16	1.95±0.37	1.99±0.33	0.586		0.16	5.11±5.82	3.89±5.88	0.514		0.16	21.25± 5.17	22.43 ± 3.90	0.314		0.16	0.081±0.008	0.073±0.007	8.5750e-14
	0.17	2.06±0.39	2.09±0.35	0.586		0.17	5.11±5.82	3.89±5.88	0.514		0.17	21.25± 5.17	22.43 ± 3.90	0.314		0.17	0.082±0.008	0.075±0.007	1.5882e-15
	0.18	2.16±0.41	2.19±0.37	0.586		0.18	5.11±5.82	4.47±5.98	0.742		0.18	21.25± 5.17	22.43 ± 3.90	0.314		0.18	0.084±0.008	0.076±0.007	2.6968e-16
	0.19	2.26±0.42	2.30±0.38	0.609		0.19	5.11±5.82	5.05±6.03	0.986		0.19	21.25± 5.17	22.43 ± 3.90	0.314		0.19	0.085±0.008	0.077±0.007	7.0511e-17
	0.20	2.36±0.44	2.40±0.40	0.609		0.20	5.11±5.82	5.62±6.01	0.804		0.20	21.25± 5.17	22.43 ± 3.90	0.314		0.20	0.086±0.008	0.079±0.006	2.3287e-18
	0.21	2.46±0.46	2.50±0.42	0.609		0.21	6.34±5.72	6.27±6.00	0.986		0.21	21.25± 5.17	22.43 ± 3.90	0.314		0.21	0.088±0.008	0.080±0.006	8.9543e-20
	0.22	2.56±0.48	2.60±0.43	0.586		0.22	6.34±5.72	6.80±5.83	0.811		0.22	21.25± 5.17	22.43 ± 3.90	0.314		0.22	0.089±0.007	0.081±0.006	6.3341e-20
	0.23	2.65±0.49	2.70±0.45	0.586		0.23	6.34±5.72	6.80±5.83	0.811		0.23	21.25± 5.17	22.43 ± 3.90	0.314		0.23	0.090±0.007	0.081±0.006	9.4969e-21
	0.24	2.75±0.51	2.79±0.47	0.609		0.24	6.34±5.72	7.35±5.62	0.600		0.24	21.25± 5.17	22.43 ± 3.90	0.314		0.24	0.090±0.007	0.083±0.006	4.0661e-21
	0.25	2.84±0.53	2.89±0.48	0.656		0.25	6.34±5.72	7.35±5.62	0.600		0.25	21.25± 5.17	22.43 ± 3.90	0.314		0.25	0.091±0.007	0.083±0.006	1.8483e-22
	0.26	2.94±0.55	2.98±0.50	0.632		0.26	6.93±5.54	7.94±5.35	0.580		0.26	21.25± 5.17	22.43 ± 3.90	0.314		0.26	0.092±0.007	0.084±0.006	6.9448e-24
	0.27	3.03±0.56	3.08±0.52	0.632		0.27	7.51±5.28	7.94±5.35	0.713		0.27	21.25± 5.17	22.43 ± 3.90	0.314		0.27	0.093±0.007	0.085±0.005	2.1223e-24
	0.28	3.12±0.58	3.17±0.53	0.632		0.28	7.51±5.28	8.66±5.09	0.415		0.28	21.25± 5.17	22.43 ± 3.90	0.314		0.28	0.094±0.006	0.086±0.005	6.777e-25
	0.29	3.21±0.59	3.26±0.55	0.656		0.29	7.51±5.28	8.66±5.09	0.415		0.29	21.25± 5.17	22.43 ± 3.90	0.314		0.29	0.095±0.006	0.086±0.005	1.2527e-25
	0.30	3.30±0.61	3.36±0.56	0.632		0.30	7.51±5.28	9.08±4.62	0.370		0.30	21.25± 5.17	22.43 ± 3.90	0.314		0.30	0.095±0.006	0.087±0.005	3.1413e-26
	0.31	3.39±0.63	3.45±0.58	0.632		0.31	7.51±5.28	9.44±4.09	0.328		0.31	21.25± 5.17	22.43 ± 3.90	0.314		0.31	0.095±0.006	0.088±0.005	1.3237e-26
	0.32	3.48±0.64	3.54±0.59	0.656		0.32	7.51±5.28	9.44±4.09	0.328		0.32	21.25± 5.17	22.43 ± 3.90	0.314		0.32	0.096±0.006	0.089±0.005	1.1296e-27

* continues in next page

Modulariy	PTh	CNT	MSC	p-value	Global Effiency	PTh	CNT	MSC	p-value	Global Flow Coefficient	PTh	CNT	MSC	p-value	Assortativity	PTh	CNT	MSC	p-value
	0.06	0.261±0.051	0.272±0.061	0.656		0.06	0.074±0.029	0.075±0.027	0.805		0.06	0.053±0.037	0.062±0.039	0.542		0.06	0.245±0.109	-0.240±0.090	0.908
	0.07	0.250±0.049	0.257±0.057	0.856		0.07	0.084±0.031	0.087±0.028	0.704		0.07	0.056±0.038	0.067±0.040	0.438		0.07	-0.245±0.110	-0.234±0.087	0.987
	0.08	0.240±0.048	0.246±0.054	0.805		0.08	0.093±0.032	0.095±0.029	0.856		0.08	0.058±0.040	0.069±0.040	0.458		0.08	-0.245±0.109	-0.232±0.080	0.934
	0.09	0.230±0.046	0.237±0.051	0.779		0.09	0.101±0.032	0.102±0.027	0.856		0.09	0.061±0.040	0.071±0.041	0.499		0.09	-0.244±0.109	-0.229±0.077	0.830
	0.10	0.224±0.048	0.228±0.050	0.830		0.10	0.108±0.033	0.110±0.024	0.961		0.10	0.062±0.040	0.074±0.041	0.382		0.10	-0.242±0.110	-0.225±0.076	0.805
	0.11	0.217±0.047	0.222±0.048	0.908		0.11	0.114±0.033	0.118±0.022	1.000		0.11	0.064±0.042	0.077±0.041	0.314		0.11	-0.240±0.112	-0.224±0.074	0.754
	0.12	0.209±0.046	0.215±0.048	0.704		0.12	0.119±0.032	0.124±0.021	0.987		0.12	0.065±0.042	0.079±0.043	0.347		0.12	-0.241±0.111	-0.224±0.075	0.729
	0.13	0.203±0.044	0.209±0.048	0.754		0.13	0.125±0.029	0.129±0.020	0.856		0.13	0.067±0.042	0.081±0.043	0.419		0.13	-0.239±0.110	-0.224±0.074	0.805
	0.14	0.198±0.043	0.203±0.047	0.609		0.14	0.130±0.029	0.134±0.020	0.856		0.14	0.069±0.043	0.082±0.043	0.438		0.14	-0.240±0.110	-0.221±0.075	0.729
	0.15	0.193±0.043	0.198±0.045	0.704		0.15	0.135±0.027	0.138±0.020	0.934		0.15	0.070±0.044	0.084±0.043	0.382		0.15	-0.238±0.109	-0.220±0.075	0.704
	0.16	0.186±0.043	0.193±0.045	0.542		0.16	0.139±0.027	0.141±0.020	0.961		0.16	0.072±0.044	0.086±0.044	0.364		0.16	-0.237±0.108	-0.218±0.076	0.632
	0.17	0.183±0.041	0.188±0.043	0.656		0.17	0.142±0.026	0.143±0.020	0.830		0.17	0.073±0.045	0.088±0.044	0.382		0.17	-0.236±0.108	-0.215±0.077	0.564
	0.18	0.177±0.039	0.184±0.041	0.564		0.18	0.145±0.025	0.146±0.020	0.754		0.18	0.075±0.046	0.090±0.045	0.364		0.18	-0.235±0.108	-0.214±0.076	0.564
	0.19	0.173±0.038	0.179±0.041	0.564		0.19	0.148±0.024	0.148±0.021	0.779		0.19	0.076±0.046	0.091±0.045	0.347		0.19	-0.233±0.109	-0.213±0.076	0.564
	0.20	0.170±0.037	0.175±0.040	0.680		0.20	0.150±0.024	0.150±0.021	0.729		0.20	0.077±0.046	0.093±0.045	0.347		0.20	-0.232±0.107	-0.218±0.076	0.564
	0.21	0.166±0.035	0.171±0.039	0.680		0.21	0.152±0.024	0.151±0.022	0.754		0.21	0.078±0.046	0.094±0.045	0.299		0.21	-0.230±0.108	-0.209±0.076	0.609
	0.22	0.162±0.036	0.168±0.039	0.586		0.22	0.154±0.023	0.153±0.023	0.779		0.22	0.079±0.047	0.096±0.046	0.314		0.22	-0.227±0.107	-0.206±0.077	0.586
	0.23	0160±0.034	0.165±0.038	0.632		0.23	0.156±0.023	0.154±0.023	0.830		0.23	0.081±0.047	0.097±0.046	0.299		0.23	-0.224±0.106	-0.204±0.077	0.586
	0.24	0.157±0.032	0.160±0.037	0.805		0.24	0.157±0.023	0.155±0.024	0.908		0.24	0.082±0.047	0.099±0.046	0.283		0.24	-0.221±0.106	-0.202±0.076	0.564
	0.25	0.154±0.033	0.158±0.037	0.704		0.25	0.158±0.023	0.156±0.025	0.882		0.25	0.083±0.048	0.100±0.046	0.255		0.25	-0.220±0.106	-0.199±0.076	0.564
	0.26	0.152±0.033	0.155±0.037	0.830		0.26	0.159±0.023	0.157±0.025	0.882		0.26	0.084±0.048	0.102±0.047	0.241		0.26	-0.217±0.106	-0.197±0.076	0.564
	0.27	0.149±0.032	0.152±0.036	0.754		0.27	0.160±0.023	0.158±0.026	0.830		0.27	0.085±0.047	0.103±0.047	0.241		0.27	-0.214±0.105	-0.195±0.076	0.542
	0.28	0.146±0.031	0.150±0.035	0.704		0.28	0.161±0.024	0.158±0.026	0.779		0.28	0.086±0.047	0.105±0.047	0.241		0.28	-0.212±0.104	-0.192±0.076	0.520
	0.29	0.144±0.031	0.147±0.034	0.805		0.29	0.162±0.024	0.159±0.027	0.805		0.29	0.087±0.048	0.106±0.047	0.241		0.29	-0.209±0.103	-0.190±0.076	0.520
	0.30	0.142±0.031	0.146±0.035	0.754		0.30	0.163±0.024	0.159±0.027	0.779		0.30	0.089±0.048	0.108±0.047	0.241		0.30	-0.206±0.103	-0.187±0.076	0.458
	0.31	0139±0.030	0.144±0.035	0.805		0.31	0.163±0.025	0.160±0.027	0.754		0.31	0.090±0.048	0.109±0.047	0.228		0.31	-0.203±0.102	-0.185±0.074	0.458
	0.32	0.137±0.031	0.141±0.035	0.729		0.32	0.164±0.025	0.160±0.028	0.729		0.32	0.091±0.048	0.110±0.047	0.241		0.32	-0.1999±0.102	-0.181±0.074	0.458

II. Local/nodal Connectivity measures – Results

Table 15- **(RUN V1MT)** Regions with local connectivity measures statistically different between groups in the range of 0.06–0.32 of PTh values, and a significance level of 0.05. The minimum p-value and corresponding PTh for each region, as well as the difference between the measure of the two groups (MSC-CNT) across the PTh's are positioned in each cell of the table. When the difference in that measure is higher in the MSC group the cell is grey, when is higher in the CNT group is white.

ROI	Total degree	In degree	Out degree	Total strength	In strength	Out strength	Subgraph centrality	K-coreness centrality	Betweenness centrality	Participation coefficient	PageRank centrality	Local efficiency	Node flow coefficient	Total flow coefficient	Eccentricity
PreCG_L (1)		P=0.0131 (0.07) 10.5310												P=0.0306 (0.20) 118.4967	
SFG_L (2)															
OLF_L (9)											P=0.0167 (0.28) 0.0013			P=0.0048 (0.26) 149.5425	
PFCventmed_L (11)	P=0.0026 (0.09) 24.7810	P=0.0011 (0.09) 13.1176		P=0.0065 (0.07) 6.1042	P=0.0065 (0.10) 3.6843			P=0.0013 (0.09) 5.2810					P=0.0105 (0.32) 0.0656	P=0.0058 (0.32) 745.4706	
OFCant_L (14)			P=0.0167 (0.22) -3.2810			P=0.0183 (0.25) -6.9201									
OFClat_L (16)													P=0.0238 (0.26) 0.0390		
HIP_L (21)														P=0.0200 (0.30) 178.7908	
PHG_L (22)											P=0.0127 (0.06) 0.0037		P=0.0028 (0.32) 0.0585	P=0.0018 (0.22) 502.2810	
AMYG_L (23)	P=0.0121 (0.06) 14.7418							P=0.0034 (0.30) 10.8529					P=0.0013 (0.24) 0.0664	P=2.0477e-4 (0.31) 365.4837	
CAL_L (24)															
MOG_L (28)			P=0.0257 (0.15) 16.7778			P=0.0200 (0.24) 2.7816									
FFG_L (30)													P=0.0043 (0.23) 0.0496		
PUT_L (39)		P=0.0189 (0.25) -12.3399											P=0.0133 (0.13) 0.0420		

* continues in next page

ROI	Total degree	In degree	Out degree	Total strength	In strength	Out strength	Subgraph centrality	K-coreness centrality	Betweenness centrality	Participation coefficient	PageRank centrality	Local efficiency	Node flow coefficient	Total flow coefficient	Eccentricity
HES_L (42)	P=0.0127 (0.28) -11.6373	P=0.0181 (0.32) -14.1520													
STG_L (43)		P=0.0127 (0.21) -19.4542													
CER4-5_L (51)													P=0.0116 (0.14) 0.0528		
CER6_L (52)													P=0.0333 (0.20) 0.0388		
tAV_L (57)				P=0.0282 (0.11) -8.6240		P=0.0282 (0.25) -8.7140									
tVA_L (59)													P=0.0105 (0.29) 0.0361		
tVPL_L (61)			P=0.0120 (0.08) -22.4967			P=0.0152 (0.08) -3.9647		P=0.0020 (0.23) -15.8219							
tRE_L (63)													P=0.0028 (0.25) 0.0535		
tMDl_L (65)						P=0.0200 (0.27) -5.0546									
tPuA_L (68)				P=0.0282 (0.23) -5.2042		P=0.0333 (0.14) -4.3111							P=0.0153 (0.19) 0.0447		
tPuM_L (69)						P=0.0065 (0.08) -7.5591							P=0.0091 (0.06) 0.0426		
tPuI_L (71)											P=0.0127 (0.23) 0.0023		P=0.0183 (0.25) 0.0357		
ACCpre_L (73)											P=0.0035 (0.29) 0.0019		P=0.0023 (0.17) 0.0657	P=0.0063 (0.10) 440.5229	
SNpc_L (77)		P=0.0115 (0.27) 13.9771											P=0.0065 (0.15) 0.0555	P=0.0053 (0.19) 465.8758	
RedN_L (79)													P=0.0018 (0.29) 0.0479		
VER1-2 (81)				P=0.0391 (0.06) -6.8892		P=0.0218 (0.25) -6.5451									

* continues in next page

ROI	Total degree	In degree	Out degree	Total strength	In strength	Out strength	Subgraph centrality	K-coreness centrality	Betweenness centrality	Participation coefficient	PageRank centrality	Local efficiency	Node flow coefficient	Total flow coefficient	Eccentricity
VER4-5 (83)				P=0.0183 (0.08) -4.3977											
MFG_R (93)		P=0.0109 (0.15) 8.4412													
ROL_R (97)		P=0.0292 (0.28) -15.2124			P=0.0361 (0.21) -5.7028			P=0.0075 (0.17) -3.3725							
SFGmedial_R (100)	P=0.0011 (0.32) 23.2451	P=0.0021 (0.09) 15.7647		P=0.0065 (0.09) 6.3739	P=0.0039 (0.09) 5.3948			P=6.7496e-5 (0.13) 5.2484	P=4.9765e-4 (0.30) -212.7778						
PFCventmed_R (101)	P=8.9637e-4 (0.18) 23.8203	P=0.0023 (0.06) 15.4510		P=0.0065 (0.07) 5.8040	P=0.0043 (0.06) 4.1037			P=0.0079 (0.26) 7.1634						P=0.0048 (0.30) 401.4935	
REC_R (104)					P=0.0054 (0.06) 3.1672										
OFCant_R (105)		P=0.0026 (0.06) 11.3775			P=0.0039 (0.06) -3.3607										
OFCpost_R (111)	P=0.0110 (0.18) 16.7614													P=0.0087 (0.30) 3278.33791	
HIP_R (112)	P=0.0133 (0.16) 15.3922													P=0.0238 (0.22) -15.9935	
PHG_R (113)								P=0.0148 (0.12) 4.6373					P=0.0139 (0.10) 0.0442		
AMYG_R (119)		P=0.0257 (0.21) 9.1879			P=0.0333 (0.24) 2.0359			P=0.0085 (0.13) 8.0588							
IOG_R (120)													P=0.0185 (0.06) 0.0451		
FFG_R (130)		P=0.0199 (0.26) -12.3611			P=0.0333 (0.20) -4.8040										
PAL_R (132)		P=0.0033 (0.11) -15.5686													
HES_R (133)		P=0.0058 (0.30) -17.6797			P=0.0183 (0.12) -6.0970										

* continues in next page

ROI	Total degree	In degree	Out degree	Total strength	In strength	Out strength	Subgraph centrality	K-coreness centrality	Betweenness centrality	Participation coefficient	PageRank centrality	Local efficiency	Node Flow coefficient	Total Flow coefficient	Eccentricity
STG_R (134)													P=0.0079 (0.28) 0.0481		
TPOsup_R (140)													P=0.0218 (0.19) 0.0735	P=0.0096 (0.08) 829.0261	
CER3_R (141)													P=0.0105 (0.20) 0.0448		
CER4-5_R (144)													P=0.0096 (0.28) 0.0895		
CER8_R (148)													P=0.0200 (0.21) 0.0555		
tLP_R (149)	P=0.0115 (0.30) -22.585	P=0.0181 (0.18) -15.7778		P=0.0218 (0.18) -7.2300	P=0.0160 (0.18) -4.8267									P=0.0096 (0.08) -348.3856	
tVA_R (150)								P=0.0204 (0.32) -5.9869	P=0.0057 (0.09) 156.8170						
tVL_R (151)	P=0.0018 (0.17) -27.3039			P=0.0116 (0.19) -7.9175				P=0.0016 (0.08) -8.4379	P=0.0015 (0.29) 127.4641		P=0.0116 (0.32) -0.0029				
tVPL_R (152)						P=8.0812e-4 (0.26) -6.7264							P=0.0031 (0.19) 0.0624		
tMDm_R (154)													P=0.0139 (0.29) 0.0383		
tLGN_R (156)													P=0.0023 (0.13) 0.0482		
tMGN_R (157)		P=7.9925e-4 (0.12) 25.6111			P=0.0010 (0.12) 6.1997								P=7.1698e-4 (0.18) 0.0706	P=4.9720e-4 (0.18) 423.4673	
tPuA_R (158)													P=0.0039 (0.16) 0.0469		
tPuI_R (161)													P=0.0139 (0.12) 0.0495		
SNpr_R (168)									P=0.0016 (0.08) 157.1797						

Table 16- (**RUN BM**) Regions with local connectivity measures statistically different between groups in the range of 0.06–0.32 of PTh values, and significance level of 0.05. The minimum p-value and corresponding PTh for each region, as well as the difference between the measure of the two groups (MSC-CNT) across the PTh's are positioned in each cell of the table. When the difference in that measure is higher in the MSC group the cell is grey, when is higher in the CNT group is white.

ROI	Total degree	In degree	Out degree	Total strength	In strength	Out strength	Subgraph centrality	K-coreness centrality	Betweenness centrality	Participation coefficient	PageRank centrality	Local efficiency	Node flow coefficient	Total flow coefficient	Eccentricity
IFGorb_L (6)			P=0.0095 (0.30) 13.0784			P=0.015 1 (0.25) 3.8809							P=0.0386 (0.06) 0.0407		
ACC_L (18)				P=0.0087 (0.08) -9.5394	P=0.0105 (0.08) -7.1901										
MOG_L (28)	P=0.0293 (0.23) -14.2451		P=0.0085 (0.25) -11.1503	P=0.0282 (0.31) -5.2276		P=0.006 8 (0.25) -3.9132									
PoCG_L (31)	P=0.0133 (0.32) 19.5163		P=0.0021 (0.32) 16.1307	P=0.0238 (0.27) 5.4738		P=0.002 7 (0.24) 4.7791	P=0.0026 (0.14) -3.11e12	P=0.0146 (0.27) 14.8464	P=4.3849e-4 (0.13) -434.7843	P=4.5098e-4 (0.18) 0.5294	P=8.0812 e-4 (0.23) 0.0034		P=0.0015 (0.19) 0.0848	P=0.0118 (0.29) 116.4216	
SPG_L (32)													P=0.0020 (0.23) 0.0517		
ANG_L (35)			P=0.0119 (0.28) 10.8954			P=0.017 2 (0.28) 3.0023				P=0.0143 (0.09) 0.3562	P=0.0096 (0.28) 0.0028		P=0.0021 (0.12) 0.0773	P=0.0184 (0.16) 225.4542	
PCUN_L (36)		P=0.0079 (0.32) -11.0621			P=0.0105 (0.08) -4.3820										
CAU_L (38)		P=0.0354 (0.08) -16.1993													
CERCRU1_L (48)													P=0.0213 (0.17) 0.0489		
tVA_L(59)													P=0.0132 (0.16) -0.0349		
tMDm_L (64)													P=0.0068 (0.10) -0.0427		
tMDl_L (65)	P=0.0053 (0.18) -28.1242			P=0.0087 (0.23) -10.7961		P=0.030 6 (0.09) -7.6897									
ACCpre_L (73)											P=0.0116 (0.21) 0.0038				
tRe_L (79)			P=0.0055 (0.20) 24.1111			P=0.009 1 (0.20) 8.1637					P=0.0053 (0.09) 0.0074				

* continues in next page

ROI	Total degree	In degree	Out degree	Total strength	In strength	Out strength	Subgraph centrality	K-coreness centrality	Betweenness centrality	Participation coefficient	PageRank centrality	Local efficiency	Node flow coefficient	Total flow coefficient	Eccentricity
LC_L (80)											P=0.0059 (0.16) 0.0039				
VER4_5 (83)											P=0.01 (0.32) -0.0032				
VER9 (87)		P=0.0086 (0.22) 17.8301			P=0.0113 (0.19) 6.8225										
ROL_R (97)									P=0.0023 (0.15) 172.9248						
OFCant_R (104)															P=0.0391 (0.11) 2.2706
OFCpost_R (105)		P=0.0067 (0.06) -12.4312			P=0.0053 (0.06) -4.8302						P=0.0035 (0.32) 0.0031	P=0.0167 (0.06) -0.0350			
INS_R (107)											P=0.0087 (0.20) 0.0067				
ACC_R (108)		P=0.0105 (0.06) -14.0163		P=0.0167 (0.12) -7.8357	P=0.0043 (0.32) -7.5372							P=0.0079 (0.07) -0.0264			
AMYG_R (113)		P=0.0120 (0.08) 15.6209			P=0.0160 (0.08) 5.8971						P=0.0096 (0.31) -0.0032				
FFG_L (120)												P=0.0333 (0.18) -0.0175			
SPG_R(122)									P=2.6449e-4 (0.11) -569.6928		P=0.0043 (0.25) 0.0013		P=2.2482e -4 (0.21) 0.0927	P=0.0216 (0.22) 150.0719	
SMG_R (124)			P=0.0113 (0.18) 11.8562			P=0.011 4 (0.17) 4.0264							P=0.0094 (0.13) 0.0613		
ANG_R (125)													P=0.0054 (0.13) 0.0603		
PUT_R (129)								P=0.0100 (0.26) 15.1046							
CERCRU2_R (139)		P=0.0173 (0.13) 13.2092													

* continues in next page

ROI	Total degree	In degree	Out degree	Total strength	In strength	Out strength	Subgraph centrality	K-coreness centrality	Betweenness centrality	Participation coefficient	PageRank centrality	Local efficiency	Node flow coefficient	Total flow coefficient	Eccentricity
CER3_R (140)						P=0.0172 (0.07) 4.4279									
CER6_R (142)	P=0.0050 (0.31) -21.9967			P=0.0035 (0.30) -8.3024		P=0.0056 (0.27) 5.0155		P=0.0195 (0.06) -13.6961	P=0.0012 (0.17) 252.0196		P=0.0087 (0.29) -0.0018			P=0.0110 (0.27) -176.5359	P=0.0042 (0.07) 1.8007
CER10_R (146)		P=0.0031 (0.31) 16.9248			P=0.0259 (0.28) 6.2233										
tRe_R (153)	P=0.0040 (0.31) -27.6569		P=0.0278 (0.07) -18.2582	P=0.0065 (0.16) -11.6923										P=0.0035 (0.07) -441.0850	
tMDm_R (154)			P=0.0091 (0.21) -25.1275			P=0.0139 (0.21) -10.5654							P=0.0043 (0.31) -0.0470	P=0.0079 (0.24) -574.8954	
VTA_R (166)	P=0.0021 (0.36) 27.7320		P=0.0082 (0.11) 18.2222	P=0.0087 (0.14) 8.7359				P=0.0090 (0.26) 11.6601						P=0.0013 (0.12) 324.0686	

Table 17- (**RUN RS**) Regions with local connectivity measures statistically different between groups in the range of 0.06–0.32 of PTh values, and a significance level of 0.05. The minimum p-value and corresponding PTh for each region, as well as the difference between the measure of the two groups (MSC-CNT) across the PTh's are positioned in each cell of the table. When the difference in that measure is higher in the MSC group the cell is grey, when is higher in the CNT group is white.

ROI	Total degree	In degree	Out degree	Total strength	In strength	Out strength	Subgraph centrality	K-coreness centrality	Betweenness centrality	Participation coefficient	PageRank centrality	Local efficiency	Node flow coefficient	Total flow coefficient	Eccentricity
ROL_L (7)			P=0.0143 (0.12) 7.4535			P=0.0183 (0.18) 2.1343							P=0.0200 (0.22) 0.0541		
REC_L (12)			P=0.0281 (0.32) -20.6732												
OFCmed_L(13)		P=0.0169 (0.06) 7.9869													
INS_L (17)										P=0.0092 (0.11) 0.2353					
ACC_L (18)					P=0.0218 (0.08) -8.9431										
AMYG_L (23)													P=0.0116 (0.14) 0.0361	P=0.0035 (0.08) 399.2647	
CUN_L (25)		P=0.0131 (0.10) 10.6046						P=0.0078 (0.12) 9.2974							
LING_L (26)								P=0.0237 (0.17) 6.9183							
SOG_L (27)								P=0.0245 (0.16) 10.1307							
IOG_L (29)	P=7.4899e-4 (0.16) 16.7418	P=0.0058 (0.18) 12.5784		P=0.0039 (0.06) 4.7269	P=0.0166 (0.06) 3.6693			P=3.8454e-4 (0.06) 9.9346						P=0.0056 (0.11) 108.5294	
SPG_L (32)	P=0.0070 (0.06) 17.7484	P=0.0064 (0.12) 12.9346		P=0.0079 (0.06) 5.8987	P=0.0079 (0.06) 5.1835			P=0.0052 (0.12) 8.6961							
PUT_L (39)					P=0.0282 (0.25) -7.1969										
MTG_L (45)	P=0.0227 (0.25) 21.9967		P=0.0075 (0.27) 10.1373			P=0.0116 (0.27) 2.3438								P=0.0109 (0.12) 417.0980	
CERCRU1_L (48)			P=0.0033 (0.17) -22.7974	P=0.0153 (0.28) -6.3729		P=0.0071 (0.17) -8.3807									

* continues in next page

ROI	Total degree	In degree	Out degree	Total strength	In strength	Out strength	Subgraph centrality	K-coreness centrality	Betweenness centrality	Participation coefficient	PageRank centrality	Local efficiency	Node flow coefficient	Total flow coefficient	Eccentricity
CER3_L (50)		P=0.0225 (0.20) 8.9346													
CER4-5_L (51)			P=0.0109 (0.06) -16.3366			P=0.0053 (0.09) -7.1996					P=0.0218 (0.23) -0.0035				
CER7b_L (53)														P=0.0160 (0.11) 569.3072	
tVPL_L (61)	P=0.0198 (0.09) -23.3170	P=0.0023 (0.16) -13.0556		P=0.0167 (0.21) -7.8951	P=0.0020 (0.15) -4.1740			P=6.5854e-4 (0.08) -8.9510	P=0.0011 (0.22) 240.5098					P=0.0017 (0.08) -311.0817	
tRE_L (63)					P=0.0167 (0.27) -2.5668										
tMDm_L (64)				P=0.0200 (0.32) -8.3575											
tMDl_L (65)	P=0.0100 (0.14) -27.1209			P=0.0087 (0.13) -9.4547				P=0.0077 (0.06) -6.5654							P=0.0078 (0.06) 1.6333
tPuL_L (70)					P=0.0218 (0.07) -3.7631										
ACCpre_L (73)															P=0.0424 (0.11) 2.3581
LC_L (80)														P=0.0293 (0.25) 266.3399	
RapheD (89)									P=0.0044 (0.10) 254.7026						
RapheM (90)		P=0.0029 (0.27) -5.3529			P=0.0025 (0.27) -2.6373										
PreCG_R (91)														P=0.0183 (0.24) 254.1895	
ROL_R (97)		P=0.0095 (0.30) -18.8464			P=0.0183 (0.15) -8.3377										
REC_R (102)		P=0.0173 (0.24) 6.5915													

* continues in next page

ROI	Total degree	In degree	Out degree	Total strength	In strength	Out strength	Subgraph centrality	K-coreness centrality	Betweenness centrality	Participation coefficient	PageRank centrality	Local efficiency	Node flow coefficient	Total flow coefficient	Eccentricity
OFCant_R (104)		P=0.0236 (0.20) 11.7255													
OFCpost_R (105)		P=0.0037 (0.29) 14.9575			P=0.0218 (0.22) 4.3145										
INS_R (107)		P=0.0121 (0.13) -24.9837	P=0.0163 (0.11) 5.3922	P=0.0183 (0.09) -10.6960	P=0.0127 (0.13) -12.0657	P=0.0126 (0.16) 1.3868				P=0.0029 (0.15) 0.2941			P=0.0128 (0.15) 0.0342		
ACC_R (108)		P=0.0159 (0.32) -14.0229	P=0.0173 (0.32) 6.8889		P=0.0259 (0.12) -6.9966								P=0.0075 (0.11) 0.0448		
CUN_R (115)	P=0.0105 (0.17) 19.9314	P=0.0105 (0.20) 12.7288			P=0.0183 (0.23) 3.4061			P=0.0086 (0.17) 10.0784							
SPG_R (117)	P=0.0198 (0.27) 16.4412	P=0.0133 (0.31) 11.8105			P=0.0096 (0.31) 3.4694										
MOG_R (118)	P=0.0081 (0.10) 15.8758	P=0.0149 (0.07) 12.2222		P=0.0055 (0.09) 4.3303	P=0.0158 (0.07) 3.7339			P=0.0028 (0.09) 9.4673							
IOG_R (119)	P=0.0151 (0.09) 11.3170	P=0.0017 (0.09) 10.8954			P=9.0916e-4 (0.09) 3.0636			P=0.0124 (0.09) 9.5098						P=0.0167 (0.26) 78.5784	
FFG_R (120)														P=0.0014 (0.10) 229.5784	
PUT_R (129)			P=0.0049 (0.25) 9.2190		P=0.0333 (0.26) -7.3174	P=0.0116 (0.25) 2.5359									
PAL_R (130)			P=0.0208 (0.11) 16.7647			P=0.0167 (0.16) 5.5886					P=0.0071 (0.11) 0.0031				
HES_R (132)			P=0.0115 (0.25) 11.0000			P=0.0238 (0.14) 3.2792							P=0.0025 (0.12) 0.0484		
TPOmid_R (136)														P=0.0075 (0.26) 195.8170	
CERCRU1_R (138)			P=0.0095 (0.25) -23.2745			P=0.0183 (0.25) -7.8989					P=0.0096 (0.18) -0.0071				
CER4-5_R (141)						P=0.0259 (0.15) -4.5888									

* continues in next page

ROI	Total degree	In degree	Out degree	Total strength	In strength	Out strength	Subgraph centrality	K-coreness centrality	Betweenness centrality	Participation coefficient	PageRank centrality	Local efficiency	Node flow coefficient	Total flow coefficient	Eccentricity
CER7b_R (143)	P=0.0087 (0.32) 19.2712													P=0.0105 (0.15) 556.2026	
tLP_R (148)			P=0.0182 (0.06) -27.2876	P=0.0183 (0.08) -11.0840		P=0.0096 (0.12) -11.7924									
tVL_R (150)			P=0.0059 (0.07) -15.5033			P=0.0057 (0.07) -4.7200					P=0.0079 (0.07) -0.0034				P=0.0087 (0.12) 2.9898
tVPL_R (151)								P=0.0060 (0.12) -6.3497	P=0.0043 (0.23) 203.8301						
tMDm_R (154)	P=0.0061 (0.26) -23.6601			P=0.0167 (0.19) -8.1932				P=0.0069 (0.28) -7.3697	P=0.0017 (0.06) 194.4706						P=0.0127 (0.06) 1.5618
tMDl_R (155)															P=0.0151 (0.06) 1.6841
tLGN_R (156)								P=0.0109 (0.12) -8.4346							P=0.0259 (0.11) 3.5422
tMGN_R (157)		P=0.0013 (0.28) -14.5327			P=8.0812e-4 (0.28) -4.6565									P=0.0105 (0.32) -331.9739	
tPuL_R (160)		P=0.0100 (0.22) -16.0948			P=0.0065 (0.23) -5.6218			P=0.0102 (0.23) -7.8595							
ACCsub_R (162)															P=0.0306 (0.06) 1.0766
ACCpre_R (163)															P=0.0391 (0.06) 1.3886
VTA_R (166)			P=0.0181 (0.10) 12.7484			P=0.0259 (0.23) 3.4240					P=0.0059 (0.25) 0.0028				